HIGH STRENGTH REINFORCING STEEL BARS: CONCRETE SHEAR FRICTION INTERFACE

Final Report – Part A

SPR 762

Oregon Department of Transportation

HIGH STRENGTH REINFORCING STEEL BARS: CONCRETE SHEAR FRICTION INTERFACE

Final Report – Part A

SPR 762

by
André R. Barbosa, Ph.D., David Trejo, Ph.D., Drew Nielson
Oregon State University

for

Oregon Department of Transportation
Research Section
555 13th Street NE, Suite 1
Salem OR 97301

and

Federal Highway Administration
1200 New Jersey Avenue SE
Washington, DC 20590

March 2017

Technical Report Documentation Page

1. Report No. FHWA-OR-RD-17-08	2. Government Accession No.	3. Recipient's Catalog No.
4. Title and Subtitle High Strength Reinforcing Steel Bars: Concrete Shear Friction Interface		5. Report Date -March 2017- 6. Performing Organization Code
7. Author(s) Andre R. Barbosa, David Trejo, Drew Nielson		8. Performing Organization Report No. SPR 762 – Part A
9. Performing Organization Name and Address Oregon State University 101 Kearney Hall Corvallis, OR 97331		10. Work Unit No. (TRAIS) 11. Contract or Grant No.
12. Sponsoring Agency Name and Address Oregon Dept. of Transportation Research Section and Federal Highway Admin. 555 13th Street NE, Suite 1 1200 New Jersey Avenue SE Salem, OR 97301 Washington, DC 20590		13. Type of Report and Period Covered Final Report – Part A 14. Sponsoring Agency Code

15. Supplementary Notes

16. Abstract

High-strength steel (HSS) reinforcement, specifically ASTM A706 Grade 80 (550), is now permitted by the AASHTO LRFD Bridge Design Specifications for use in reinforced concrete bridge components in non-seismic regions. Using Grade 80 (550) steel reinforcement instead of Grade 60 (420) steel reduces material and construction costs. However, state highway agencies (SHAs) only allow Grade 80 (550) reinforcing steel in bridge structural elements that are not expected to undergo large strain reversals. AASHTO and SHAs have concerns with using Grade 80 (550) reinforcement in elements designed for concrete shear interfaces experimental data and currently limit the design value to the yield value of the Grade 60 (420) reinforcing steel bars. The report presents research developed to date on performance of Grade 80 (550) steel in resisting interface shearing actions, which is critical for characterizing the performance of precast girders and shear-keys in which Grade 80 (550) reinforcing steel may be used. A push-off test based experimental program was designed using ASTM A706 Grade 60 (420) and Grade 80 (550) reinforcing steel. A total of twenty push-off specimens were constructed and tested to discern if the design can account for the higher strength-steel nominal yield values.

17. Key Words	18. Distribution Statement Copies available from NTIS, and online at http://www.oregon.gov/ODOT/TD/TP_RES/		
19. Security Classification (of this report) Unclassified	20. Security Classification (of this page) Unclassified	21. No. of Pages 129	22. Price

SI* (MODERN METRIC) CONVERSION FACTORS

APPROXIMATE CONVERSIONS TO SI UNITS

Symbol	When You Know	Multiply By	To Find	Symbol
		LENGTH		
in	inches	25.4	millimeters	mm
ft	feet	0.305	meters	m
yd	yards	0.914	meters	m
mi	miles	1.61	kilometers	km
		AREA		
in^2	square inches	645.2	millimeters squared	mm^2
ft^2	square feet	0.093	meters squared	m^2
yd^2	square yards	0.836	meters squared	m^2
ac	acres	0.405	hectares	ha
mi^2	square miles	2.59	kilometers squared	km^2
		VOLUME		
fl oz	fluid ounces	29.57	milliliters	ml
gal	gallons	3.785	liters	L
ft^3	cubic feet	0.028	meters cubed	m^3
yd^3	cubic yards	0.765	meters cubed	m^3
NOTE: Volumes greater than 1000 L shall be shown in m^3.				
		MASS		
oz	ounces	28.35	grams	g
lb	pounds	0.454	kilograms	kg
T	short tons (2000 lb)	0.907	megagrams	Mg
		TEMPERATURE (exact)		
°F	Fahrenheit	(F-32)/1.8	Celsius	°C

APPROXIMATE CONVERSIONS FROM SI UNITS

Symbol	When You Know	Multiply By	To Find	Symbol
		LENGTH		
mm	millimeters	0.039	inches	in
m	meters	3.28	feet	ft
m	meters	1.09	yards	yd
km	kilometers	0.621	miles	mi
		AREA		
mm^2	millimeters squared	0.0016	square inches	in^2
m^2	meters squared	10.764	square feet	ft^2
m^2	meters squared	1.196	square yards	yd^2
ha	hectares	2.47	acres	ac
km^2	kilometers squared	0.386	square miles	mi^2
		VOLUME		
ml	milliliters	0.034	fluid ounces	fl oz
L	liters	0.264	gallons	gal
m^3	meters cubed	35.315	cubic feet	ft^3
m^3	meters cubed	1.308	cubic yards	yd^3
		MASS		
g	grams	0.035	ounces	oz
kg	kilograms	2.205	pounds	lb
Mg	megagrams	1.102	short tons (2000 lb)	T
		TEMPERATURE (exact)		
°C	Celsius	1.8C+32	Fahrenheit	°F

*SI is the symbol for the International System of Measurement

ACKNOWLEDGEMENTS

The authors would first like to acknowledge the Oregon Department of Transportation (ODOT) and the Pacific Northwest Transportation Consortium Region 10 (PacTrans) for providing the funding for this research project. At ODOT, we would like to acknowledge Steven Soltesz, Matthew Mabey, Tanarat Potisuk, Craig Shike, and other engineers at the ODOT's Bridge Standards and Bridge Design units. At PacTrans, the authors appreciate the support provided by Christopher Bell and Linda Boyle, former PacTrans board members. The authors thank Jeff Gent and James Batti for their technical assistance during testing at Oregon State University. Several graduate and undergraduate students also contributed at various levels to work performed in the laboratory; their help on this project is truly appreciated. NuCor steel provided reinforcing steel bars for this project. Special thanks to Thomas Murphy and Dennis Lauber from Cascade Steel (McMinnville, OR) for producing a special heat of the Grade 80 [550] HSS steel reinforcement.

DISCLAIMER

This document is disseminated under the sponsorship of the Oregon Department of Transportation and the United States Department of Transportation in the interest of information exchange. The State of Oregon and the United States Government assume no liability of its contents or use thereof.

The contents of this report reflect the view of the authors who are solely responsible for the facts and accuracy of the material presented. The contents do not necessarily reflect the official views of the Oregon Department of Transportation or the United States Department of Transportation.

The State of Oregon and the United States Government do not endorse products of manufacturers. Trademarks or manufacturers' names appear herein only because they are considered essential to the object of this document.

This report does not constitute a standard, specification, or regulation.

EXECUTIVE SUMMARY

INTRODUCTION

The use of Grade 80 (550) steel reinforcement instead of Grade 60 (420) steel, if used at its full design strength, could reduce material and construction costs of bridge and building projects. However, current federal and state codes have restrictions on the use of HSS in some cases. This is why Grade 80 [550] steel, though commercially available, is not commonly or widely used. More research needs to be done to determine the behavior of HSS in bridge and building components in order for designers to receive the full economic benefit of HSS for their projects.

This section summarizes results of a report entitled *High Strength Reinforcing Steel Bars: Concrete Shear Friction Interface Behavior*. The report provides an analysis and evaluation of the application of high-strength steel (HSS) for use in concrete interface shear friction applications using HSS.

Current bridge and building code provisions limit the contribution of the reinforcing steel to the strength of Grade 60 (420) reinforcing bar. Thus, the strength of Grade 80 (550) reinforcing steel, or other HSS reinforcing steel, are not considered for in concrete shear interface design. To date, only a limited number of tests have been performed to determine the behavior of HSS in concrete shear friction interface applications. The tests that have been conducted indicated that using HSS reinforcing bars to their full design capacity tends to overestimate the shear interface capacity of the specimens tested. In addition, limiting the design stress to 60 ksi (420 MPa) has been empirically determined to be appropriate for reinforcing bars across the shear interface. The research in this part of the report presents results on the behavior of Grade 80 (550) reinforcing steel meeting ASTM A706 specifications in shear friction applications and compares the results to current US design equations.

OBJECTIVES

The overall objective of this research is to study the behavior of HSS so that designers can use the reinforcing steel in more types of bridge components reliably.

The main objective of this research is to improve the current understanding of the behavior of HSS in concrete shear friction interfaces through laboratory testing to determine if the reinforcing steel can be used at its full design potential.

METHODOLOGY

A total of 20 push-off test specimens were constructed with varying reinforcing bar sizes (#4 and #5 [#13M and #16M]) and reinforcing steel grades (ASTM A706 Grade 60 [420] and ASTM

A706 Grade 80 [550]). The specimens were instrumented and tested with an applied load through the shear interface. The general research methodology followed is:

(1) A literature review on the topic was performed first. This included reviewing: (a) the shear friction theory; (b) published experimental research on concrete interface shear behavior estimated from push-off test specimens; (c) published experimental research on concrete interface shear behavior estimated from full-scale composite beam specimens; and (d) applicable codes and specifications for the design of interface shear in reinforced concrete structures.
(2) An experimental program was developed, which included: (a) experimental setup design; (b) specimen design and reinforcing steel layout; (c) push-off test procedures including the test setup and rate of loading; (d) instrumentation layout and plan; (e) construction procedure of the specimens; and (f) post-processing of experimental results.
(3) Materials used to construct the push-off test specimens were analyzed. This included tensile testing of the reinforcing steel that was to be used across the interface to determine the material properties. In addition, testing on the concrete was completed to determine its material properties.
(4) The experiment was conducted and the results were analyzed and discussed. The interface shear force versus the interface shear displacement, strain, and crack width behavior was reported. In addition, pertinent values from the test were reported and analyzed. Results and analysis of specimen type tested was discussed and compared to US codes.
(5) Conclusions were drawn from the discussion and recommendations for future testing were made.

SUMMARY OF MAIN FINDINGS

Overall, the results show a promising step forward for the utilization of HSS in bridge and building components. All push-off specimens were designed to have similar interface shear resistance using current AASHTO design equations. The main findings from of this research are that while the peak strength capacity of the specimens reinforced with Grade 80 #5 bars was greater than that of the Grade 60 #5 bars, a similar increase was not observed in the #4 specimens where negligible differences were observed in the peak strength. However, the use of HSS reinforcement increased the post-peak sustained loads. The mixed observations in terms of the increasing strength in the specimens with #4 and #5 reinforcement can be explained with the fact that the interface reinforcement for the #4 specimens did not reach yielding strains. However, two different varying conditions, the reinforcement bar size and the spacing between the bars, may have played a role in this difference. To clarify this point, and to gain a better understanding of the effects of HSS reinforcement for shear friction applications, further research is still needed, especially concerning other test variables not considered in SPR 762, including for example, concrete strength, interface roughness, rebar spacing, rebar grade, among others.

TABLE OF CONTENTS

LIST OF TABLES

LIST OF FIGURES

1.0 INTRODUCTION

Although high strength steel (HSS) is commercially available, its use is limited. In US design specifications and codes, such as ACI 318 *(ACI 2011)* and AASHTO *(AASHTO 2012)*, the design strength of HSS reinforcing bars in shear friction interfaces is currently limited to 60 ksi [420 MPa]. More research is being performed on using HSS in concrete structural members, such as in concrete columns for highway bridges *(Trejo et al. 2014)*. Full use of HSS strength in design could provide benefits in construction. Advantages could include reduction of reinforcing bar congestion as well as reductions in material and construction costs.

1.1 OBJECTIVE OF THE RESEARCH

The objective of this research report is to provide a better understanding of the behavior of Grade 80 (550) reinforcing steel meeting ASTM A706 specifications across a concrete-concrete interface connection subjected to a shear force. A total of twenty push-off specimens were tested at the Structural Engineering Research Laboratory at Oregon State University to gain more knowledge about the effects of grade of reinforcing steel bars, bar size, and reinforcement parameter in concrete interface shear friction behavior.

1.2 OULINE OF THE RESEARCH REPORT

This report includes 6 chapters. A brief description of each chapter follows. Chapter 1 introduces each chapter of the report and provides a basic description of the contents in each chapter. Chapter 2 includes a literature review for the experimental program. The review covers basic concepts of shear friction theory, reviews research completed with push-off test specimens and full-scale girder-slab composite beams, and discusses current code specifications. Chapter 3 presents the experimental program and design of the push-off test specimens including (i) the considerations for design; (ii) shear interface assumptions; (iii) shear connector layout; (iv) reinforcement layout; (v) construction procedure; (vi) external and internal instrumentation of the test specimens; (vii) the test setup and test procedure; and (viii) post-processing of experimental results. Chapter 4 is an overview of the materials used for the experimental program including what specifications were used to test the specimens, steel capacity and characterization, and the mixture proportions for the concrete used in the research program. In addition, this chapter provides the results from the materials testing. The chapter is separated into steel and concrete materials sections. Chapter 5 presents the experimental results for all sets of push-off test specimen. There is also a section for the analysis of the results, where the results of the test are discussed. The last two sections of this chapter include a proposed design equation and a comparison of the results to current US codes. Finally, chapter 6 provides a summary of the research program and states the main conclusions obtained.

2.0 LITERATURE REVIEW

This chapter presents a review of the literature on concrete-concrete shear interface behavior. Shear friction theory in concrete-concrete interfaces is presented first. A review of the research with push-off test specimens is then presented before research results from full-scale composite beam specimens is presented. Finally, current code equations for predicting in-service performance are reviewed.

Shear friction is defined in this paper as the resistance to displacement of an interface of two elements when acted upon by a shear force. The force is considered to be across a given plane at an existing or potential crack location, an interface between dissimilar materials, an interface between two concretes cast at different times, or the interface between different elements of the cross section *(AASHTO 2012).* Examples of this include corbels, bearing shoes, ledger beam bearings, and a host of connections between precast concrete elements *(Mansur et al. 2008).* This includes the connection between a girder and deck, such as the types designed in AASHTO *(AASHTO 2012).*

2.1 SHEAR FRICTION THEORY

Harries et al. *(Harries et al. 2012)* reported that one of the commonly known names for the shear-carrying mechanism, when force is transferred to an interface parallel to the shear force applied, is "shear friction." The authors noted that the mechanics are complex and are a function of concrete properties, constituent materials, the interaction between the reinforcing steel bars crossing the interface, and the interface surface roughness. Concrete materials and properties include aggregate and mixture proportions and the bond between the new and old concrete. This section will present a brief survey of the mechanics of shear friction. The discussions of the mechanics will include: (i) the commonly accepted general analogy; (ii) aggregate interlock; (iii) dowel action; (vi) concrete-concrete bond or cohesion; (v) and bar development or steel-concrete bond. The topics are discussed as each may play a controlling role in shear friction behavior.

Schematics showing the shear friction analogy proposed by Birkeland and Birkeland *(Birkeland and Birkeland 1966)* are shown in Figure 2.1 through Figure 2.3. This analogy is commonly used in the literature to explain the theoretical interface shear behavior. Figure 2.1 shows that the shear resistance, V, is related to the force, N, normal to the interface. The normal force, as shown as a clamping force, P, acts across the interface, m-m. The shear resistance, V, is equal to the friction coefficient, μ, multiplied by the clamping force, P. This only includes friction resistance and assumes no concrete-concrete bond resistance. As concrete-concrete interfaces include aggregate particles protruding through the interface, it is necessary to compensate for this "aggregate interlock." Aggregate interlock is the locking of the aggregate particles and depends on the surface roughness of the concrete and the clamping force in the system.

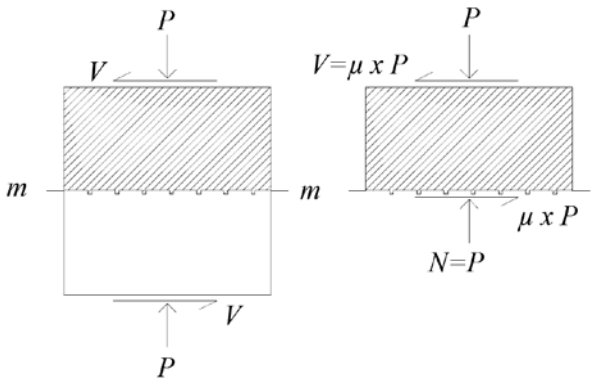

Figure 2.1: Shear friction hypothesis (adapted from Birkeland and Birkeland *(Birkeland and Birkeland 1966)*)

Figure 2.2 shows the reinforcement normal to interface *m-m*. When an interface is subjected to a lateral load, the interface separates a distance, δ, due to the interaction of the interface as illustrated in Figure 2.2. From this displacement, the tension, *T*, in the reinforcing bars increase, thus increasing the clamping force, *P*. The interface surface roughness is often simplified as a sawtooth surface at the interface, *m-m*, with an angle, ϕ. The reinforcing bars are assumed to be properly anchored on both sides of the interface and at their full yield strength at the ultimate shear capacity. Therefore, the tension, *T*, or clamping force, *P*, is the area of the steel, A_s, multiplied by the yield stress, f_y. This clamping force and surface roughness causes the aggregate at the interface to lock together and resist the shear force. This phenomenon is defined as aggregate interlock.

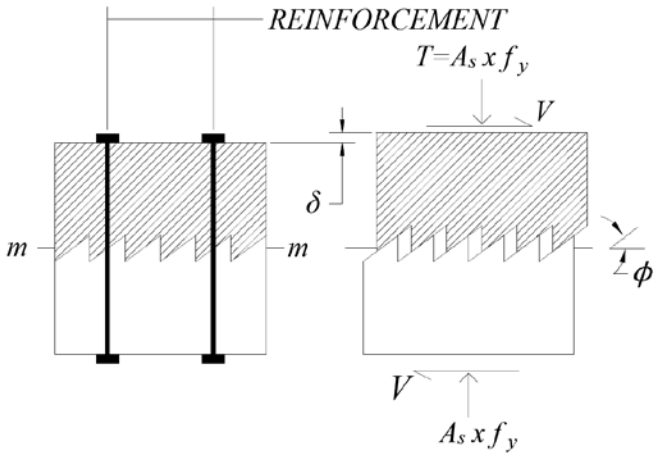

Figure 2.2: Shear friction hypothesis reinforcement analogy (adapted from Birkeland and Birkeland *(Birkeland and Birkeland 1966)*)

Figure 2.3 further illustrates the internal forces of the interface that were shown in Figure 2.2. The shear resistance, *V*, is the tension in the reinforcement multiplied by the tangent of the angle between the tension from the reinforcing bars and the normal force, *N*, reaction on the interface. The normal force, *N*, is from the interaction of *V* with the simplified sawtooth surface roughness.

Therefore, the shear resistance is the horizontal component of the aggregate interlock resistance or normal force, *N*, and is a function of the tanϕ.

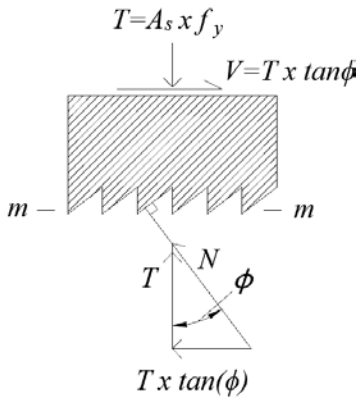

Figure 2.3: Shear friction hypothesis roughness analogy (adapted from Birkeland and Birkeland *(Birkeland and Birkeland 1966)*)

With additional roughness, more aggregate interlock is assumed and greater theoretical resistances can be obtained. The ultimate shear capacity or shear resistance at maximum load, V_u, is given by Birkeland and Birkeland *(Birkeland and Birkeland 1966)* as:

$$\mathbf{V_u = A_s f_y \tan(\phi)} \qquad \mathbf{(2.1)}$$

The term *tan(ϕ)* increases with increased roughness of the interface. Its value is reported to be 1.7 for monolithic concrete, 1.4 for artificially roughened joints, 1.0 for ordinary construction joints, and 0.8 for concrete-steel interfaces. Ordinary construction joints are interfaces where the concrete is cast on hardened concrete without artificial roughening *(Birkeland and Birkeland 1966)*. Artificially roughened joints are joints that are roughened with, for example, a rake, broom, or steel tined instrument. Birkeland and Birkeland *(Birkeland and Birkeland 1966)* specify that Equation 2-1 is applicable only for interfaces where the concrete strength is greater than 4000 psi (27.6 MPa). This equation is applicable when the reinforcing steel bar size is #6 (#19M) and smaller or when the headed stud size is 1/2 in. (12.7 mm) diameter and smaller. Headed studs are unthreaded rods with an upset head and are usually welded to steel beams for steel-concrete shear resistance purposes. No current codes use the Birkeland and Birkeland *(Birkeland and Birkeland 1966)* equation for design calculations, as more research has been completed and more accurate estimations formulated. Although much of the following research and codes are based on this general theory, the sawtooth simplification is not representative of the physical concrete interface.

To understand more about the behavior of the physical concrete interface, Kim et al. *(Kim et al. 2010)* analyzed aggregate interlock for self-consolidating concrete (SCC) and conventional concrete (CC). Specimen dimensions were 26 in. x 6 in. x 15.75 in. (660 mm x 152 mm x 400 mm) and were similar to common push-off test specimens with the two interlocking L shape geometries, as shown in Figure 2.4. Twelve SCC mixture proportions were evaluated with two (2) different aggregate types (river gravel and limestone), two (2) concrete strengths (5 and 7 ksi (34 and 48 MPa)), and three (3) coarse aggregate volumes. The specimens were pre-cracked

along the interface to ensure minimal or no concrete-concrete bonding. An external, stiff system of rods and plates were used to ensure the interface did not widen. This would ensure that only the capacity of the aggregate interlock would be tested. The specimen was tested vertically in line with the shear plane interface as shown in Figure 2.4 (b).

The general concept of aggregate interlock is illustrated in Figure 2.5 as an aggregate particle represented by a circle. Note this schematic assumed cohesion has been broken as cohesion would be represented as tensile stresses resisting the separation and slip of the interface. The stresses shown in the figure are from the engaged reinforcing bars resisting separation of the interface. There are vertical and horizontal components to the normal stresses that are similar to the simplification in Figure 2.3.

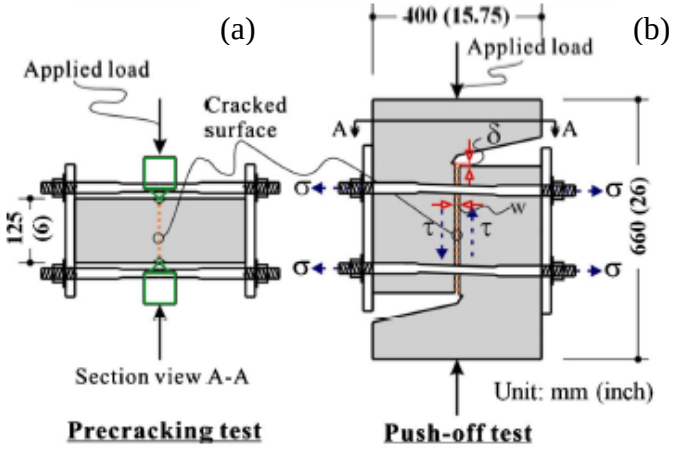

Figure 2.4: Test specimen for evaluating aggregate interlock: schematic test setup *(Kim et al. 2010)*

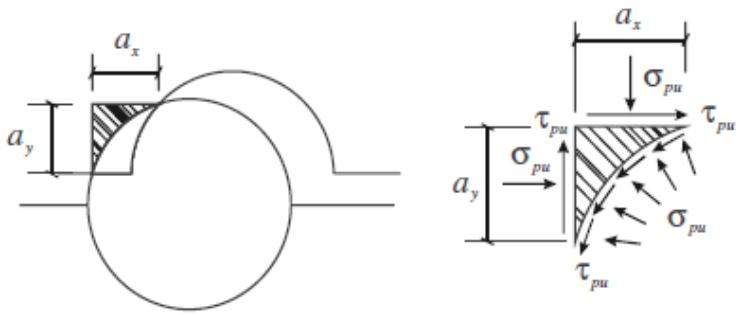

Figure 2.5: Schematic of aggregate interlock from Walraven's theory (adapted from Walraven and Reinhardt *(Walraven and Reinhardt 1981)* by Kim et al. *(Kim et al. 2010)*)

Figure 2.6 shows the observed behavior of the normal stress and crack width from the work by Kim et al. *(Kim et al. 2010).* As the crack width increases, the normal stress, which is a resultant of the clamping force, increases linearly as the aggregate collides and separates the interface.

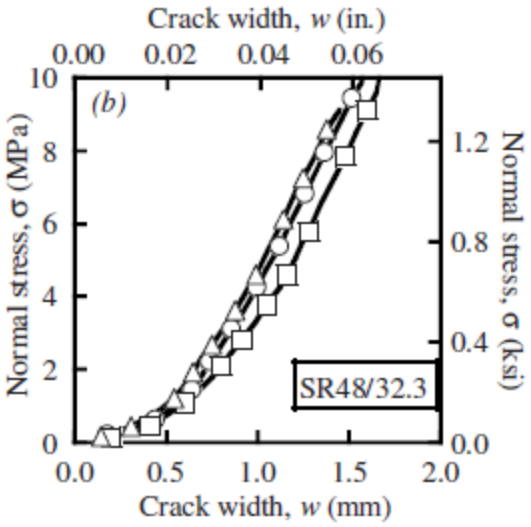

Figure 2.6: Typical plot of measured parameters *(Kim et al. 2010)*

The authors determined friction coefficients using a mixed procedure using the energy absorption calculated from the test. The authors found that the theoretical friction coefficients for SSC and CC mixtures were 0.32 and 0.30 respectively, while mixtures with river gravel (0.40) had higher friction coefficients than limestone gravel (0.23). The authors reported that the limestone gravel was weaker than the river gravel and thus was not able to maintain interlock as effectively. Aggregate interlock is dependent on the strength of the aggregate and the clamping force provided by the reinforcing bars. A previous study by Walraven and Reinhardt *(Walraven and Reinhardt 1981)* on aggregate interlock explored other areas of the mechanism.

Walraven and Reinhardt *(Walraven and Reinhardt 1981)* compared the shear resistance for an interface with and without cohesion to study how aggregate interlock and cohesion interact. The authors also studied the influence of dowel action on the shear resistance. The authors tested specimens with a shear plane area of 55.8 in^2 (36,000 mm^2) using two series of specimens.

The first series had embedded reinforcing bars across the interface. The authors made the assumption that the embedded bars had a bond characteristic similar to those found by Rehm *(Rehm 1961)*. This was done so the authors could estimate the clamping force from the interface separation. For the first series, the reinforcement ratio (6), bar diameter (4), concrete strength (3), inclination of stirrups to crack plane (8), dowel action (4), and surface roughness (2) were variables of the test. For the second series of the test, there was no embedded steel. External bars similar to what was shown in Figure 2.4 were used instead. The clamping force was measured directly from the force on the external bars. The variables for this series included the concrete strength (3) and the width of initial cracking (3). An additional increase in crack width was not possible as the external rods restrained the width of the interface.

The authors reported that for the embedded reinforcing steel bars the behavior of the load and crack opening was approximately consistent for all steel to concrete ratios tested for the same concrete strength. The steel reinforcing bar area to concrete area ratios ranged from 0.6 to 3.4%. The authors reported two other notes of interest: (i) larger aggregate sizes did not significantly influence the behavior of the aggregate interlock; (ii) when the cracks were loaded and unloaded,

considerable hysteresis was noticed. Because aggregate size did not influence behavior the aggregate strength seemed to control the behavior. The hysteresis provided evidence for frictional action as illustrated in Figure 2.1. Aggregate interlock is the locking of the aggregate and is caused by the clamping force from the reinforcing steel. In addition to that clamping force, the reinforcing steel also contributes to the shear resistance through dowel action.

The dowel action in specimens with embedded reinforcing bars was tested by Walraven and Reinhardt *(Walraven and Reinhardt 1981)*. The authors evaluated dowel action by debonding reinforcing steel bar stirrups with soft sleeves over a distance of 0.79 in. (20 mm) on each side of the crack as shown in Figure 2.7.

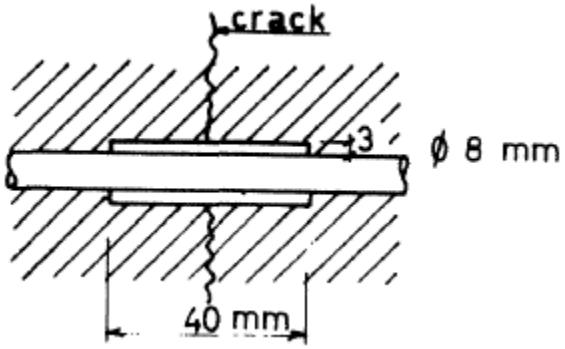

Figure 2.7: Soft sleeves around the bars Walraven and Reinhardt *(Walraven and Reinhardt 1981)*

The specimens tested by Walraven and Reinhardt *(Walraven and Reinhardt 1981)* with the "interrupted" bond at the interface showed that dowel action does not control at small crack widths. This indicates that aggregate interlock is the source of the most significant shear resistance. After the aggregate interlock is broken, dowel action then controls. Figure 2.9 illustrates the calculated contribution of the dowel action to the overall shear strength. Dowel action can be approximated with the following variables: (i) geometry of the interface; (ii) position of reinforcing bar; (iii) crack location; (iv) interface displacement; (v) bar diameter; and (vi) concrete strength.

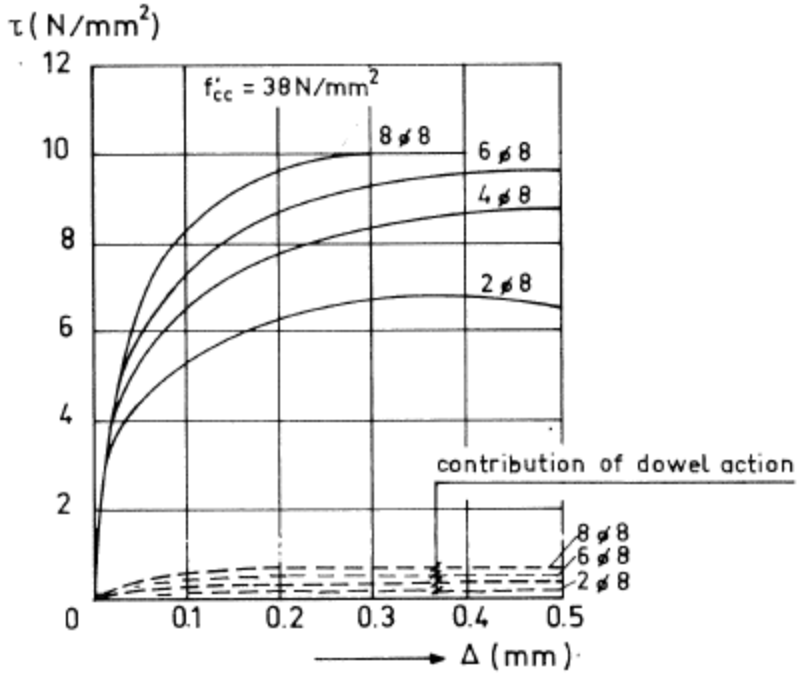

Figure 2.8: Contribution of dowel action to the total shear stress in a crack *(Walraven and Reinhardt 1981)* (145.04 psi = 1 N/mm^2)

The lack of dowel action contribution at small crack widths was reported to be most likely due to its mechanisms or dowel mode. Park and Paulay *(Park and Paulay 1975)* illustrated the calculations for dowel action mechanisms and this is shown in Figure 2.9. The authors reported that the dowel mode could be flexure, shear, or kinking. Flexure dowel action is resisted by the moment resistance of the reinforcing bar. Shear dowel action is only the shear resistance of the reinforcing bar. Kinking assumes a pure tensile resistance at an angle between two plastic hinge points on the reinforcing bar, which would create horizontal and vertical resistances. Each mechanism may require significant slip on the interface to engage significantly. In addition to dowel action, concrete-concrete cohesion is also a parameter in shear resistance.

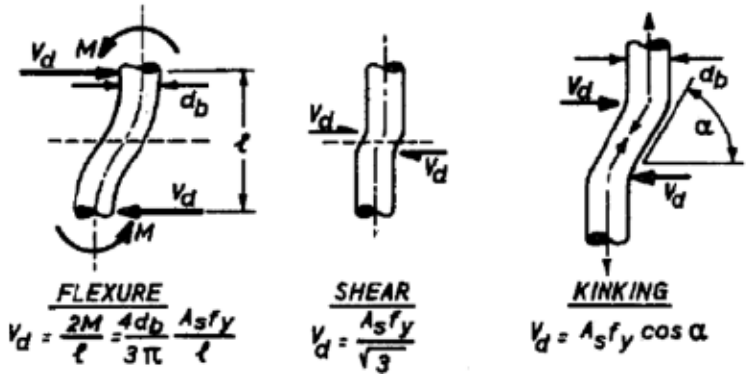

Figure 2.9: Three mechanisms of dowel action *(Park and Paulay 1975)*

To study concrete-concrete cohesion, Júlio et al. *(Júlio et al 2004)* completed slant shear and pull-off tests with five varying interface preparations and five cylinder specimens per type of preparation. Sizes of the cylinders for the slant shear test and pull-off test were 7.9 in. x 7.9 in. x

15.75 in. (0.2 m x 0.2 m x 0.4 m) and 7.9 in. x 7.9 in. x 7.9 in. (0.2 m x 0.2 m x 0.2 m), respectively. The interface on the slant shear specimens was 30 degrees to the vertical. The authors found that the surfaces that had the substrate surface sand-blasted had the highest values of cohesion. This method showed stronger cohesion than the partially chipped and wire-brushed interfaces that the authors tested. The authors also noted from previous tests that increasing the concrete strength increases the bond strength of the interface. Cohesion is dependent on concrete strength and surface preparation. Another consideration for shear resistance, in addition to cohesion, is the concrete-steel bond, bar development, or bond resistance.

Menzel *(Menzel 1939)* defined concrete-steel bond or bond resistance as the resistance of an embedded reinforcing bar to relative motion under stress. This bond resistance is important to ensure reinforcing bars efficiently interact with the concrete to form a composite unit. An efficient bond would theoretically reduce the length of the reinforcing bar that could strain within the interface, thus increasing the stiffness of the reinforcement. The increased stiffness would help ensure aggregate interlock by increasing the clamping force per unit displacement. The authors completed tests on single bars embedded in a concrete prism. All bars were 1 in. (25 mm) diameter round bars or square bars free from mill scale and rust. Plain bars with no deformations or ribs, such as cold rolled and polished steel, were tested with bars with deformations that were designed to improve the bond length. The authors noted that for the cold rolled polished bar, the specimens that had an as-received, unmodified surface had considerably less bond strength than the sand-blasted, cold-rolled polished bars. It was also noted that the reinforcing bar deformations significantly increase the bond resistance, even though reinforcing bars without deformations do exhibit some bond resistance. The authors concluded that bond resistance is greatly increased by reinforcing bar surface preparation and the presence of deformations.

Santos and Júlio *(Santos and Júlio 2012)* provided a detailed review on shear-friction research, recommendations, and code development. See Santos and Júlio *(Santos and Júlio 2012)* for an in-depth analysis. A general review is provided here. The authors found that the shear resistance is due to: (i) cohesion; (ii) friction; and (ii) dowel action. The authors also noted that dowel action shear resistance is usually “disguised” in the data as either cohesion or friction. Figure 2.9 shows the general behavior of dowel action and the theoretical contribution to the shear strength of the interface for each dowel mode of flexure, shear, and kinking. General parameter curves compiled from Santos and Júlio *(Santos and Júlio 2012)* are shown in Figure 2.10. This figure graphically shows the shear strength as a function of reinforcement parameter design curves from many works. In general, there is a strong linear relation between the shear strength and reinforcement parameter, which is the reinforcement ratio, ρ, multiplied by the yield stress, f_y. However, many parameter curves have a limit to this relation, as seen in the Santos and Júlio *(Santos and Júlio 2012)* curve in Figure 2.10.

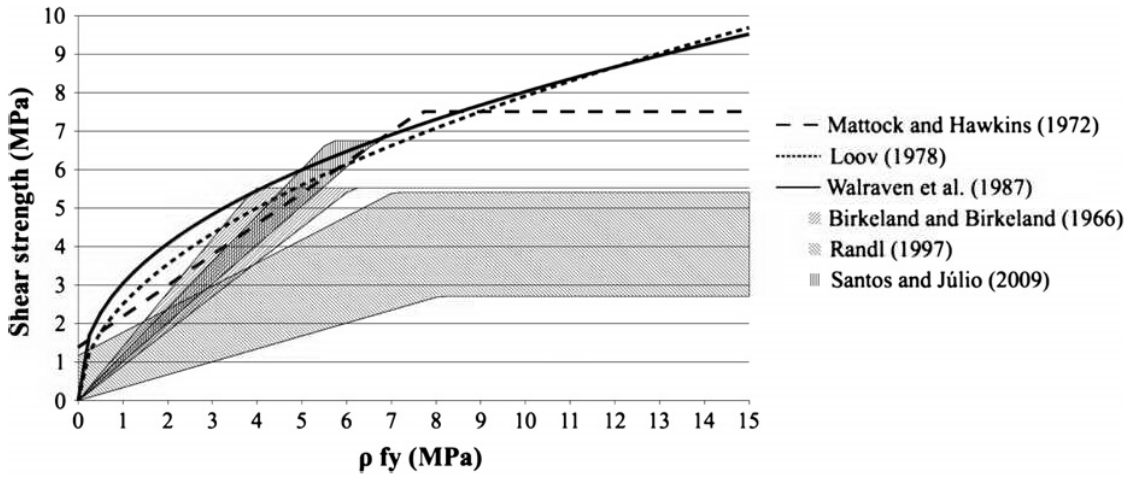

Figure 2.10: Comparison of design expressions *(Santos and Júlio 2012)* (1 ksi = 6.89 MPa)

2.2 RESEARCH WITH PUSH-OFF TEST SPECIMENS

This section reviews the literature concerning interface shear tests conducted with push-off test specimens. Table 2.1 shows the basic parameters of each reference in chronological order. The shear planes for the tested specimens were perpendicular and parallel to the ground for vertical and horizontal load directions, respectively. See the following reviews for additional information about the test and general observations.

Hofbeck et al. *(Hofbeck et al. 1969)* tested specimens with and without pre-existing cracks along the shear plane. This was done to find the effect of the concrete-concrete cohesion as it related to aggregate interlock. Cracked specimens were cracked with an applied line load to the side of the specimens along the shear interface. After testing, the authors reported that imposed cracks along the interface increased the slip at all stages of loading and decreased the ultimate shear strength. However, the reduction in ultimate shear strength from the uncracked specimens to the pre-cracked specimens was less at higher reinforcement parameters. Also, for the higher strength reinforcing bars in the pre-cracked specimens, the ultimate shear strength was consistently higher, except at relatively high reinforcement parameters. The authors noted that overall, shear-friction theory provides a reasonable and conservative estimate of shear transfer strength for the parameters listed in the study assuming that the $\tan \phi = 1.4$, according to Equation 2-1.

Mattock et al. *(Mattock et al. 1976)* conducted research on push-off test specimens using lightweight aggregate to determine its effect on the aggregate interlock. The aggregates included in the test program were naturally occurring gravel and sand, rounded lightweight aggregate, crushed angular lightweight aggregate, and a sanded lightweight aggregate. For the sanded lightweight aggregate, most of the lightweight sand particles were replaced by normal weight sand. Cracked and uncracked specimens were tested. Maximum aggregate sizes varied from 3/8 in. (9.5 mm) to 1/2 in. (12.7 mm). Diagonal tension cracks formed between 400 psi and 700 psi (2.7 MPa and 4.8 MPa) shear stress resistance over the interface. Results showed that an increase in the reinforcement parameter increased the ultimate shear stress. The authors noted that a crack along the interface reduced the ultimate strength for a given reinforcement parameter by a nearly constant amount. Diagonal tension cracks along the interface for the uncracked specimens were

inclined 20 degrees to 45 degrees to the shear plane. No diagonal tension cracks occurred in the initially cracked specimens. The results showed that the shear transfer strength for concrete specimens with lightweight aggregate is less than the shear transfer strength at concrete containing normal weight gravel aggregate and sand concrete mixtures.

Kahn and Mitchell *(Kahn and Mitchell 2002)* evaluated the performance of regular-and high-strength concretes to determine shear friction behavior. The authors noted that for all tests, the failure crack went through the aggregate rather than the interface. This is atypical because for shear tests with normal strength concrete, the binder between the coarse aggregate typically fails first. The authors recommended an upper limit of shear stress of 20% of the concrete strength for strengths up to 18 ksi (124.1 MPa). The authors also recommended that the yield stress in the transverse reinforcement not be taken more than 60 ksi (420 MPa) for high strength concrete. This is to limit the slip along the smooth cracks. Also, limiting the yield stress provides a uniform friction coefficient for both normal-and high-strength concretes. Note that even though all reinforcement tested was Grade 60 (420 MPa) steel, the yield strengths that were measured from testing were 69.5 ksi (479.2 MPa) and 83.0 ksi (572.3 MPa). When the authors used f_y = 60 ksi (420 MPa) for their friction calculations instead of the actual steel yield values, the results had less variance.

Wallenfelsz *(Wallenfelsz 2006)* and Scholz *(Scholz 2007)* corresponded on the same research. The Wallenfelsz *(Wallenfelsz 2006)* paper is a thesis on the push-off test specimen portion of the study and provides more detail on the push-off test than the Scholz *(Scholz 2007)* paper. Headed studs and reinforcing bars were tested in this research in a girder-haunch-deck system. Interfaces were grouted with a shear pocket and tested horizontally on roller supports. A vertical ram was used to simulate dead load on the interface. The authors noted that the peak shear load occurred around the same time a crack was visible on the interface. The test was taken to a displacement of 1.5 in. (38 mm) before it was ended. Typical load behavior includes a peak load after a linear load relation, followed by a drop of load before a consistent sustained load, as seen in Figure 2.11. Also seen in Figure 2.11, is that the ratio of the theoretical steel contribution and concrete contribution make a large difference in the behavior of the push-off test. A higher steel ratio ensures a higher and more consistent post-peak sustained shear resistance.

Scholz et al. *(Scholz et al. 2007)* tested girder-haunch-deck system interfaces to better understand the shear friction. The surface of the interface was roughened with a rake. Tests were conducted with a simulated dead load. The authors performed a total of 13 series with two tests in each series. Nine of the series evaluated specimens with reinforcing bars across the interface, one series had no reinforcement, and the remaining series contained headed studs across the interface. Various grout types for the haunch were tested. Slant cylinder tests with similar surface treatments were conducted to verify the bond strength for each grout type. These tests specimens contained no reinforcing bars. The authors also noted that the grout cohesion was a controlling characteristic of the shear strength for specimens containing grout. The authors noted that there was only a small increase in the measured shear stress at peak load from the #4 (#13M) to #5 (#16M) bar specimens. However, the specimens with the #5 (#16M) bar held a higher post-crack load as illustrated in Figure 2.12.

Table 2.1: Reference parameters for push-off test specimens

Reference	Load direction V=Vert. H=Horiz.	Specimen size	Number of specimens	Bar Size(s)	Steel ratios, ρ, %	Yield Stress, fy, ksi (MPa)	Concrete Strength, f'c, ksi (MPa)
Hofbeck et al.*(Hofbeck et al. 1969)*	V	21.5 in. x 10 in. x 5 in. (546 mm x 254 mm x 127 mm)	38	1/8 in. (3.2 mm),#2 (6.4 mm), #3 (#10M), #4 (#13M), #5 (#16M)	0.00% -2.64%	48.0-66.1 (331-456)	4 (27.6)
Mattock et al. *(Mattock et al. 1976)*	V	22 in. x 12 in. x 12 in. (559 mm x 305 mm x 305 mm)	62	#3 (#10M)	0.00%-3.79%	47.7-53.6 (328.9-369.6)	2.5 (17.2), 6.0 (41.4)
Kahn and Mitchell *(Kahn and Mitchell 2002)*	V	24 in. x 12 in. x 10 in. (610 mm x 305 mm x 254 mm)	50	#3 (#10M)	0.37%-1.47%	69.5 (479.2), 83.0 (572.3)	6.8 (46.7), 17.9 (123.4)
Scholz et al. *(Scholz et al. 2007)/*Wallenfelsz *(Wallenfelsz 2006)*	H	48 in. x 18 in. x 16 in. (1219 mm x 457 mm x 406 mm)	26	#4 (#13M), #5 (#16M)	0.10%, 0.16%	73 (503.3)	4.3-6.0 (23.6-41.4)
Mansur et al. *(Mansur et al. 2008)*	V	29.5 in. x 15.75 in. x 5.9 in. (750 mm x 400 mm x 150 mm)	19	0.315 in. (8 mm), #3 (#10M)	0.45%-2.67%	43.5 (300)	10.6 (73), 12.3 (85), 13.8 (95), 15.4 (106)
Scott *(Scott 2010)*	H	50 in. x 18 in. x 16 in. (1270 mm x 457 mm x 406 mm)	36	#4 (#13M), #5 (#16M), #6 (#19M)	0.00%, 0.10%, 0.5%, 1.2%	60 (410)*	5.7-6.2 (39.3-42.7)
Trejo and Kim *(Trejo and Kim 2011)*	H	48 in. x 18 in. x 16 in. x (1219 mm x 457 mm x 406 mm)	8	#4 (#13M), #5 (#16M)	0.10%	62 (428)	5.9-7.5 (40.7-51.7)
Zeno *(Zeno 2009)*	V	44 in. x 24 in. x 10 in. (1118 mm x 610 mm x 254 mm)	8	#3 (#10M), #4 (#13M)	0.41%, 0.75%	61.5 (424.0)-140.0 (965.3)	5 (34.5)

*Actual yield stress unknown. Nominal yield stress stated.

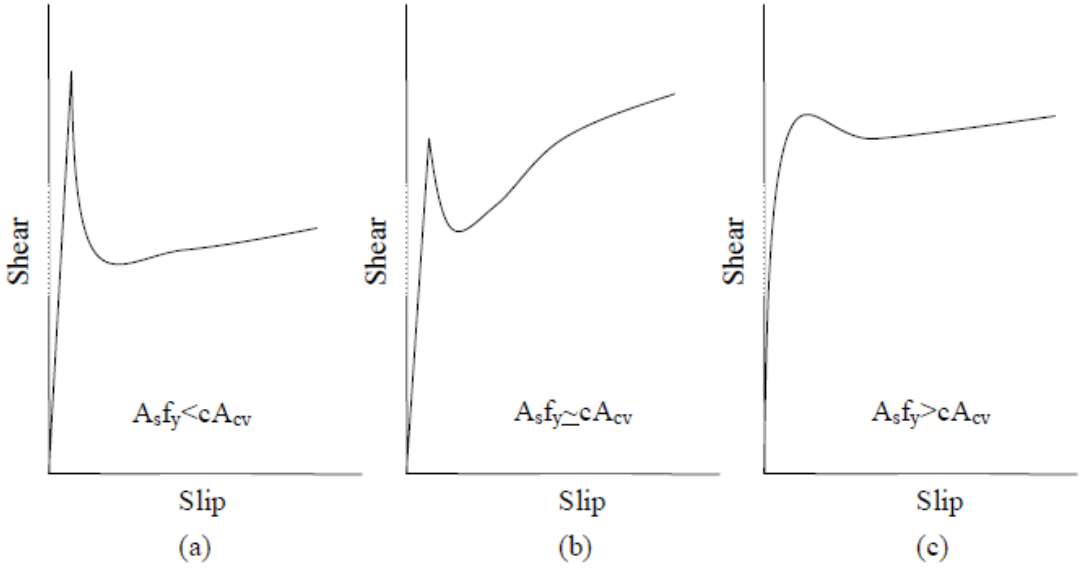

Figure 2.11: Typical Load vs. Slip Plots (Wallenfelsz 2006)

Strain gauges were installed in the haunch. The authors noted that increased cross-sectional area of the connectors increased the strain at peak load. The authors reasoned that if the contribution to the shear resistance from the cohesion is greater than the contribution from the reinforcing bars, then the reinforcing bars will yield by the peak load. If not, then yielding happens sometime after the peak load when the concrete-concrete bond has fractured. For the specimens tested, the authors reported that the bond fractured after a slip in the range of 0.15 in. (3.8 mm) to 0.30 in. (7.6 mm). The authors stated that the AASHTO (2004) equation is flawed in that a friction coefficient is not applicable until a crack is formed, which always occurs beyond the peak load. The authors recommended splitting the components so that the nominal shear capacity is the maximum of the concrete contribution and the steel reinforcement contribution.

Mansur et al. (2008) tested pre-cracked push-off specimens. The researchers investigated the effect of the reinforcement parameter and the strength of concrete on the aggregate interlock. Specimens were cracked with a pair of steel wedges across the interface before the shear capacity test was conducted. To better visualize the test behavior, the researchers split the behavior into three branches: (i) a initial linear response; (ii) a nonlinear response; and (iii) the residual shear strength. The researchers reported that the stiffness of the nonlinear response increased with an increase in concrete strength. In addition, a higher reinforcement parameter produced an increase in peak shear strength and interface slip at the ultimate shear strength. The researchers noted that it is important to balance the concrete strength and reinforcement parameter to efficiently design higher shear resistance values.

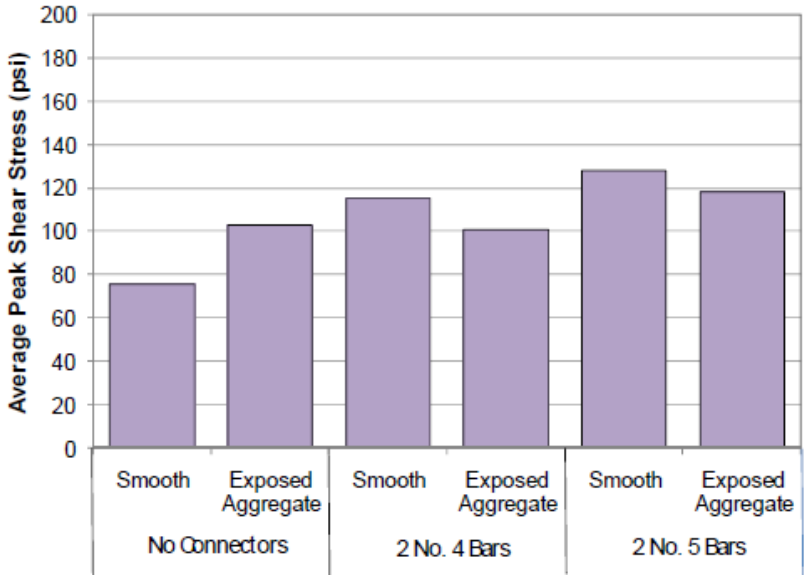

Figure 2.12: Average shear stress at peak load (Scholz et al. 2007) (1 ksi = 6.89 MPa)

Scott *(Scott 2010)* investigated the interaction of lightweight concrete with normal-weight concrete in shear friction applications. There were three test specimen configurations: (i) a normal weight concrete girder with a lightweight concrete deck; (ii) a lightweight concrete girder with a lightweight concrete deck; and (iii) a normal-weight concrete girder with a normal-weight concrete deck. The researcher placed strain gauges on both sides of each reinforcing bar. This allowed the measured strain to be adjusted to remove any potential reinforcing bar bending moment effect on the strain. The unreinforced specimens exhibited similar bond failure loads. However, the lightweight concrete girder and deck had a fracture plane that deviated from the interface plane. The authors noted that an increase in reinforcement area led to a decrease in the strain of the shear reinforcement right before or right after cracking at the interface. This serves as evidence that additional area of the reinforcing bars ensure adequate clamping force for aggregate interlock, but do not prevent bond failure.

Trejo and Kim *(Trejo and Kim 2011)* conducted tests with cold-joint (aka construction joints) connections with grouted interfaces in an eight-series push-off test with varying parameters. The purpose of the tests was to determine the effect of shear friction with grouted interfaces. Six (6) of the eight (8) series completed were for shear connector/coupler connections and two were for reinforcing bar connections. The authors used a superimposed dead load, or clamping force. From their test results, the authors noted five stages of a typical failure mode, as seen in Figure 2.13: (i) adhesion loss, where interface slips at constant load, V_{loss}; (ii) engagement of shear key components; (iii) peak load shear key failure, V_{peak}; (iv) dowel action of connectors or beginning of sustained load; and (v) system failure.

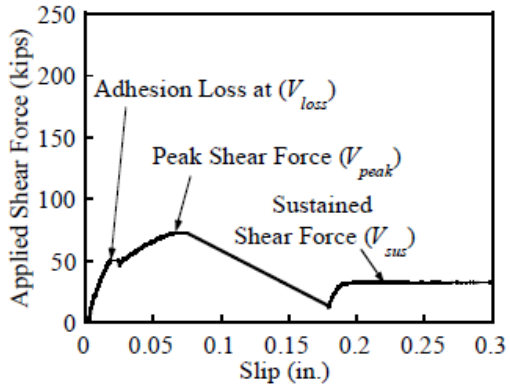

Figure 2.13: Typical failure mode and the plot of the system (Trejo and Kim 2011)

It was reasoned that kinking, as shown in Figure 2.9, was the primary dowel action mode of the reinforcing bars and these contributed to most of the sustained load. Shear slip reached approximately 0.05 in. (1.3 mm) when the installed strain gauges read that the clamping force of the reinforcing bar roughly corresponded to the yield stress.

Shear interface behavior with high-strength steel, or steel with a yield stress greater than 60 ksi (420 MPa) for shear friction applications was investigated by Harries et al. *(Harries et al. 2012)* and Zeno *(Zeno 2009)*. The experimental study consisted of push-off test specimens that simulated the connection between an AASHTO *(AASHTO 2012)* girder and a slab. Zeno *(Zeno 2009)* tested specimens that included 60 ksi (420 MPa) and 100 ksi (690 MPa) steel. The interface was prepared with a 1/4 in. (6.4 mm) amplitude roughness and was cleared of laitance before casting the second layer following the recommendation of AASHTO *(AASHTO 2007)* 5.8.4.3. The objective of the experiment was to compare the performance of the horizontal shear capacity for specimens containing ASTM A615 and ASTM A1035 reinforcing bars. The experimental setup included a compression machine that applied a monotonically increasing load across the interface. The load was applied in alignment with the shear interface. Test results showed that three of the four ASTM A615 (Grade 60) specimens reached the calculated AASHTO *(AASHTO 2007)* design values and none of the four ASTM A1035 specimens reached the design values when taking the steel design stress as 100 ksi (690 MPa). However, the ASTM A1035 steel did reach the design value if the steel design stress was limited to 60 ksi (420 MPa), as specified by AASHTO *(AASHTO 2007)*.

Figure 2.14 shows the results and Figure 2.15 shows the linearized average results for the four #3 (#10M) and four #4 (#13M) bars of the ASTM A615 and ASTM A1035 steel specimens. There are four curves shown for the combination of A615 Grade 60 ksi (420 MPa) reinforcement steel with #3 (#10M) bars (P-615-3 A/B) and A615 Grade 60 #4 (#13M) bars (P-615-4 A/B). In addition, there are four curves shown for the A1035 Grade 100 (690 MPa) reinforcement steel with #3 (#10M) bars (P-1035-3 A/B) and #4 (#13M) bars (P-1035-4 A/B). Figure 2.15 and Figure 2.15 show that the peak loads (at the end of stage 2) are higher for the larger bars as there is more area of reinforcing bar through the interface. The authors stated that the drop in the load was more pronounced for the ASTM A1035 steel. In addition, the sustained loads are larger with the higher grade, ASTM A1035 steel.

The study reported three phases of load-deflection as shown in Figure 2.14 and Figure 2.15:

The first stage begins at the start of the test and lasts until the concrete begins to crack. It is recognizable by its linear-elastic load-deflection relationship and low steel strain in the interface reinforcing bars.

The second stage follows the initial cracking and ends at the ultimate shear load. It is characterized by a softer response as the concrete begins to crack. The linearization in Figure 2.15 does not show the curvature in the load-deflection relationship as the concrete cracks, though it does demonstrate the overall softening of the resisting elements until peak load.

The last stage, the post ultimate load stage, is the stage where the shear interface is fully cracked, which is characterized by a sustained load that was, for this study, less than the ultimate load.

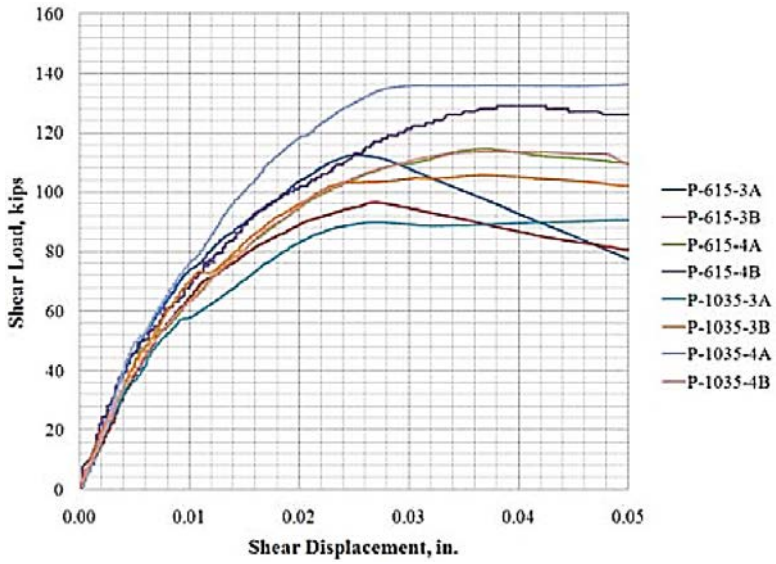

Figure 2.14: Shear load versus shear displacement showing the described stages of the shear friction mechanism *(Zeno 2009)*

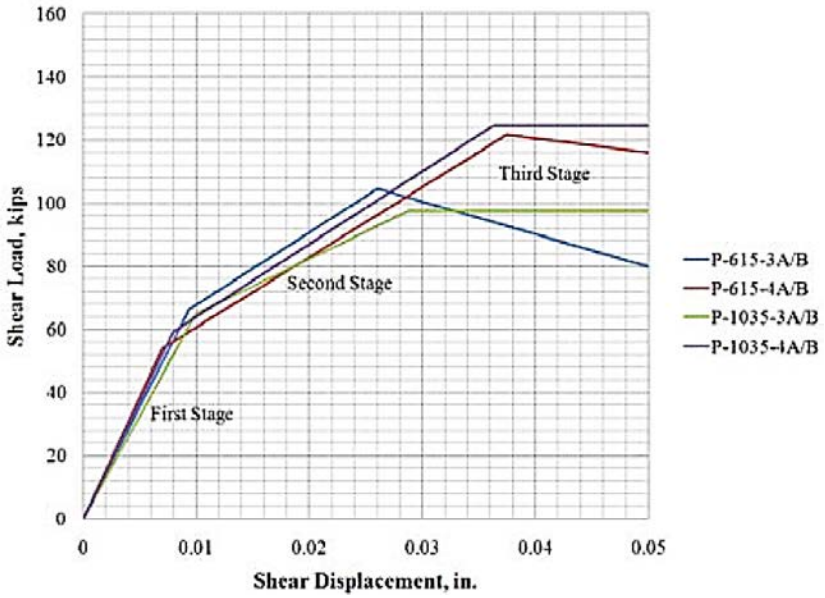

Figure 2.15: Linearization of shear load versus shear displacement showing the described stages of the shear friction mechanism *(Zeno 2009)*

Strain gauges were installed in the reinforcing bars 3 in. (76 mm) above the interface to ensure the instruments would not be damaged due to concrete fracturing at the interface. The strain for all of the specimens was taken throughout the test. Figure 2.16 shows the strain measurements versus the shear load and Figure 2.17 shows the linearization. The results indicated that the bars never yielded before reaching the peak shear loads and that stresses in the reinforcing steel are negligible until the cracking load (until the beginning of Stage 2).

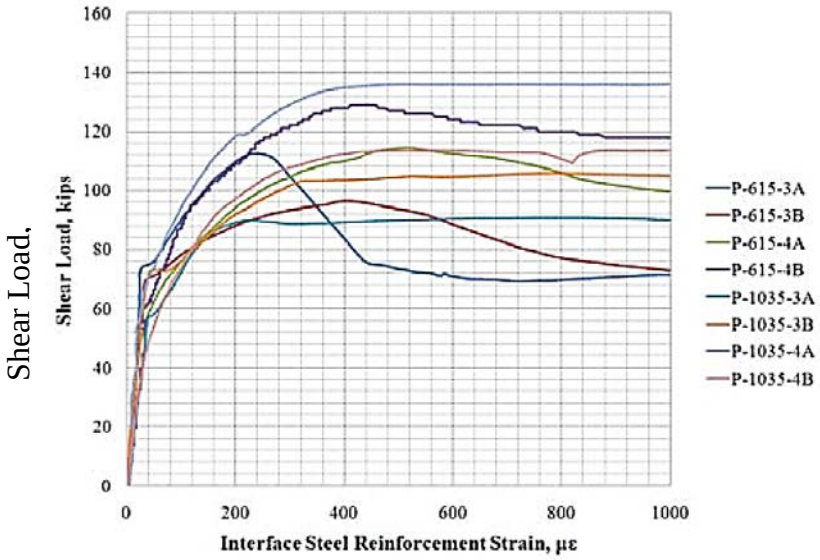

Figure 2.16: Shear load versus average interface steel strain showing described stages of the shear friction mechanism *(Zeno 2009)*

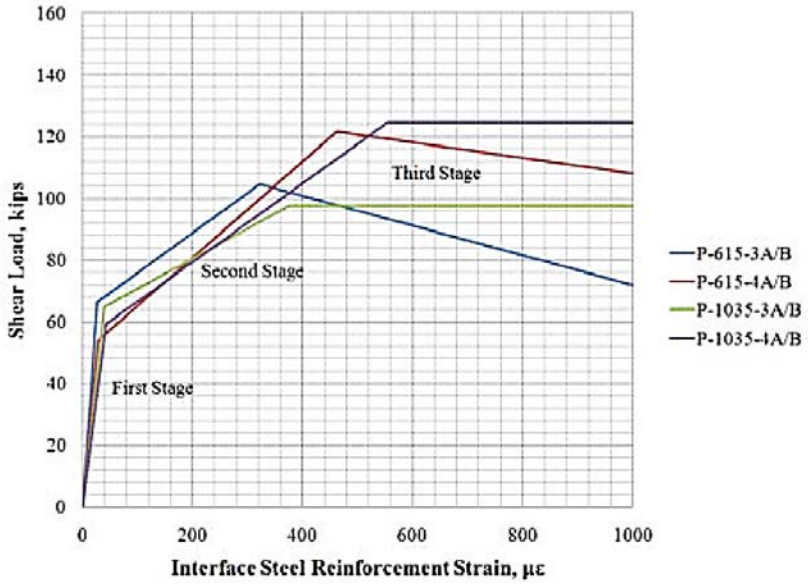

Figure 2.17: Linearization of shear load versus average interface steel strain showing described stages of the shear friction mechanism *(Zeno 2009)*

Figure 2.16 and Figure 2.17 also show that the stiffness of the interface is a function of the bar size during the first stage of loading. Adding stiffness to the interface system by using more reinforcing bar area results in the peak load being higher. This is because it makes the response from the crack width stiffer, ensuring better aggregate interlock before the concrete-concrete cohesion fails. The authors noted that the strain of the steel corresponding to approximately 60 ksi (420 MPa) works for predicting the shear resistance of the interface. However, raising the yield stress of the steel is not beneficial as the steel is only strained to a stress of about 60 ksi (420 MPa). If the higher grade steel had an increased modulus of elasticity or stiffness, then increased peak load would be anticipated due to greater clamping force per unit of crack width. However, this assumes that the aggregate would not fracture. As the modulus of elasticity for all steel is approximately 29,000 ksi (200 GPa), it is not economical to increase the stiffness because another, potentially more expensive, material would need to be used. The results from Zeno *(Zeno 2009)* indicate that increasing the yield strength does enable the sustained load to be higher. However, the strains obtained 3 in. (76 mm) from the interface were well below the approximately 2000 microstrain yield threshold of Grade 60 (420) steel. ASTM A615 steel reinforcement strain values were less than the ASTM A1035 steel reinforcement strain values for bars of the same size and geometric configuration. Zeno *(Zeno 2009)* attributed this behavior to potential enhanced bonding characteristics of the ASTM A1035 steel.

In summary, the specimens with reinforcing steel meeting ASTM A1035 Grade 100 specifications across the interface did not reach the calculated AASHTO *(AASHTO 2007)* design values when taking the steel design stress as 100 ksi (690 MPa). However, these specimens did reach the design value if the steel design stress was limited to 60 ksi (420 MPa), as specified by AASHTO *(AASHTO 2007).* The results indicated that the measured strain of the reinforcing bar across the interface did not reach a strain corresponding to a yield stress of 60 ksi (420 MPa) before reaching the peak load. This is why increasing the yield stress of the reinforcing steel across the interface did not increase the peak load. However, increasing the area of reinforcing

bar across the interface did increase the peak load. This is because an increase in reinforcing steel area across the interface stiffens the interface system, which ensures aggregate interlock.

2.3 RESEARCH WITH FULL-SCALE COMPOSITE BEAM SPECIMENS

This section reviews research from full-scale composite beam tests. Table 2.2 shows the main references reviewed and the basic parameters of each reference in chronological order. See the following reviews for additional information about the tests and corresponding general observations from each test.

Seamann and Washa *(Seamann and Washa 1964)* tested specimens to determine the shear friction behavior of full composite beams. The interface roughness varied for the tests and the maximum aggregate size was 3/4 in. (190 mm). The authors noted that as the top slab began to slip, the beam acted partially composite, becoming less composite as it continued to displace. The authors also briefly discussed the effect on the peak shear strength of the neutral axis location relative to the position of the slab. The authors stated that there was an increase in shear strength with beams that had a neutral axis below the slab when compared with the shear-strength of beams with the neutral axis above the slab. However, the slabs tested were twice as thick as the other slabs and therefore had a greater clamping force from self-weight. This may have had a larger effect on the peak shear strength than the location of the neutral axis, though it is difficult to determine. It was reported that the ultimate shear strength increased with higher concrete strengths.

Loov and Patnaik *(Loov and Patnaik 1994)* tested how beam flange length, reinforcement parameter, and beam cross section shape affected shear friction behavior. Beams were simply supported with the load at centerspan. The surface of the beam was roughened to 0.25 in. (6.4 mm) amplitude. Flexural cracks from the beam propagated into the interface, where the cracks converged to a single crack that extended the length of the interface. The authors estimated from the literature that the reinforcing bars would yield at a slip of 0.02 in. (0.5 mm). However, larger slips were observed before reinforcing bar yield. The authors recommended an equation for shear resistance based off the test results. The authors stated that the equation represented both full-scale and push-off test specimen results from the literature far better than previous shear-friction equations.

Patnaik *(Patnaik 2001)* studied the behavior of shear friction behavior on smooth concrete interfaces. The authors tested 18 rectangular-shaped section beams and six T-shaped section beams. Concrete strength and depth of the tensile reinforcing steel divided by the spacing of the horizontal shear reinforcing steel (d/s), had no significant influence on the shear strength. However, clamping stress had a significant, linear relationship to shear strength. The authors noted that the beams were able to develop flexural capacity while assuming a completely composite (monolithic) section, despite slight slipping. In addition, many of the beams had reinforcing stirrups that exceeded 93 ksi (641 MPa) yield strength. All of the results from the higher yield stress specimens fit well with the other specimens in a linear plot of shear strength versus the clamping stress.

Kahn and Slapkus *(Kahn and Slapkus 2004)* tested high strength concrete composite T-beams to gain more perspective on shear friction with varying concrete strengths and reinforcement parameters. The beams were intended to duplicate the beams tested by Loov and Patniak *(Loov and Patnaik 1994)*. Maximum aggregate size ranged from 3/4 in. (19.0 mm) to 3/8 in. (9.5 mm). The authors considered flange failure when the interface cracked and slip occurred between the flange and the interface. The load decreased while the deflection increased after the interface slip exceeded 0.01 in. (0.25 mm). The shear strength recorded exceeded twice the load anticipated with the AASHTO *(AASHTO 1998)* and ACI *(ACI 2002)* equations. It was noted that the concrete strength and clamping stress contribute to the overall shear strength and that both AASHTO *(AASHTO 1998)* and ACI *(ACI 2002)* equations were conservative for concrete compressive strengths as high as 11 ksi (75.8 MPa). No strain gauges were installed in the reinforcing bars so it is unknown if the bars provided the full theoretical clamping force.

Table 2.2: Reference parameters for the full scale composite beam specimens

Reference	Specimen size	Number of specimens	Bar Size	Reinforcement ratio, ρ, %	Yield Stress, f_y, ksi (MPa)	Concrete Quality, f'c, ksi (MPa)
Seamann and Washa *(Seamann and Washa 1964)*	96 in., 144 in., 240 in. x 17 in. x 15 in. (2438 mm, 3658 mm, 6096 mm x 432 mm x 381 mm)	42	#3 (#10M), #4 (#13M)	0.00-1.07%	42.6 (293.7), 53.7 (370.2)	3 (20.7), 4.5 (31.0), 5.5 (37.9)
Loov and Patnaik *(Loov and Patnaik 1994)*	118.1 in. x 15.75 in. x 13.78 in. (3 m x 0.4 m x 0.35 m)	16	#3 (#10M)	0.10-1.89%	59.0-63.5 (407-438)	2.8-7.5 (19.3-51.7)
Patnaik *(Patnaik 2001)*	Rectangular Beams: 106.3 in. x 13.78 in. 9.84 in. (2.7m x 0.35m x 0.25m) T-Section Beams: 126.0 in. x 13.78 in. x 15.75 in. (3.2m x 0.350m x 0.4m)	18	0.22 in. (5.6 mm), 0.25 in. (6.4 mm), 0.34 in. (8.7 mm), 0.35 in. (8.9 mm), 0.56 in. (14.1 mm)	0.05-1.05%	49.3-102.1 (339.9-704.0)	2.5-5.0 (17-34.8)
Kahn and Slapkus *(Kan and Slapkus 2004)*	120 in. x 16.5 in. x 15.5 in. (3048 mm x 419 mm x 394 mm)	6	#3 (10M)	0.19-0.37%	80.7 (556)	7.3 (50.3), 11.3 (77.9)
Kovach *(Kovach 2008)*	130 in. x 12 in. x 11.5 in. (3302 mm x 305 mm x 292 mm)	35	N/A	0.00%	N/A	3 (20.7), 6 (41.4)

Kovach *(Kovach 2008)* questioned the accuracy of push-off tests. The author noted that because the shear loads from such tests could produce eccentricities across the interface or may cause areas of high stress concentration, the test may not be valid. High stress concentrations result in non-conservative estimates of the horizontal shear capacity. The authors stated that the accuracy of push-off tests is not certain and highly recommended evaluating composite interfaces as part of a beam section. The author tested, in two phases, prestressed/precast T-beams with varying surface finishes. This was to determine the cohesion properties of the connection without reinforcing bars. The surface finishes tested included: (i) as-placed; (ii) broom finish; (iii) ¼ in. (6.4 mm) rake finish; and (iv) sheepsfoot finish. A sheepsfoot finish included circular indents like a sheepsfoot to roughen the surface. The beams were tested with 5-point and 3-point load configurations. The author reported that the horizontal shear capacity for unreinforced interfaces was considerably higher than the code estimate for AASHTO *(AASHTO 2007)*, which utilizes the same equation as AASHTO *(AASHTO 2012)*. The author noted that the surface roughness had a considerable effect on the shear capacity.

2.4 CODE REVIEW

This section discusses the relevant codes for determining horizontal interface shear capacity. The specifications from the American Association of State Highway and Transportation Officials (AASHTO), State Highway Agencies, and American Concrete Institute (ACI) are discussed.

2.4.1 American Association of State Highway and Transportation Officials (AASHTO) Design

AASHTO *(AASHO 2012)* is similar to the Birkeland and Birkeland *(Birkeland and Birkeland 1966)* analogy in that it assumes that concrete cohesion and clamping force contribute to the interface shear resistance. However, the AASHTO *(AASHTO 2012)* equation splits these two components into separate parameters, as shown in Equation 2.2. The equations in AASHTO *(AASHTO 2012)* Section 5.8.4.1 are shown below as Equation 2.2 through Equation 2.6. The equations quantify the horizontal shear strength, V_{ni} (kip [kN]).

$$\mathbf{V_{ni} = cA_{cv} + \mu\,(A_{vf}f_y + P_c)} \qquad \mathbf{(2.2)}$$

where

$$\mathbf{A_{cv} = b_{vi}L_{vi}} \qquad \mathbf{(2.3)}$$

c = cohesion factor specified in Article 5.8.4.3 (ksi [MPa]);
Acv = area of concrete considered to be engaged in interface shear transfer (in.^{2} [mm2]);
μ = friction factor specified in Article 5.8.4.3;
Avf = area of interface reinforcement crossing the shear plane (in.^{2} [mm2]);
fy = yield stress of reinforcement but design value not to exceed 60 ksi (420 MPa);
Pc = permanent net compressive force normal to the shear plane; if force is tensile, Pc is taken equal to 0.0 (kip [kN]);
bvi = interface width considered to be engaged in shear transfer (in. [mm]);
Lvi = interface length considered to be engaged in shear transfer (in. [mm]).

AASHTO (AASHTO 2012) notes that shear resistances using higher yield reinforcing bar stress, f_y, values have overestimated the capacity for pre-cracked specimens. The code also states that limited testing has been performed. Equation 2.2 is the general shear equation and adds the contribution from concrete-concrete cohesion (cA_v) with aggregate interlock $\mu(A_{vf}f_y+P_c)$, which is the clamping force times a friction factor, μ, empirically determined from testing. Equation 2.4 limits the nominal interface shear capacity to values empirically determined from testing as the fraction of concrete available to resist interface shear, which is a function of the design concrete compressive strength, f'_c. The horizontal shear strength, V_{ni}, must be less than the factor, K_1, multiplied by the strength and area of the concrete:

$$\mathbf{V_{ni} < K_1 f'_c A_{cv}} \qquad \textbf{(2-4)}$$

where

K_1 = fraction of concrete available to resist interface shear, as specified in AASHTO *(AASHTO 2012)* Article 5.8.4.3;
f'_c = *specified 28-day compressive strength of the weaker concrete on either side of the interface (ksi [MPa]).*

Equation 2.5 is another empirical limitation on the interface shear, which limits the horizontal shear strength, V_{ni}, the shear interface stress and is similar to the limitations shown for each analogy in Figure 2.1 through 2.3.

$$\mathbf{V_{ni} < K_2 A_{cv}} \qquad \textbf{(2.5)}$$

where

K_2 = limiting interface shear resistance specified in AASHTO *(AASHTO 2012)* Article 5.8.4.3 (ksi [MPa]).

Factors for Equation 2.2 through Equation 2.5 are listed in AASHTO *(AASHTO 2012)* Section 5.8.4.3 and factors used in Chapter 5 of this paper for calculating the ultimate shear strengths from AASHTO *(AASHTO 2012)* Section 5.8.4.3 are listed below. For a cast-in-place concrete slab on clean concrete girder surfaces, free of laitance with surface roughened to an amplitude of 0.25 in. (6.4 mm), AASHTO *(AASHTO 2012)* recommends the following:

c = 0.28 ksi (1.93 MPa);
μ = 1.0;
K_1 = 0.3;
K_2 = 1.8 ksi (12.4 MPa) for normal-weight concrete;
= 1.3 ksi (9.0 MPa) for lightweight concrete.

In addition to the interface cohesion and friction factors, AASHTO *(AASHTO 2012)* Section 5.8.4.4 enacts a minimum steel area of 5% of the concrete shear interface area divided by the yield strength of the reinforcing steel across the interface, f_y. The minimum steel area equation is shown in Equation 2.6:

$$\mathbf{A_{vf} \geq \frac{0.05A_{cv}}{f_y}} \qquad \textbf{(2-6)}$$

where A_{vf} is governed by applicable code restrictions.

The minimum interface shear reinforcement, A_{vf}, need not exceed the lesser of the amount determined using Equation 2.6 and the amount needed to resist $1.33V_{ui}/\phi$ as determined using Equation 2.2. This is intended as an overstrength factor as the minimum is waived or lowered if the shear resistance without reinforcing steel exceeds $1.33V_{ui}/\phi$. In addition, the minimum reinforcement provisions specified shall be waived for girder/slab interfaces with surface roughened to an amplitude of 0.25 in. (6.4 mm) where the factored interface shear stress, v_{ui} of AASHTO *(AASHTO 2012)* 5.8.4.2-1 is extended across the interface and adequately anchored in the slab.

wherein this case, the variables are:

V_{ui} = the factored horizontal shear force;
ϕ = resistance factor (AASHTO (2012) section 5.5.4.2.1).

2.4.2 American Concrete Institute (ACI) Design

The American Concrete Institute (ACI) 318-11 standard and commentary section 17 specifies the horizontal shear capacity. The capacity is to be taken as a concrete-concrete cohesion factor of 260 psi (1.79 MPa). This is added to the reinforcement parameter from the literature times a factor of 0.6. It is all multiplied by the width of the interface to determine the nominal horizontal shear strength, V_{nh} (kip [kN]), as shown below *(ACI 2011)*:

$$\mathbf{V_{nh} = (260 + 0.6\rho_v f_y)\,\lambda\, b_v\, d} \qquad \textbf{(2.7)}$$

where

ρ_v = reinforcement ratio (in.^{2}/in.^{2} [mm^2/mm^2]);
f_y = yield stress of steel (psi [MPa]);
λ = value from 11.6.4.3;
b_v = width of shear interface (in. [mm]);
d = distance from the top face of the beam to the centroid of the tensile longitudinal reinforcement (in. [mm]);

Note that ACI *(ACI 2011)* does not limit the yield stress of steel in the reinforcing. However, it does limit the interface shear stress, as shown in Equation 2.8 and Equation 2.9. ACI *(ACI 2011)* states that if the interface shear stress parameter is exceeded, that the design of horizontal shear shall be in accordance to ACI *(ACI 2011)* Section 11.6.4. This section does limit the yield stress of the reinforcing steel to 60 ksi (420 MPa) and the combined contribution of the concrete and steel to less than 500 psi (3.45 MPa) as shown in Equation 2.8:

$$\mathbf{V_{nh} < 500 b_v d} \qquad \textbf{(2.8)}$$

where the contact surfaces are clean, free of laitance, and intentionally roughened, V_{nh} shall not be taken more than 80 psi (0.55 MPa) as shown in Equation 2.9:

$$\mathbf{V_{nh} < 80 b_v d} \qquad \mathbf{(2.9)}$$

If ultimate design shear values exceed the maximum factored V_{nh} values, then horizontal shear is in accordance with section 11.6.4 which states that where shear-friction reinforcement is perpendicular to the shear plane, V_n, shall be computed as follows:

$$\mathbf{V_n = A_{vf} f_y \mu} \qquad \mathbf{(2.10)}$$

where A_{vf}, f_y, and μ have already been defined.

For this case, μ is 1.4 λ for concrete placed monolithically, 1.0 λ for concrete placed against hardened concrete with surface intentionally roughened as specified in section 11.6.9, 0.6 λ for concrete placed against hardened concrete not intentionally roughened, and 0.7 λ for concrete anchored to as-rolled structural steel by headed studs or by reinforcing bars. In addition, λ is 1.0 for normal weight concrete and 0.75 for all lightweight concrete. Otherwise, λ shall be determined based on volumetric proportions of lightweight and normal-weight aggregates as specified in section 8.6.1.

The reinforcing bar yield strength, f_y, is limited to 60,000 psi (420 MPa). This approach takes into account a friction angle multiplied by a clamping force, which is very similar to Equation 2.1.

For normal-weight concrete placed either monolithically or placed against hardened concrete with surface intentionally roughened as specified in ACI *(ACI 2011)* Section 11.6.9, V_n shall not exceed the lower of the following:

$$\mathbf{V_n} < \begin{cases} \mathbf{0.2 f_c' A_c} \\ \mathbf{(480 + 0.08 f_c') A_c} \\ \mathbf{1600 A_c} \end{cases} \qquad \mathbf{(2.11)}$$

where f'_c *has already been defined and* A_c is the area of the concrete at the interface (in.^{2} [cm^2]). When concretes of different strengths are cast together, the value for f'_c shall be the lower design compressive strength.

2.4.3 State Highway Agency (SHA) Design

This section provides an overview of the select SHA approach to incorporating HSS in current projects.

The Alaska Department of Transportation and Public Facilities (DOT and PF) Alaska Highway Preconstruction Manual states it interprets, amends, and augments AASHTO policies. For subjects that are not addressed by the manual, minimum AASHTO design requirements are acceptable *(DOT and PF 2013)*.

The California Department of Transportation (Caltrans) Bridge Design Practice Manual states that the LRFD specifications with California Amendments has been implemented for all new construction bridge designs in the State of California since 2006. The authors note that AASHTO *(AASHTO 2012)* is the latest version with California Amendments. These amendments were published in 2014 *(Caltrans 2014)*. Caltrans also states in Section 5.2.2 of the Bridge Design Practice Manual that reinforcing bars must be ASTM A706 with 60 ksi yield strength *(Caltrans 2010)*.

The Idaho Transportation Department (ITD) LRFD Bridge Design Manual self-lists itself as a supplement to the AASHTO LRFD Bridge Design Specifications. ITD states in the LRFD Bridge Design Manual Chapter 0.0 that new bridges must be designed with AASHTO LRFD specifications following guidelines from the ITD LRFD Bridge Design Manual *(ITD 2008)*.

ODOT *(ODOT 2014)* lists AASHTO *(AASHTO 2014)* under Section 1.2.1.1 as a standard design specification. The authors allow the use of A706 Grade 80 and state in Section 1.5.5.1.17 that the design yield strength is 80 ksi [(552 MPa)] when using A706 Grade 80 reinforcement. However, section 1.17.8.2 states to use AASHTO *(AASHTO 2014)* for shear friction, which does limit the yield strength of ASTM A706 to 60 ksi (420 MPa).

WSDOT *(WSDOT 2014)* self-lists itself as the guide for designing bridges for the Washington State Department of Transportation (WSDOT), which supplements the AASHTO LRFD Bridge Design Specifications. The specifications under section 4.2.20 states that only ASTM A706 Grade 60 (420 MPa) shall be used in members that undergo plastic hinging. ASTM A706 Grade 80 ksi (550 MPa) can be used for capacity-protected members but not for oversized shafts where ground plastic hinging is considered a part of Earthquake Resisting Systems. Further clarification is given in Section 5.1.2 for ASTM A706 Grade 80 ksi (550 MPa) steel that it may be used in Seismic Design Category (SDC) A for all components. It is not allowed in SDC B, C, and D for elements and connections that are proportioned and detailed to have significant inelastic deformation for which moment-curvature analysis was utilized to determine the plastic moment capacity. ASTM A706 Grade 80 ksi (550 MPa) steel shall also not be used for transverse and confinement reinforcement *(WSDOT 2014)*.

2.5 SUMMARY

This chapter reviewed the shear friction theory from the literature. It is noted that before and at the peak load for a concrete-concrete interface, the concrete-concrete bond or cohesion in combination with aggregate interlock controls the interface behavior. After the peak load, the dowel action of the reinforcing bars controls the interface behavior. The aggregate interlock is enhanced with increased clamping force and surface roughness. The former can either be provided externally through imposing force on the shear interface or internally by providing reinforcing bars across the shear interface. Concrete-steel bond of the reinforcing bar to the concrete in the interface affects the length of the reinforcing bar that can be elongated by the increasing crack width. The shorter the length that can be elongated, the stiffer the relation is of crack width to clamping force. A stiffer relation ensures that the clamping force is sufficient to lock the aggregate, which makes the strength of the aggregate control.

The design values for the reinforcing bars are currently limited to 60 ksi [420 MPa] by ACI *(ACI 2011)* and AASHTO *(AASHTO 2012)* equations. Limited research has been done on determining the behavior of HSS in shear friction applications. No research has been done on determining what parameters effect the contribution of the yield strength of shear friction interface reinforcing bars with the 1/8 in. (3.2 mm) roughened surface specified by ODOT. Push-off test specimens have been shown to have a good correlation to full-scale composite beam testing *(Kahn and Slapkus 2004)* and are more economical to construct. Therefore, economical results can be obtained from push-off tests and they can be conducted in smaller laboratories. However, as Kovach *(Kovach 2008)* stated, there are concerns that push-off tests have areas of high stress concentration or eccentricities that impose moments across the interface. Those effects need to be minimized by ensuring proper alignment and test setup to ensure accurate boundary conditions.

3.0 EXPERIMENTAL PROGRAM AND SPECIMEN DESIGN

3.1 INTRODUCTION

Although high strength steel (HSS) is commercially available today, its use is still limited. Currently, AASHTO limits the design yield stress of horizontal shear concrete interface reinforcing bars to 60 ksi (420 MPa). Some research on the application of HSS in bridges *(Trejo et al. 2014, Barbosa et al. 2015)* has been performed but limited research has been done on the application of HSS in concrete horizontal shear interface connections *(Zeno 2010)*. The objective of this study is to provide new data on the behavior of concrete cold joint interface connections reinforced with Grade 80 ksi (550 MPa) reinforcing steel meeting ASTM A706 specifications subjected to horizontal shear loading. To do this, specimens were designed based on ODOT *(ODOT 2014)* BR300 standard drawing. These specimens simulated a girder-deck connection. Testing of these specimens will provide data on the performance of horizontal shear interface connections reinforced with Grade 80 ksi (550 MPa) reinforcing steel.

3.2 EXPERIMENTAL DESIGN

An experimental program was developed to assess the performance of the horizontal shear interfaces of concrete containing Grade 80 ksi (550 MPa) reinforcing steel meeting ASTM A706 specifications. This experimental program included testing twenty push-off test specimens divided into two sets. In the first set, ten (10) specimens were reinforced with ASTM A706 Grade 60 ksi (420 MPa) reinforcing bars and, the second set ten (10) specimens were reinforced with ASTM A706 Grade 80 ksi (550 MPa) reinforcing bars. Five specimens from each set were detailed with #4 (#13M) reinforcing steel bars while the remaining five (5) specimens were detailed with #5 (#16M) reinforcing steel bars. All 20 specimens were designed using ODOT *(ODOT 2014)* section 1.17.8.2, which refers to AASHTO *(AASHTO 2012)* 5.8.4 for design. The spacing of the reinforcing steel bars varied from 4.0 in. (102 mm) to 8.0 in. (203 mm) for the #4 (#13M) and #5 (#16M) reinforcing steel bars, respectively. The specimens containing #4 (#13M) reinforcing bars across the interface had a shear interface reinforcement ratio, ρ, of 0.42%, and the specimens containing #5 (#16M) reinforcing bars across the interface had a shear interface reinforcement ratio, ρ, of 0.65%. All specimens were cast with nominal 4 ksi (27.6 MPa) design compressive strength concrete. Figure 3.1 shows the naming convention for the specimens. The experimental plan is shown in Table 3.1.

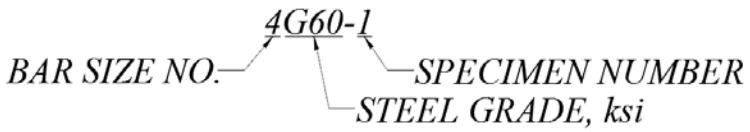

Figure 3.1: Naming convention of the push-off test specimen series

Table 3.1: Experimental test matrix

Tests	Reinf. Bar Size	ASTM A706 Grade	Interface width	Interface length	Spacing	Number of specimens
4G60	#4 (#13M)	60 ksi (420 MPa)	24 in. (610 mm)	16 in. (406 mm)	4 in. (102 mm)	5
4G80	#4 (#13M)	80 ksi (550 MPa)	24 in. (610 mm)	16 in. (406 mm)	4 in. (102 mm)	5
5G60	#5 (#16M)	60 ksi (420 MPa)	12 in. (305 mm)	24 in. (610 mm)	8 in. (203 mm)	5
5G80	#5 (#16M)	80 ksi (550 MPa)	12 in. (305 mm)	24 in. (610 mm)	8 in. (203 mm)	5

Note that to provide similar strengths for specimens built with #4 (#13M) and #5 (#16M) reinforcing steel bars, the interface areas of the concrete for the 5G60 and 5G80 were smaller than the interface area for the 4G60 and 4G80 specimens. The specimens with #5 (#16M) reinforcing bars across the interface have one-half the concrete area. Figure 3.2 shows the layout of the specimens tested with the deck (top) or girder (bottom) halves of the push-off test specimen, which are illustrated in the figure and referred to in this report as side 2 and side 1, respectively. Figure 3.3 represents the specimens reinforced with the #4 (#13M) reinforcing steel bars and Figure 3.4 represents the specimens reinforced with the #5 (#16M) reinforcing steel bars. During testing, the axial load is applied through the center of the interface where the reinforcing steel bars cross perpendicular to the interface; these reinforcing steel bars reinforce the cold-joint connection.

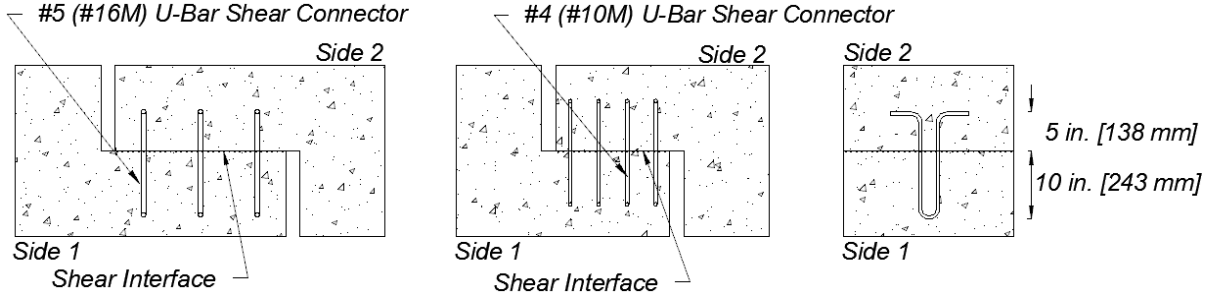

Figure 3.2: Simplified elevation schematic of push-off test specimen to show side 2 (top), side 1 (bottom), reinforcing steel bars, and shear interface.

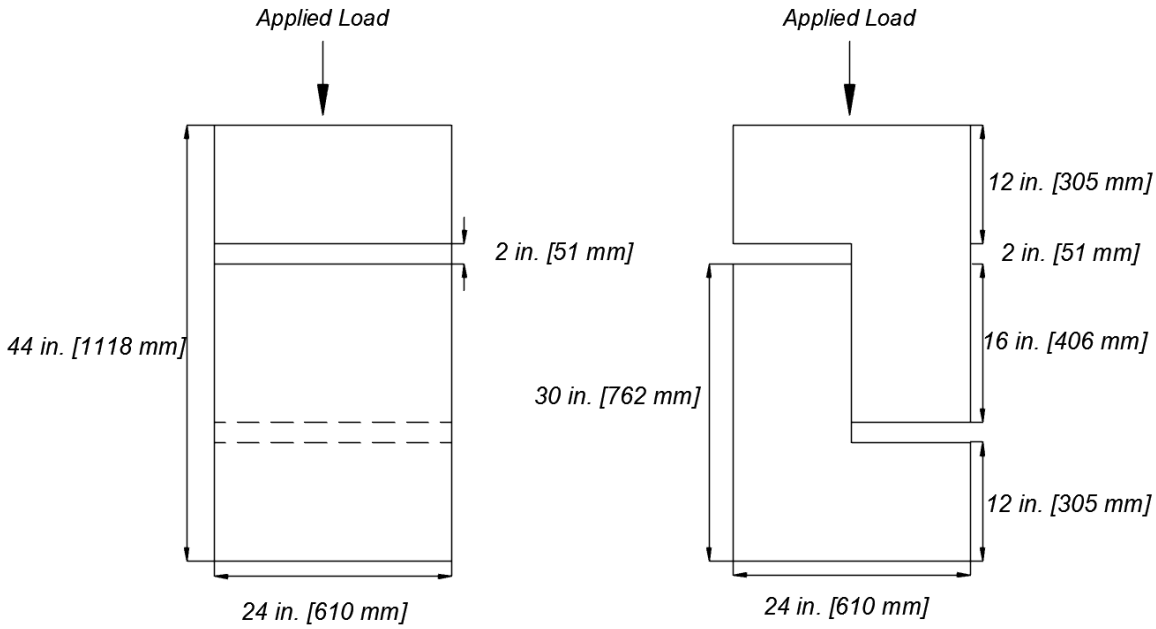

Figure 3.3: Test elevations for the specimens containing #4 (#13M) reinforcing bars across the interface: (a) Front view elevation, (b) side view elevation

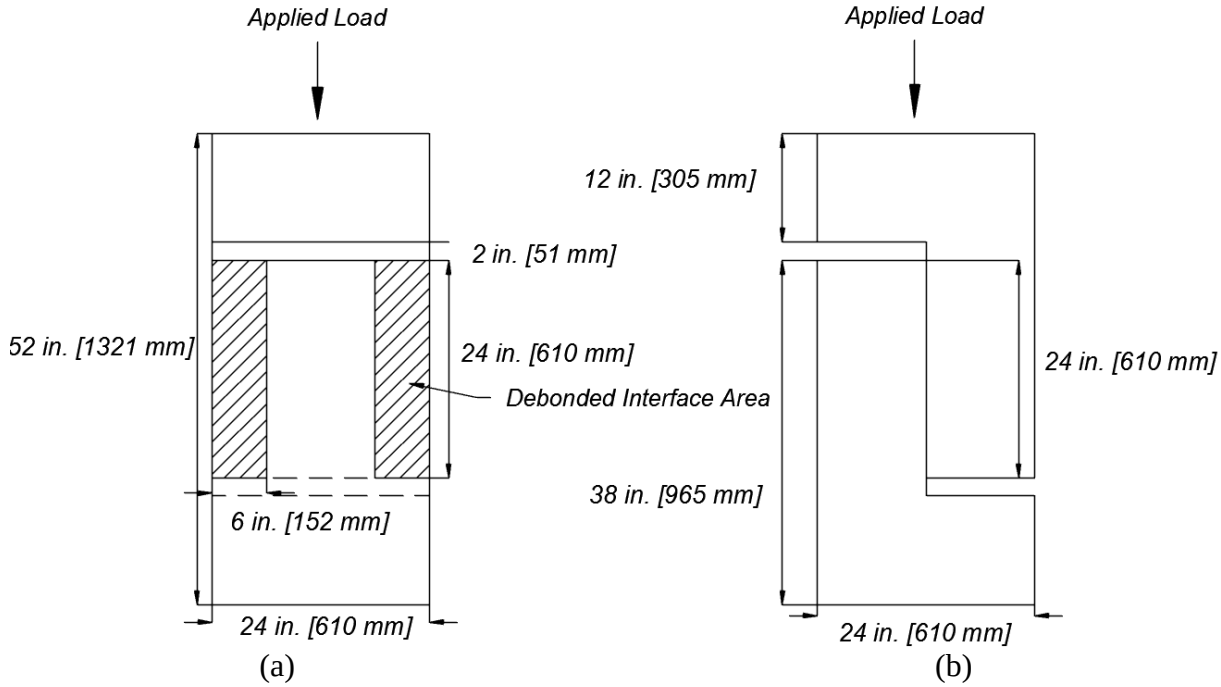

Figure 3.4: Test elevations for the specimens containing #5 (#16M) reinforcing bars across the interface: (a) Front view elevation, (b) side view elevation

3.3 PUSH-OFF TEST SPECIMENS DESIGN

Push-off test specimens were designed using ODOT *(ODOT 2014)* section 1.17.8.2, which refers to AASHTO *(AASHTO 2012)* Section 5.8.4. The concrete interface connection includes a roughened surface as specified by ODOT *(ODOT 2015),* which is a surface roughened to an amplitude of 1/8 in. (3.2 mm).

3.3.1 Interface Shear Capacity Design

The width of the specimen, reinforcing steel bar spacing, and normal force were determined from ODOT (2014) BR300 standard drawing. Normal force to the interface was estimated to be 0.003 ksi (0.0207 MPa), assuming an 8 in. (203 mm) slab, 8 foot (2438 mm) center-to-center spacing of girders, and a 24 in. (610 mm) shear interface width. This value of 0.003 ksi was applied developed and applied in the testing specimen (see descriptions below). Shear capacity was designed with AASHTO *(AASHTO 2012)* Section 5.8.4.1. The ODOT Standard Specification Section 00550.47, which specified the surface preparation requirements, has not been compared with the surface preparation descriptions in AASHTO *(AASHTO 2012)* Section 5.8.4.3. Therefore, for the analysis, it was assumed that the surface corresponded to an interpolation between the first and fifth bullet in AASHTO *(AASHTO 2012)* Section 5.8.4.3. These bullets specify a roughened interface to an amplitude of 1/4 in. (6.4 mm) and a surface that is not intentionally roughened. This is because the ODOT *(ODOT 2015)* specification is for 1/8 in. (3.2 mm) roughness and there are no AASHTO *(AASHTO 2012)* values for this roughness. The interpolated value was assumed to be the closest conservative value of the capacity anticipated. However, for the design of the specimens, the value for 1/4 in. (6.4 mm) interface was used to obtain a worst-case value for the shear strength to ensure the test setup design was adequate. Detailed calculations for the shear interface capacity with the interpolated values are provided in Appendix A.

For the specimens listed in Table 3.1, the nominal interface shear force of 215 kips (956 kN) was obtained. Thus, the experimental peak load is estimated to be 300 kips (1334 kN) (1.4 x 215 kip (956 kN)), assuming an over strength value of 1.4 is used. This over-strength factor is based on a review of Harris et al. *(Harris et al. 2012).*

Reinforcing bar locations were designed with the intention at preventing the L-shapes from failing before the interface. To ensure this, a strut-and-tie model was used to estimate specimen and interface capacity. Calculations for the strut-and-tie model can be found in Appendix B.

3.3.2 Reinforcing Steel Layout

Figure 3.5 shows the reinforcing steel layout for both specimen types. Reinforcing steel bar layout in the specimens across the interface is the same for the 4G60 and 4G80 specimens. The only difference is the steel reinforcing grade. This is also the case for the 5G60 and 5G80 specimens. For the specimens reinforced with #5 (#16M) reinforcing steel bars, half of the shear interface was debonded. Debonding was accomplished by placing 1/8 in. (3.2 mm) plywood at the interface. The U-bars terminate in 90 degree standard hooks that satisfy AASHTO *(AASHTO 2012)* Section 5.10.2.1 and all bend diameters satisfy AASHTO *(AASHTO 2012)* Table 5.10.2.3-

1. A reinforcing steel bar was placed in the middle of the U-bar to aide in the development of the side 1 and to ensure that the side 1 reinforcing steel bar would be developed.

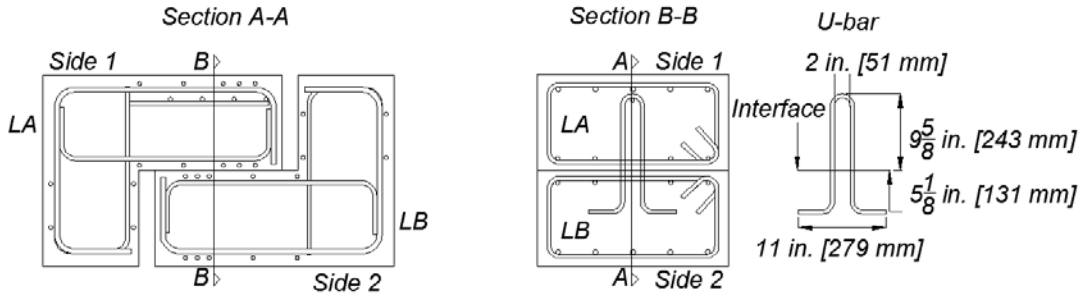

(a) #4 (#13M) Bar Specimen

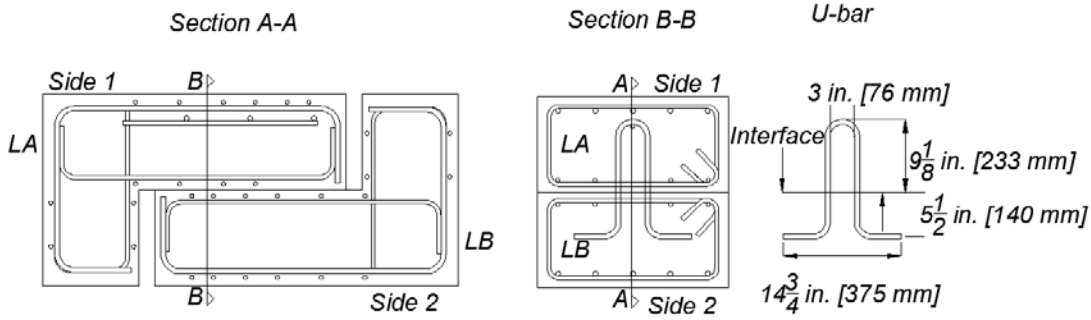

(b) #5 (#16M) Bar Specimen

Figure 3.5: Section cuts detailing reinforcing steel layout and U-bar shear connectors

All other reinforcing steel (other than the reinforcement that crossed the interface) met ASTM A706 Grade 60 ksi (420 MPa) specifications and #4 (#13M) reinforcing steel was used for all of the reinforcing except for the longitudinal reinforcement. The longitudinal reinforcement on the side opposite of the shear interface was #6 (#19M). All longitudinal bars terminate with 90 degree hooks. All transverse ties end with 135 degree hooks. Figure 3.6 shows the layout for the specimens containing #4 (#13M) bars and Figure 3.7 shows the layout for the specimens containing #5 (#16M) reinforcing steel bars.

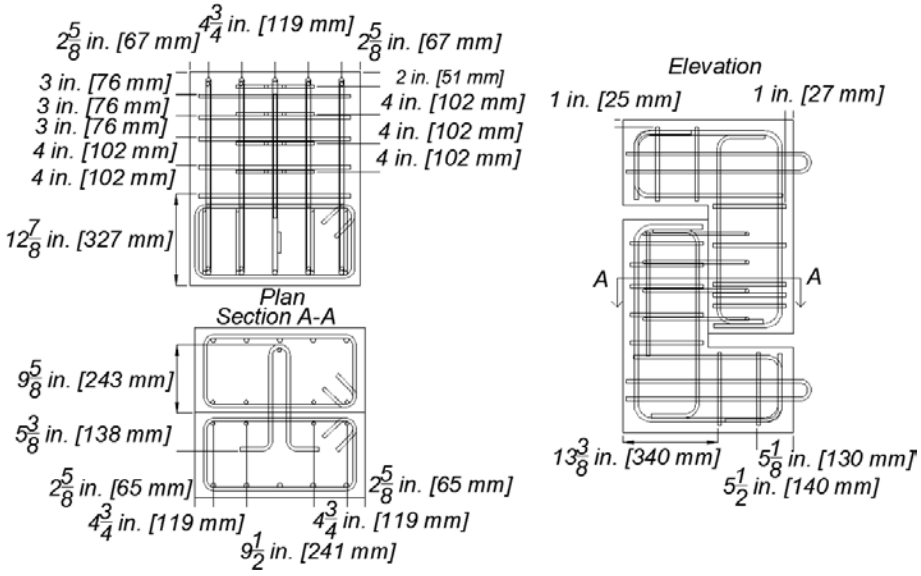

Figure 3.6: Reinforcing layout for specimens containing #4 (#13M) reinforcing bars

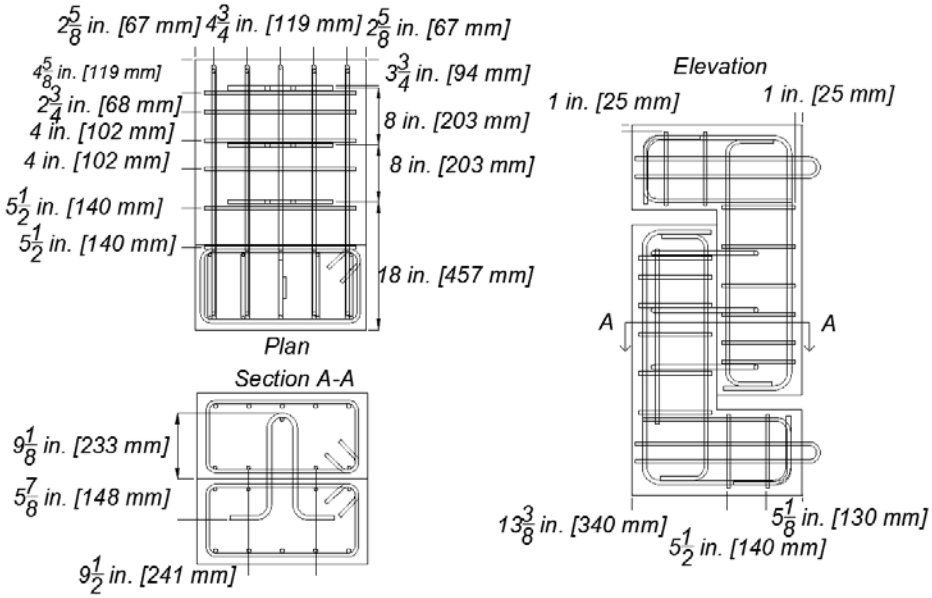

Figure 3.7: Reinforcing layout for specimens containing #5 (#16M) reinforcing bars

3.4 PUSH-OFF TEST PROCEDURES

The following section discusses the push-off test setup, instrumentation, and testing procedures. Setup procedures, instrumentation for stress and displacement measurement, and rate of loading during the test are presented.

3.4.1 Push-off Test Setup

Figure 3.8 shows an overall view of the specimen and Figure 3.9 shows a photograph of the test setup. Appendix C shows isometric views of the test specimen setups. Figure 3.10 and Figure 3.11 show the elevation views for the specimens containing #4 (#13M) reinforcing bars. Figure

3.12 and Figure 3.13 show the elevation views for the specimens containing #5 (#16M) reinforcing bars. These figures illustrate the reaction frame, actuator and load cell, actuator displacement transducer (LVDT), alignment rollers, load transfer steel plates, interface load apparatus (spring system) and corresponding load cell. As shown in the figures, the specimen size and therefore elevations of the specimen top, interface load apparatus, and the top alignment rollers vary for each size of specimen.

The test set up initiated with placing the push-off test specimen in the center of the two 4 in. (102 mm) wide stacked plates resting on top of the ground parallel to the interface. It was important to ensure that the specimen interface shear plane was aligned with the load path of the actuator. This was to minimize local stresses from an eccentric load, which could reduce the accuracy of the test. As the shear interface was located and marked, a laser was used to ensure that the interface aligned with the middle of the actuator compression cylinder at the base of the stroke on each side of the specimen. To align the specimen with the actuator in the direction perpendicular to the interface plane, the rollers perpendicular to the interface were adjusted by hammering wooden shims so that the rollers pushed the specimen into position. The roller guides on the specimen in the direction parallel to the interface plane were then adjusted to be within 0.125 in. (3.2 mm) of the specimen on each side. After the specimen was aligned and secured by the rollers, the interface string potentiometers were installed. The spring to apply simulated dead load, shown in Figure 3.8 and Figure 3.9, was engaged and the specimen alignment was checked a second time to ensure the horizontal force did not displace the top of the specimen. Instrumentation was then installed before the top loading plate was placed and aligned as well as the bottom reaction plate, which held up the specimen.

3.4.2 Rate of Loading during the Push-off Test

The actuator was placed on manual displacement and a force of about 1.0 kip (4.4 kN) was imposed on the specimen before starting the test. The rate of loading for the push-off test was 0.0004 in./min (0.01016 mm/min) until the displacement, as measured with the LVDT, was 0.60 in. (15.24 mm). The displacement rate was then doubled to 0.0008 in./min (0.02032 mm/min). After the displacement reached 1.10 in. (27.94 mm), the displacement rate was doubled again to 0.0016 in./min (0.04064 mm/min) until the end of the test. The test was over when the 2-in. gap between the L-shapes was closed.

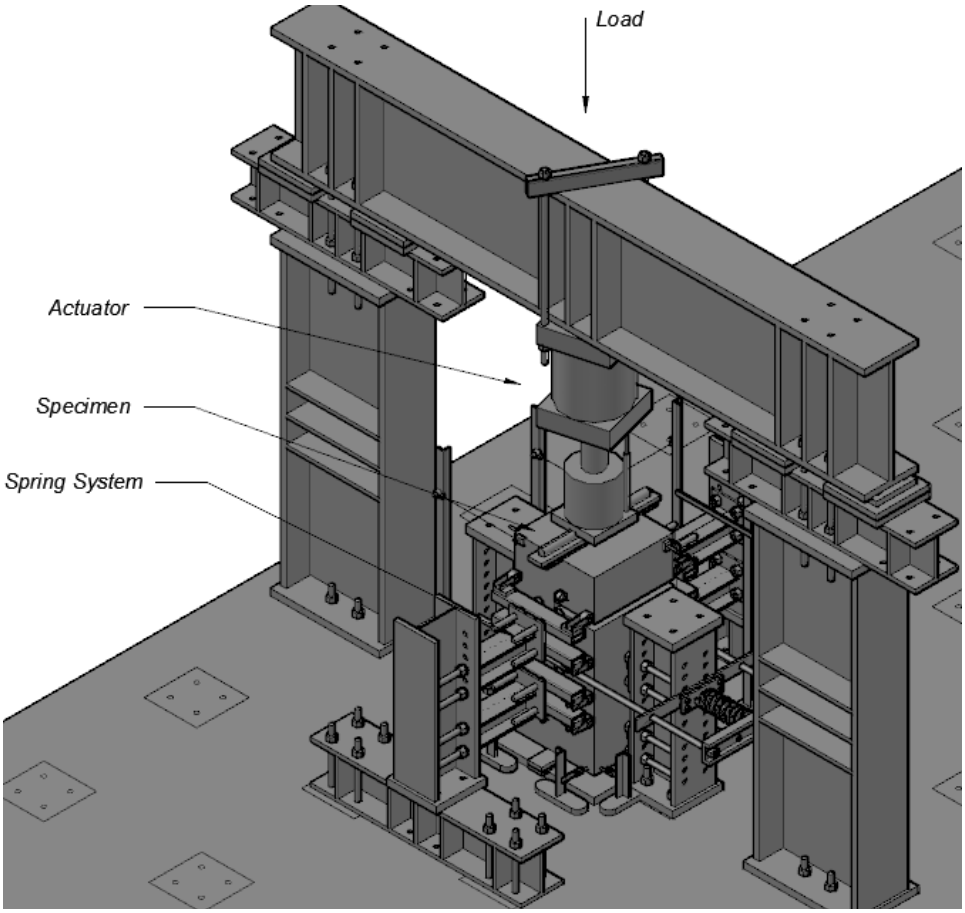

Figure 3.8: General test setup facing southeast

Figure 3.9: Photograph of specimen facing southwest during testing

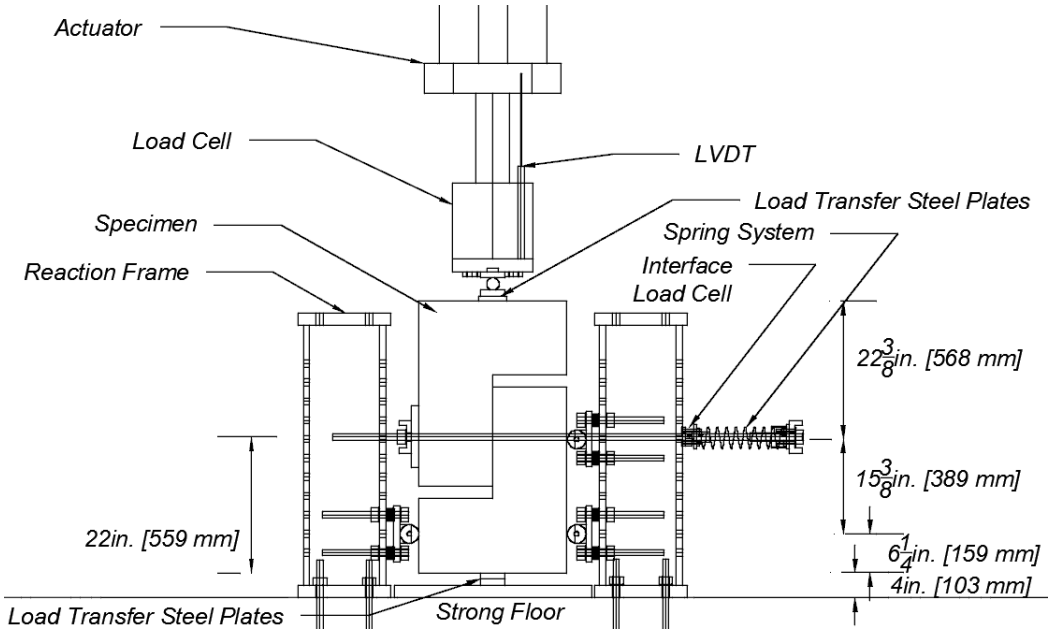

Figure 3.10: Side view elevation of test setup for the specimens containing #4 (#13M) reinforcing bars across the interface

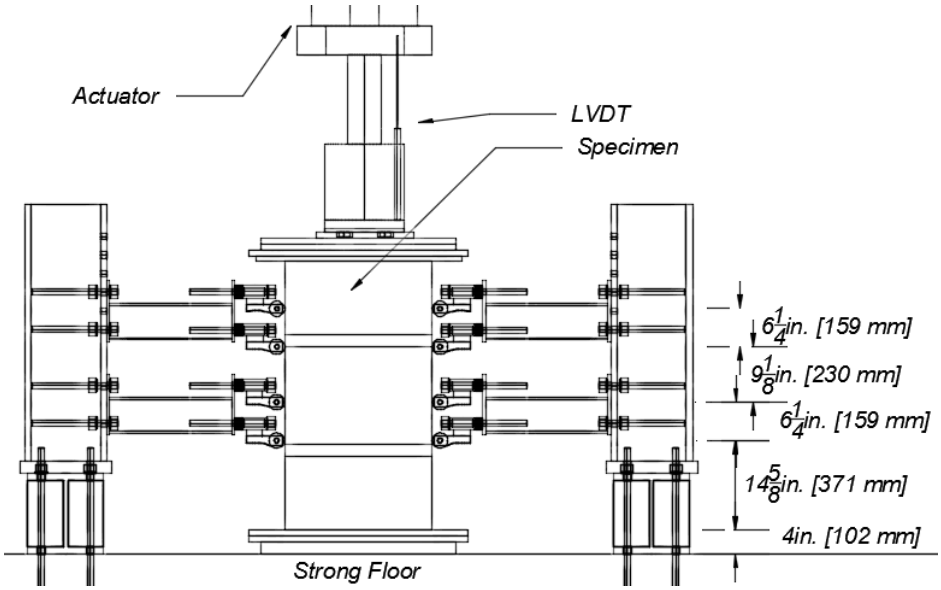

Figure 3.11: Front view elevation of test setup for the specimens containing #4 (#13M) reinforcing bars across the interface

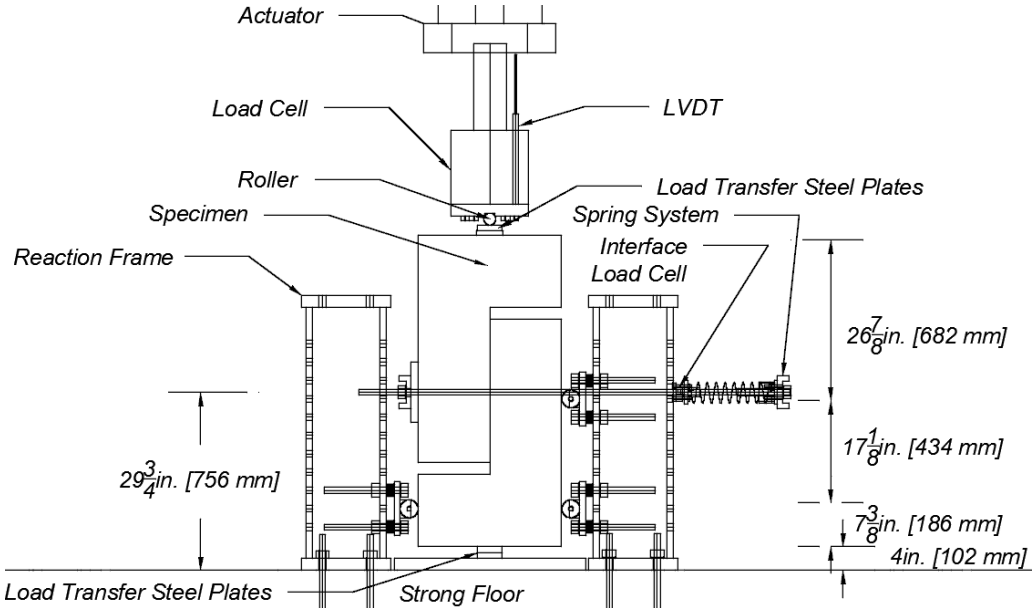

Figure 3.12: Side view elevation of the specimens containing #5 (#16M) reinforcing bars across the interface

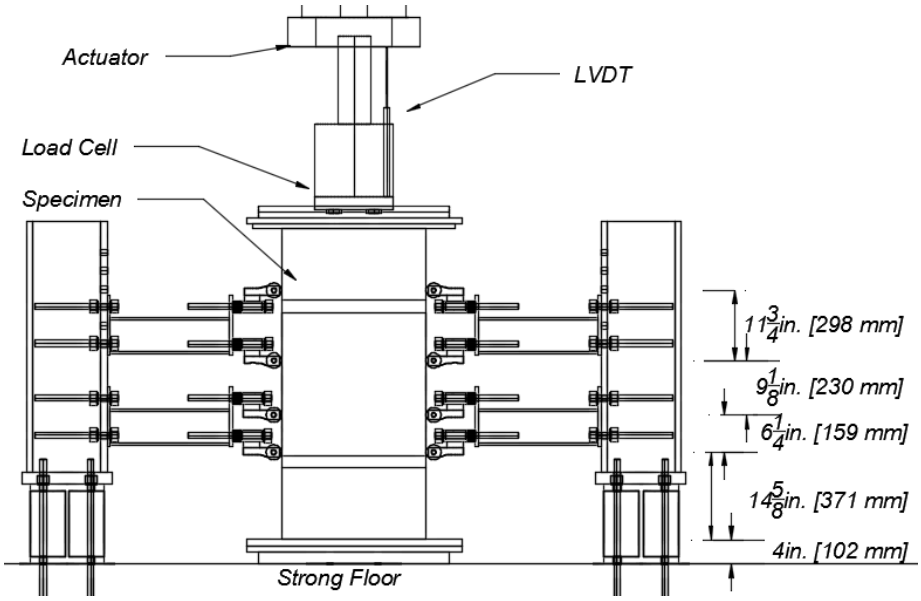

Figure 3.13: Front view elevation of the specimens containing #5 (#16M) reinforcing bars across the interface

3.5 INSTRUMENTATION

Instrumentation was used to monitor the movement of the test specimens and strains of the U-bars during testing. Figure 3.14 shows the overall view for Figure 3.15 and Figure 3.16. Figure 3.15 and Figure 3.16 show the string potentiometers used for the #4 (#13M) and #5 (#16M) reinforcing steel specimens, respectively. In each figure, the instrumentation used for the testing is shown. To monitor the movement of side 2, LVDTs placed at two bottom corners were utilized. For the side 1 movement, four (4) string potentiometers (string pots) were attached to monitor the top movement in the north-south and east-west directions. Two string pots attached on opposite sides of the top L-shape measured the vertical displacement. Four (4) string pots parallel to the shear interface and four (4) string pots perpendicular to the shear interface were installed on the outside and across the interface to measure the displacement and crack width, respectively. The vertical string pots were installed 1 in. (25 mm) parallel to the interface and the horizontal string pots were installed 4 in. (102 mm) perpendicularly at each end of the interface.

Figure 3.14 shows the overall view of the setup and the views for Figure 3.15 and Figure 3.16. Figure 3.15 and Figure 3.16 show the #4 (#13M) and #5 (#16M) external instrumentation elevation respectively. A summary of instrumentation used for the specimens is shown in Table 3.2. In addition to the instrumentation listed in Table 3.2, four (4) strain gauges were placed in each specimen. Figure 3.17 illustrates the strain gauges used. All tests used a data sampling rate of ten samples per second (10 Hz). String potentiometers were attached to aluminum pieces that were attached to the specimen. A Lebow 3130-150-500K load cell was used to determine the load during the test. A Solartron ACR-100 LVDT was used to measure the actuator displacement. The LVDT was calibrated with a Mitutoyo Absolute Digimatic Height Gage, as were all the other string potentiometers and other LVDTs used in the specimen. A National Instruments SCXI-1001 chassis was used with 27 channels to record data from the test.

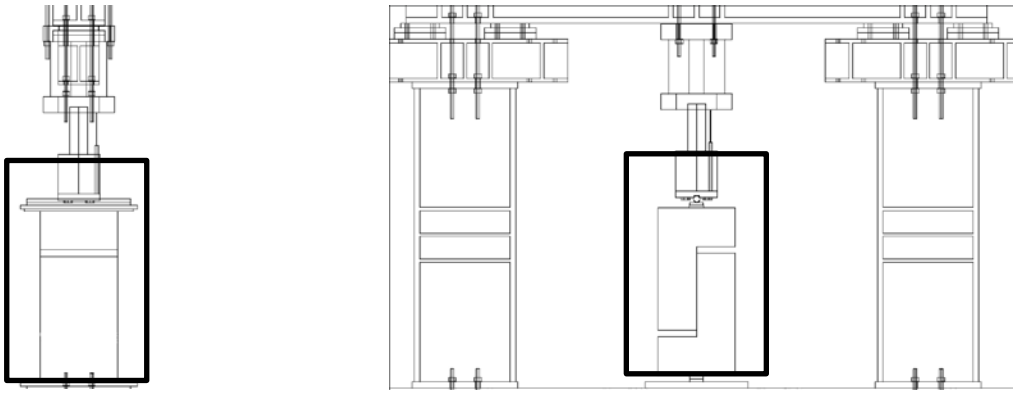

Figure 3.14: External instrumentation overall view. The two views shown in Figure 3.15 and Figure 3.16 show the zoomed in sections within each box highlighted in this figure

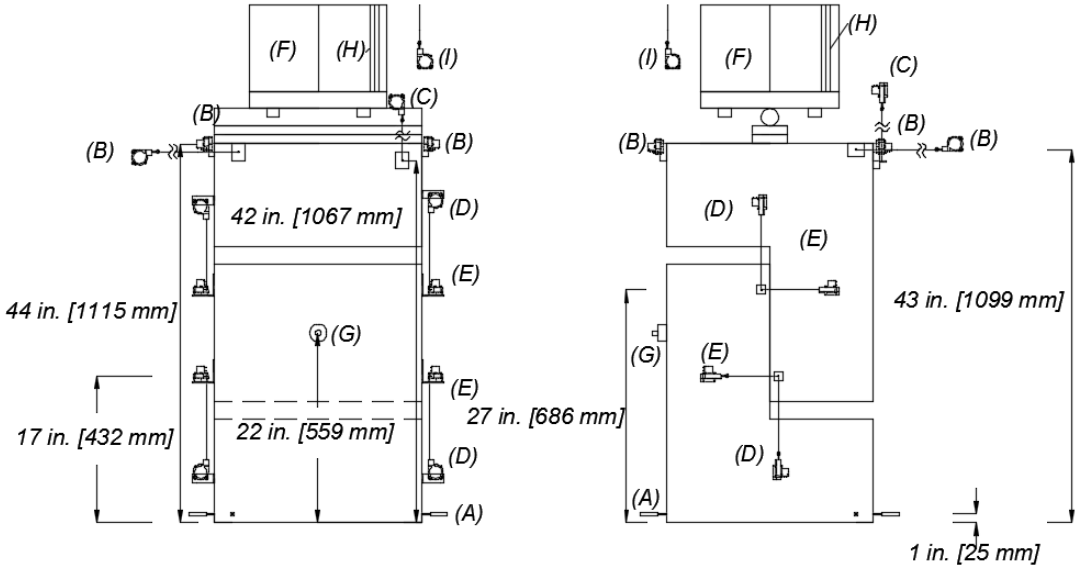

(a) (b)

Figure 3.15: External instrumentation elevation view for specimens containing #4 [#13M] reinforcing bars across the interface: (a) Front view elevation, (b) side view elevation

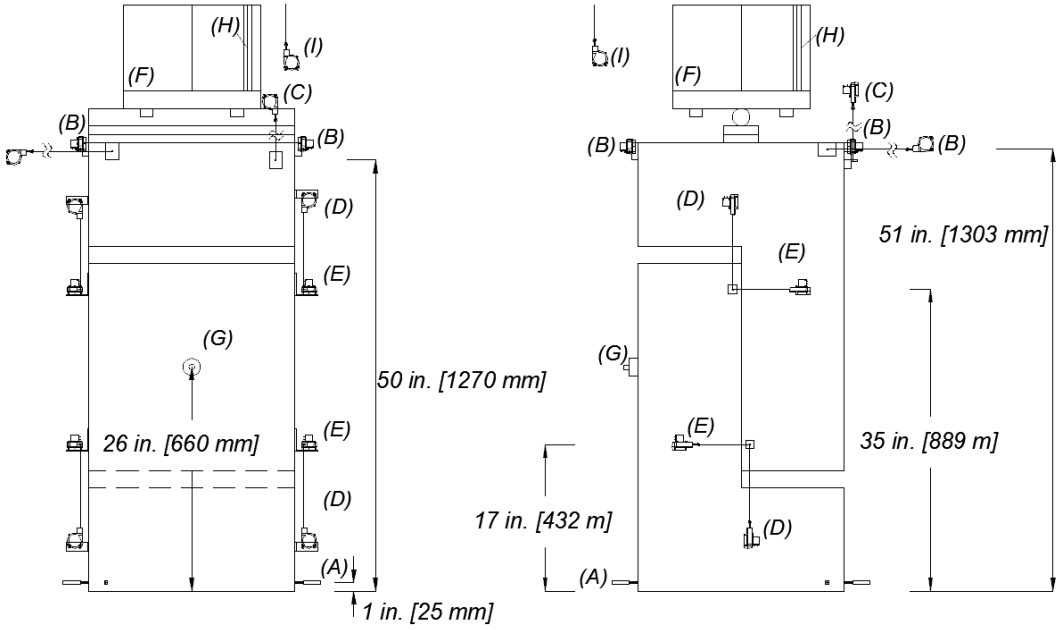

(a) (b)

Figure 3.16: External instrumentation elevation view for specimens containing #5 [#16M] reinforcing bars across the interface: (a) Front view elevation, (b) side view elevation

Table 3.2: Summary of measure observations and instrumentation

Measured observation	Instrumentation	Drawing label
Specimen base movement	4 LVDTs (horizontal)	(A)
Specimen top lateral movement	4 string pots	(B)
Specimen top vertical movement	2 string pots	(C)
Shear interface vertical movement	4 string pots	(D)
Shear interface horizontal movement	4 string pots	(E)
Applied shear load	1 load cell	(F)
Applied simulated dead load	1 load cell	(G)
Actuator displacement	1 LVDT (vertical)	(H)
Reaction frame beam displacement	1 string pot	(I)

Strain gauges were installed on the reinforcing bars across the interface to estimate the internal clamping force on the interface that contributes to aggregate interlock. Strain gauges were placed 3 in. (76 mm) from the interface on all U-bars on the same side. An additional strain gauge was added to the second U-bar 1 in. (25 mm) from the interface on the opposite leg from the strain gauges installed 3 in. (76 mm) from the interface. Strain gauges were placed 3 in. (76 mm) from the interface to ensure data was retrieved while the interface concrete fractured. The other strain gauges were intended to measure the strain in the opposite leg of the stirrup, 1 in. (25 mm) from the interface. Figure 3.17 shows the internal instrumentation elevation for both sizes of specimens. The strain gauges 3 in. (76 mm) away from the interface were located under the inside 90 degree bend of side 2 of the specimen. The strain gauges 1 in. (25 mm) from the

interface were located on the outside of the 90 degree bend on side 2 of the specimen, as shown in Figure 3.17. Figure 3.18 illustrates the strain gauges applied on the U-bar.

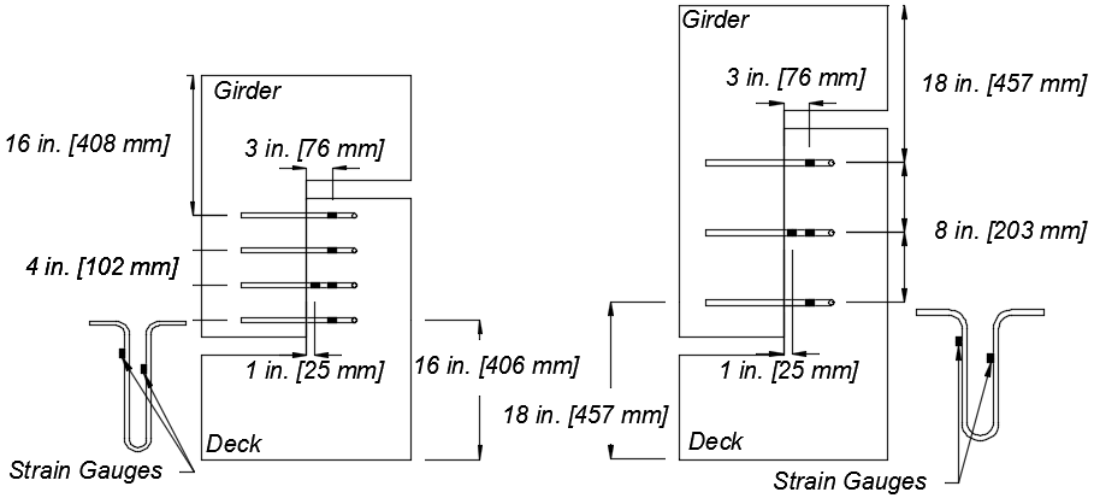

(a) (b)

Figure 3.17: Internal instrumentation elevation: (a) Specimens containing #4 [#13M] reinforcing bars across the interface and (b) specimens containing #5 [#16M] reinforcing bars across the interface.

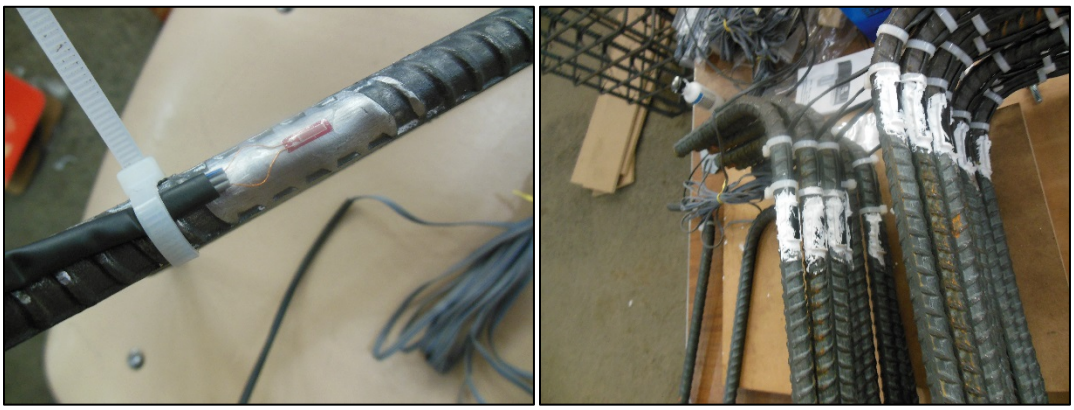

(a) (b)

Figure 3.18: Strain gauges applied to U-bar reinforcing (a) of strain gauge before protective coating and (b) view of #5 (#16M) U-bars after strain gauges are installed

3.6 CONSTRUCTION PROCEDURE

The push-off test specimens were fabricated in the Structural Engineering Research Laboratory at Oregon State University. All 20 specimens were fabricated at the same time. The test specimens were cast in two concrete placements from the same concrete mixture to minimize variability in the concrete properties. The construction of the specimens is summarized below.

(1) Application of strain gauges on U-Bar reinforcing, as shown in Figure 3.18;

Tying the L-shape cages. Cages were measured and marked at stirrup locations and tied with 16.5 gauge rebar tie wire. Cages were measured diagonally in each direction to ensure that they

would be square with the formwork. As specimens were symmetrical, both side 1 and side 2 had the same L-shape cage configuration. Specimen cages are shown in Figure 3.19;

Construction of formwork and insertion of L-shape cage into formwork. The cage was placed inside with plastic spacer guides as shown in Figure 3.20. Loose ties and other objects were cleaned out of the formwork before casting;

Installation of the U-bar (reinforcing bars that crossed the interface) on side 2 of the specimen. Blocks were used to hold the stirrups in place until they were tied. Plywood pieces with holes drilled to the correct reinforcing bar spacing were placed on top of the U-bars to ensure that they were normal to the interface and at the designed spacing, as shown in Figure 3.21;

Casting of side 2 of the specimen. All concrete for the first casting in all specimens was from the same truck. Concrete was consolidated, struck level with the surface, and interfaces were roughened with a 1/8 in. (3.2 mm) serrated trowel. Burlap and plastic were placed over the concrete immediately after casting and wetted once in the morning and once in the evening beginning the day after casting for three days. After three days, the burlap and plastic was removed. A cast specimen with burlap and plastic is shown in Figure 3.22;

Installation of the top (side 1) formwork and L-shape cage (Figure 3.23).

Concrete casting of top (side 1) L-shape. The second set of formwork was installed and the cage was placed inside with plastic spacer guides. All concrete from the second cast was from the same truck. Concrete was consolidated and struck level with the top of the formwork. Burlap and plastic was placed over the cast concrete the burlap was kept wet for three days. After three days, the burlap and plastic was removed. The formwork was removed 7 days later. Figure 3.24 shows the completed cast specimen;

Figure 3.19: Reinforcing cage for a specimen containing #5 (#16M) reinforcing bars across the interface

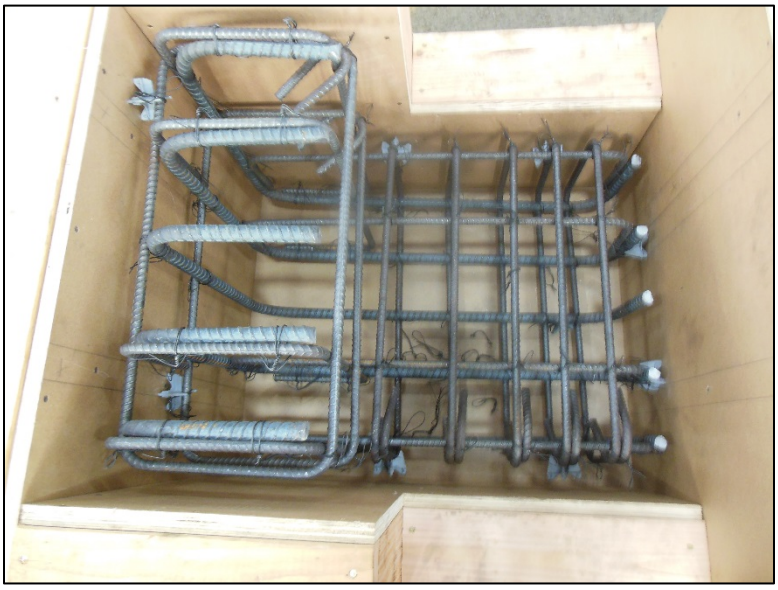

Figure 3.20: Cage for a specimen containing #4 (#13M) reinforcing bars across the interface inserted into constructed formwork

Figure 3.21: Specimen prepared for the first concrete cast

Figure 3.22: The L-shape half of a specimen containing #5 (#16M) reinforcing bars across the interface after the first concrete cast

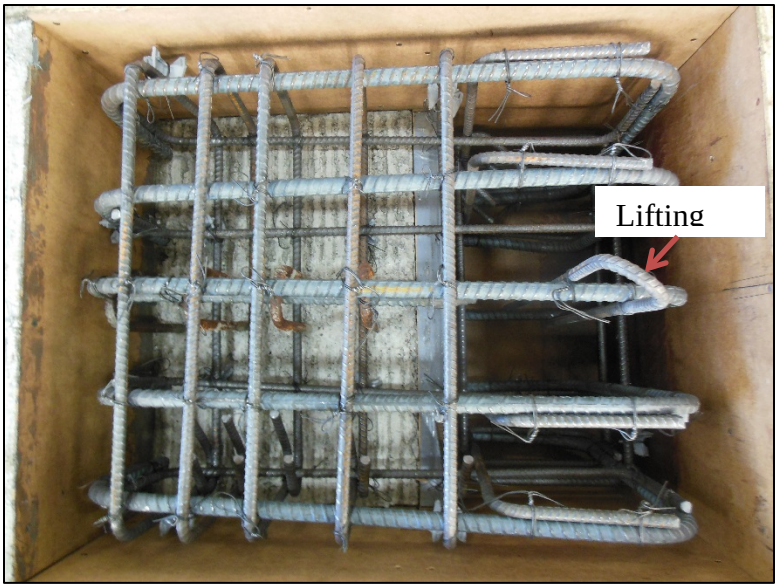

Figure 3.23: A #4 (#13M) L-shape installed in the top (side 1) side formwork

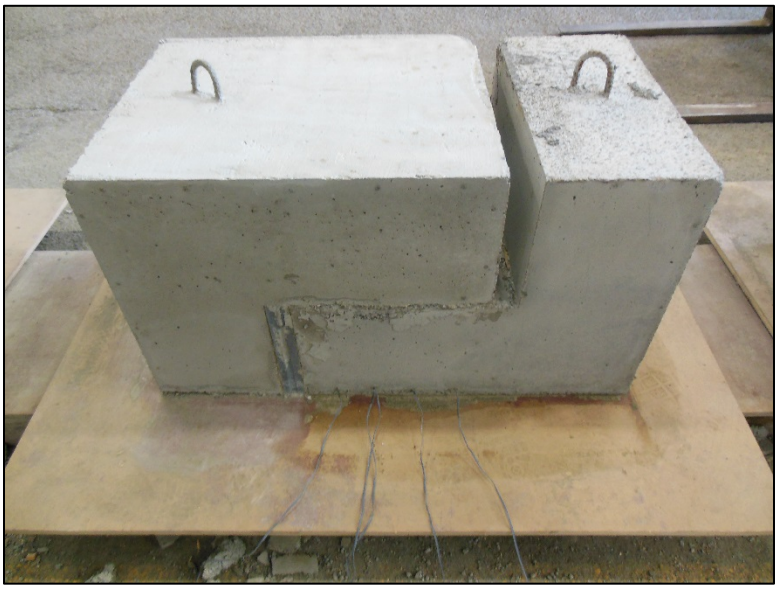
Figure 3.24: A specimen containing #4 (#13M) reinforcing bars across the interface with the formwork removed

3.7 POST-PROCESSING OF EXPERIMENAL RESULTS

Lateral movement of the lower half of the specimen and the upper half of the specimen were observed with the string potentiometers and LVDTs. It was decided that the lateral movement of all specimens was minimal and therefore not significant to the results. Results of the lateral movement are shown in Appendix D.

The interface string potentiometers and the horizontal string potentiometers were installed to measure movement on a plane. Movement of the specimen potentially influences the measurement as when the specimen displaces under interface shear force, the angles of the

strings change. To ensure the string potentiometers continue to measure along their intended planes, the values of the string potentiometers were adjusted with the following method and equation:

$$L = D + X + E \quad \textbf{(3.1)}$$

Length of the string potentiometers extension relative to the string potentiometer, *L*, was estimated by summing *D*, *X*, and *E* to obtain *L* as shown in Equation 3.1. Figure 3.25 illustrates the parameters and these are defined as follows.

D is the string potentiometer engagement zone, which was approximated with the Data Acquisition System (DAQ) using calipers to measure the extended length. The end of string must be pulled past this zone to be read by the DAQ. Pulling the string potentiometer past this length initiates the minimum reading at -5.15 in. (130.8 mm). *D* was measured to be approximately 0.435 in. (11.0 mm).

X is the string potentiometer reading, which was read from the potentiometer through the DAQ. As the string potentiometer reads from -5.15 in. to 5.15 in. (-130.8 mm to 130.8 mm), 5.15 in. (130.8 mm) is added to the reading to obtain the appropriate range for the calculations. *X* is a variable with a range from 0 in. to 10.3 in. (0 mm to 261.6 mm).

E is the length of the connection at the end of the string, which was measured with calipers. *E* was measured to be 0.65 in. (16.5 mm).

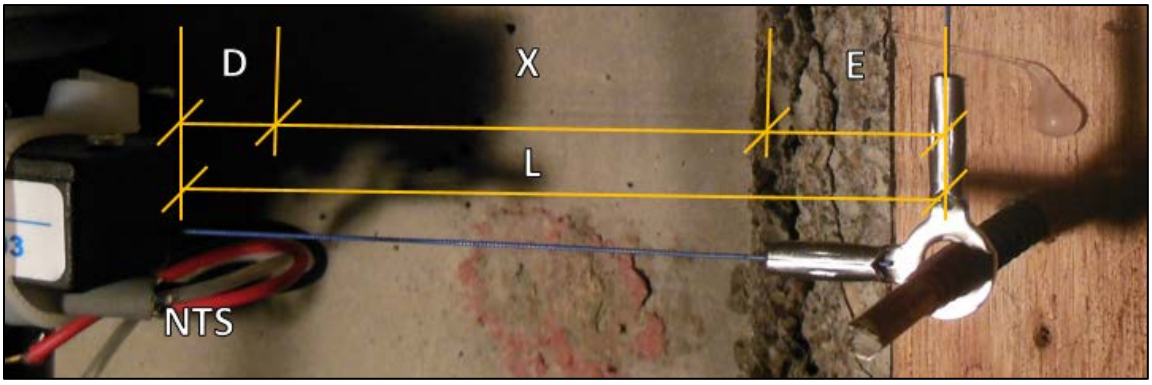

Figure 3.25: String potentiometer length determination

To calculate the correction, the average readings of the specimen top vertical movement, which captured the interface shear displacement of the specimen relative to the ground, was used. Those string potentiometers were not corrected for lateral movement as a small angle was observed from post-test observation and calculation. The calculations considered the error from taking the vertical interface shear displacement was from the shortest length of vertical string pot, which was about 10 in. (254 mm), and a maximum of 1 in. (25 mm) of side movement. The theoretical error from those measurements is 0.5% from geometry. Torqueing across the shear interface of the upper half relative to the lower half was assumed to be minimal as rollers were installed to restrain that type of motion.

The following equation shows how the horizontal string potentiometers were adjusted for specimen movement. The horizontal string potentiometers were used to calculate the crack width.

$$\mathbf{L_x = L\ cos(T)} \qquad \mathbf{(3.2)}$$

The horizontal length of the string, $L_{x,}$ was calculated using Equation 3.2 and the following parameters, which are all shown in Figure 3.26: (i) the average from the average of the specimen top vertical movement, L_y; (ii) string potentiometer length, L; (iii) the initial string potentiometer length, L_i; and (iv) the angle, T, which is equal to the inverse sin of L_y/L.

The same equation parameters are used to find the vertical interface string potentiometer correction. However, the value L_{yh}, which was obtained from the horizontal string potentiometer calculation as the difference between L_i and $L_{x,}$ was used instead of L_y to calculate the correction. The geometry for this calculation is shown in Figure 3.27.

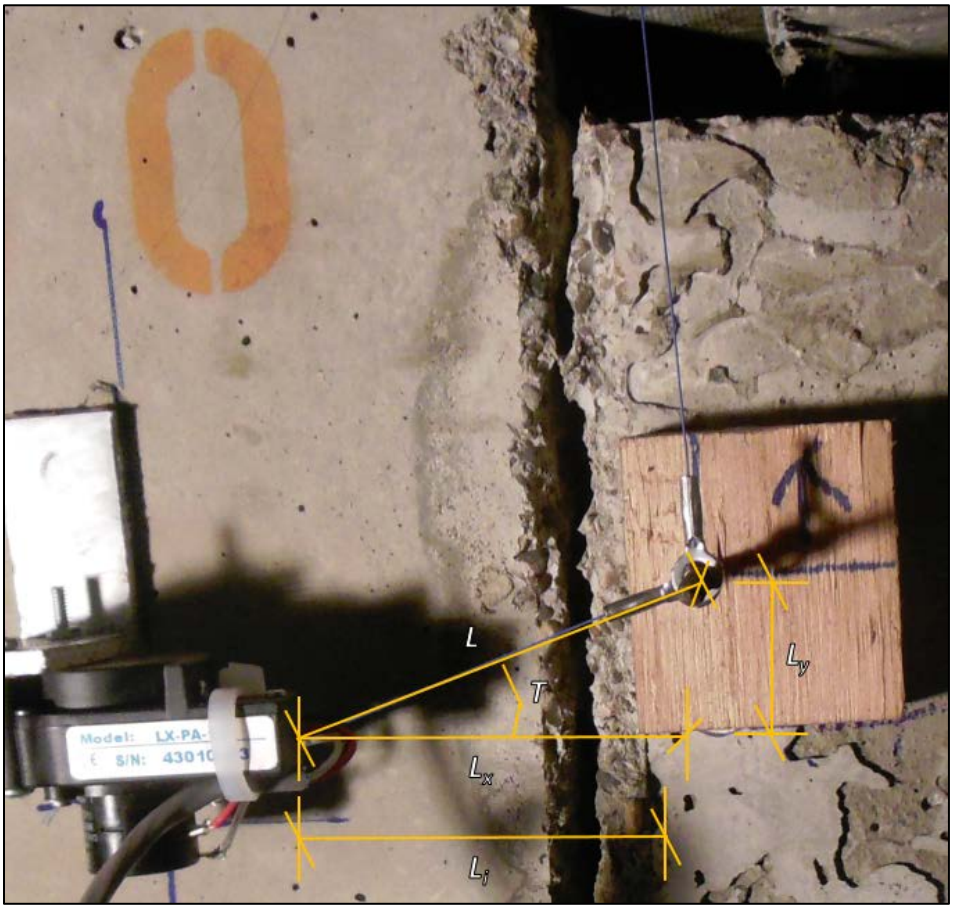

Figure 3.26: Horizontal interface string potentiometer correction

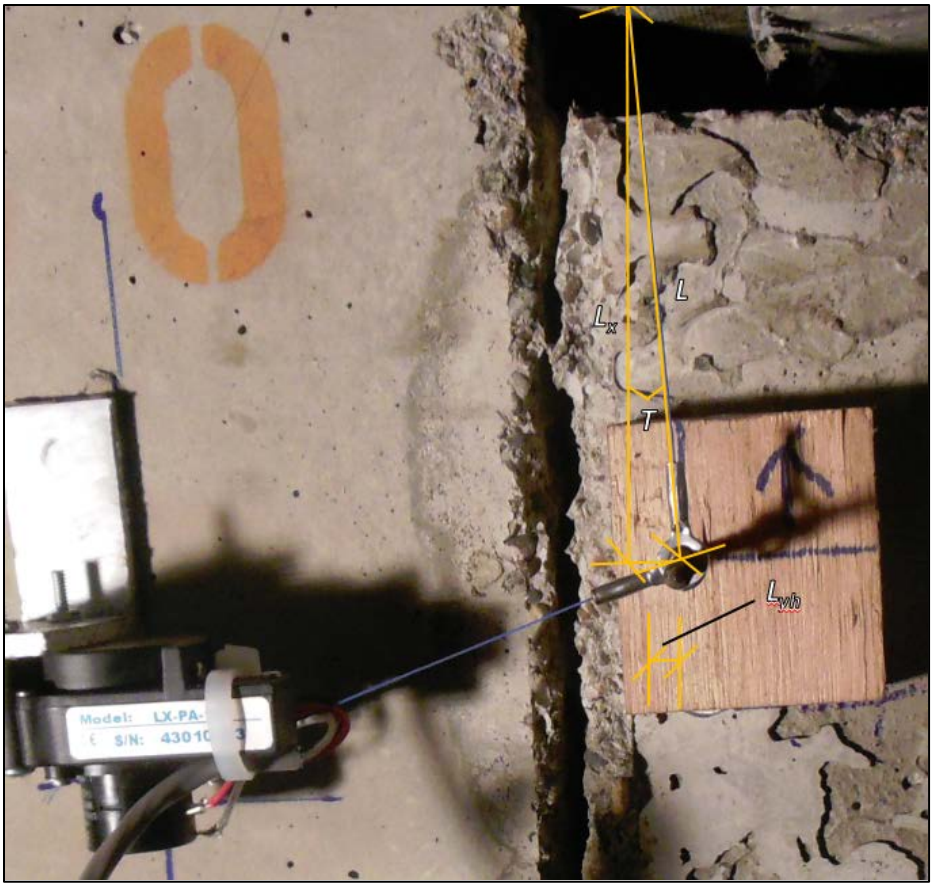

Figure 3.27: Vertical interface string potentiometer correction

4.0 MATERIALS

4.1 REINFORCING STEEL

For construction of the test specimens, two types (ASTM A615 and ASTM A706) and two grades (60 ksi (420 MPa) and 80 ksi (550 MPa)) of reinforcing bar were used. For both grades and types, #4 (#13M) and #5 (#16M) reinforcing bars were used. The #5 (#16M) ASTM A706 Grade 80 bars were provided by Cascade Steel in McMinnville, Oregon as a special heat for a previous research project *(Link et al. 2014)*. The #4 (#13M) Grade 80 bars were manufactured by Nucor in Seattle, Washington. Farwest Steel in Eugene, Oregon provided and bent all of the reinforcement except for the #4 (#13M) and #5 (#16M) ASTM A706 Grade 80 U-bars, which were cut and bent in-house. Table 4.1 shows the bar sizes and mechanical properties of the reinforcing bar as reported by the manufacturers. Table 4.2 shows the chemical composition for all steel from the steel certification.

In addition to the reported values by the manufacturers, the researchers performed additional testing of the mechanical properties. A more detailed evaluation of the reinforcing bar properties are provided in a subsequent report to be submitted by the authors on low-cycle fatigue behavior of HSS. Table 4.3 shows the results from tensile tests. Testing was completed with a Universal Testing Machine (UTM) connected to a Data Acquisition System (DAQ). The UTM force, displacement, and extensometer displacement were recorded at the frequency of 10 Hz. At least three tests of each size and grade of reinforcement was performed. Testing followed ASTM E8/E8M-13a, *Standard Test Methods for Tension Testing of Metallic Materials*. The extensometer met the requirements of ASTM E83-10a, *Standard Practice for Verification and Classification of Extensometer*. During testing, the extensometer was removed after the peak load was observed to prevent damage to the extensometer. Specimens were marked by a metal punch and gripped in the UTM machine at an 8-in. (203 mm) grip-to-grip length, according to the specifications defined by ASTM A706/A706M-14, *Standard Specification for Deformed and Plain Low-Alloy Steel Bars for Concrete Reinforcement*. Table 4.3 shows the average of the results obtained for the different bar sizes and reinforcing steel grades. The yield stress was determined using the strain computed using the 0.2% offset method and also the 0.0035 in./in. (mm/mm) strain Extension Under Load (EUL), as described in ASTM E8/E8M. In addition, tensile strength and corresponding strain, ultimate strength and corresponding strain, and also estimates of the onset of strain hardening can be found in Table 4.4.

The mill yield stress data from Table 4.1 is very similar to the tested data for the Grade 60 ksi (420 MPa) in Table 4.3. Although the Grade 80 ksi (550 MPa) steel has varying values for the milled and tested data, they are within 2 ksi (13.8 MPa) for each size of reinforcing bars tested.

Figure 4.1 through Figure 4.4 show the stress-strain curves of each of the bar types and sizes.

Table 4.1: Mechanical and physical properties of reinforcing bar (mill data)

Bar size	ASTM A706 grade ksi (MPa)	Manuf.	Heat #	Yield strength, ksi (MPa)	Tensile strength, ksi (MPa)	Elong. % 8 in. (0.2 m)*	Nom. Wt, %**
#4 (#13M)	Gr. 60 (420)	Nucor	129714	68.0 (469)	94.0 (648)	16	95
#5 (#16M)	Gr. 60 (420)	Nucor	130714	65.0 (448)	92.0 (634)	18	96
#4 (#13M)	Gr. 80 (550)	Nucor	SE14101987	89.7 (619)	117.0 (807)	12.5	95
#5 (#16M)	Gr. 80 (550)	Cascade	327612	87.5 (603)	114.0 (786)	13	96

*According to ASTM A706.
**Actual weight as percent of nominal weight specified by ASTM A706.

Table 4.2: Chemical composition of reinforcement (mill data)

Bar size	ASTM A706 grade, ksi (MPa)	C	Mn	P	S	Si	Cu	Ni	Cr	Mo	V	CE*
#4 (#13M)	Gr. 60 (420)	0.290	1.230	0.017	0.024	0.250	0.250	0.090	0.130	0.020	0.027	0.520
#5 (#16M)	Gr. 60 (420)	0.280	1.230	0.013	0.032	0.240	0.260	0.100	0.100	0.020	0.025	0.500
#4 (#13M)	Gr. 80 (550)	0.290	1.27	0.014	0.043	0.210	0.290	0.110	0.130	0.031	0.127	0.510
#5 (#16M)	Gr. 80 (550)	0.290	1.300	0.011	0.000	0.230	0.360	0.090	0.050	0.017	-	0.520

*CE is defined as the Carbon Equivalent by ASTM A706/A706M-14, Standard Specification for Deformed and Plain Low-Alloy Steel Bars for Concrete Reinforcement.

Table 4.3: Reinforcing bar tensile test results summary

Bar size	ASTM A706 grade ksi (MPa)	Yield point (0.2% offset)		Yield point (0.0035 EUL)		Tensile strength point		Ultimate strain		% Elong. in 8 in. (203 mm)
		Stress, ksi (MPa)	Strain, in./in. (-)	Stress, ksi (MPa)	Strain, in./in. (-)	Stress, ksi (MPa)	Strain, in./in. (-)	Stress, ksi (MPa)	Strain, in./in. (-)	
#4 (#13M)	60 (420)	68.9 (475)	0.0047	68.6 (473)	0.0035	98.6 (680)	0.1100	72.6 (501)	0.1585	17
#5 (#16M)	60 (420)	64.6 (445)	0.0043	64.3 (443)	0.0035	93.8 (647)	0.1180	67.6 (466)	0.2239	18
#4 (#13M)	80 (550)	87.6 (604)	0.0054	85.7 (591)	0.0035	115.4 (796)	0.0838	93.0 (641)	0.0988	11*
#5 (#16M)	80 (550)	86.2 (594)	0.0051	85.4 (589)	0.0035	114.3 (788)	0.1066	86.8 (598)	0.1555	14

*Reinforcing bars tested did not meet specified requirements

Table 4.4: Reinforcing bar strain hardening results summary

Bar size	Grade, ksi (MPa)	Strain hardening point	
		Stress, ksi (MPa)	Strain, in./in. (mm/mm)
#4 (#13M)	60 (420)	69.1 (476)	0.0098
#5 (#16M)	60 (420)	64.5 (445)	0.0089
#4 (#13M)	80 (550)	89.0 (614)	0.0102
#5 (#16M)	80 (550)	85.9 (592)	0.0084

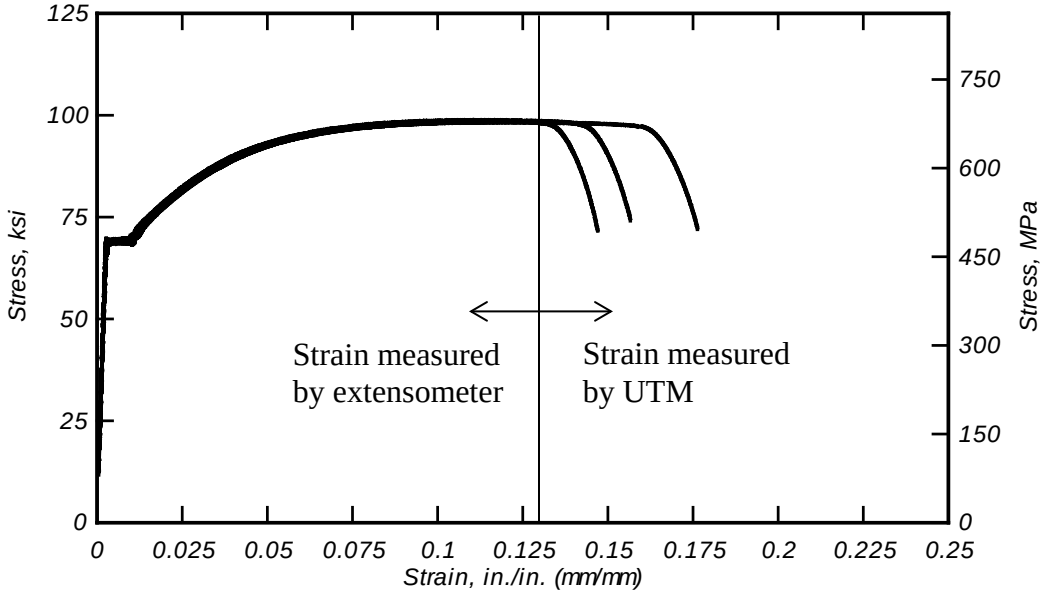

Figure 4.1: Stress-strain plot of #4 (#13M) Grade 60 reinforcing steel bar

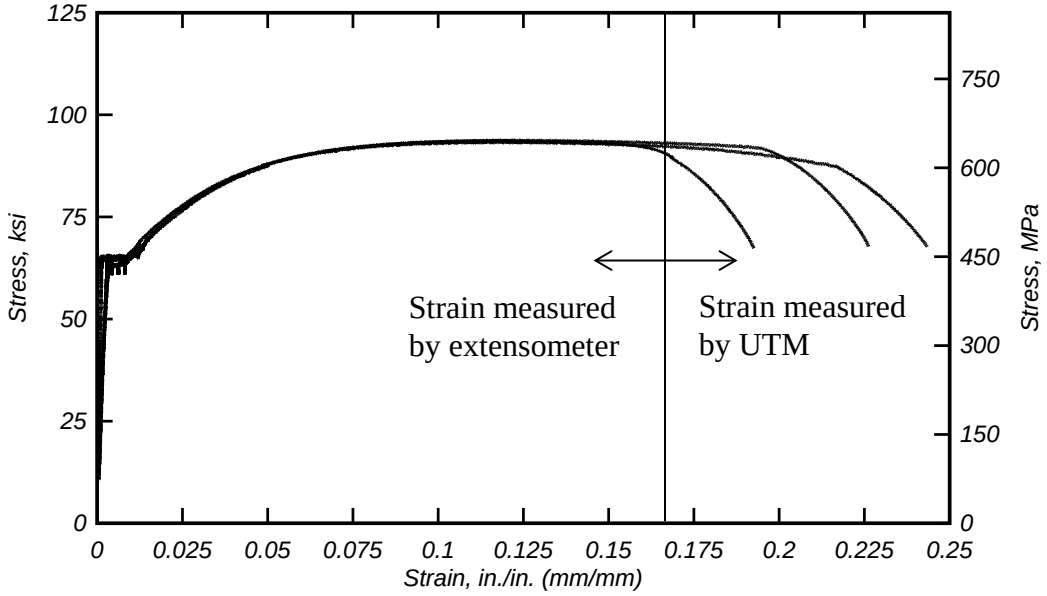

Figure 4.2: Stress-strain plot of #5 (#16M) Grade 60 reinforcing steel

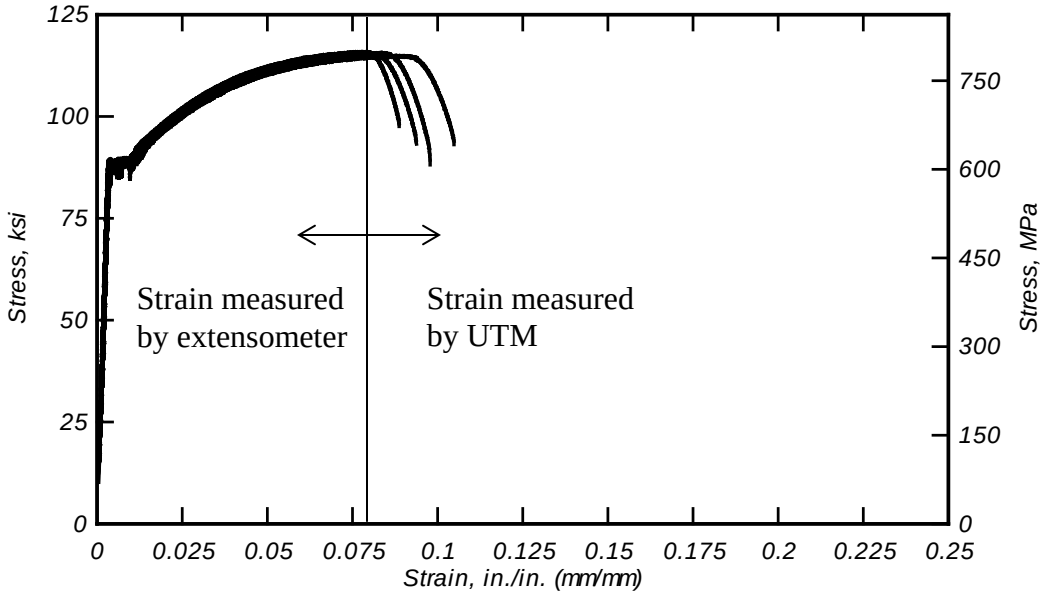

Figure 4.3: Stress-strain plot of #4 (#13M) Grade 80 reinforcing steel bar

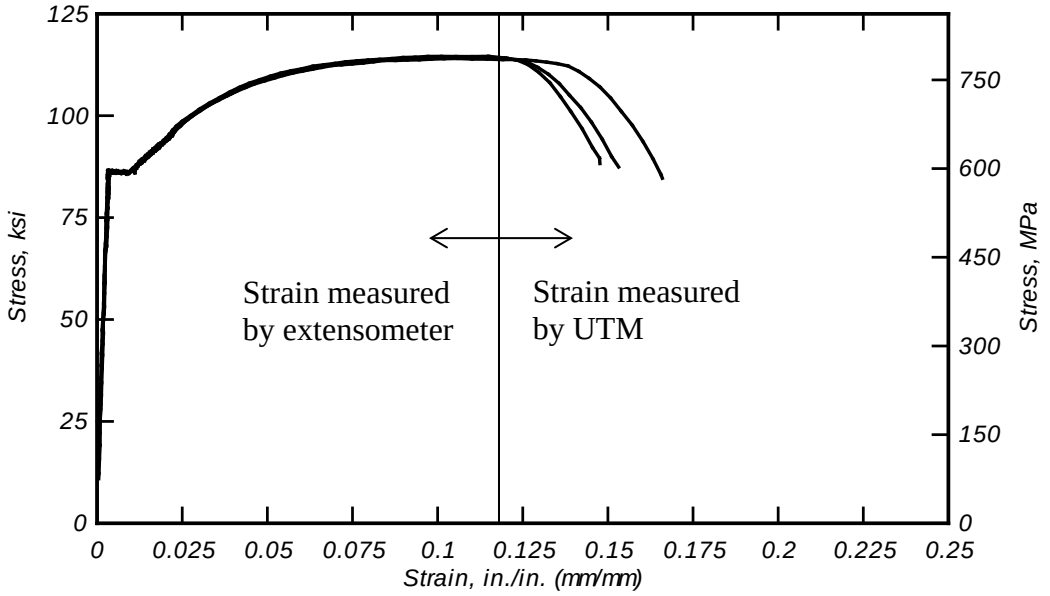

Figure 4.4: Stress-strain plot of #5 (#16M) Grade 80 reinforcing steel bar

4.2 CONCRETE

The shear specimens were cast on two different cast dates. The same concrete mixture proportions were used for both casts. Knife River Corporation provided the concrete, which was mixed at a batch plant. The maximum aggregate size was 3/8 in. (9.52 mm) and the 28-day design compression strength was 4 ksi (27.6 MPa). Table 4.5 shows the concrete mixture proportions

Table 4.6 shows the fresh concrete characteristics. Fresh concrete characteristics were evaluated using ASTM Standard C231-14, *Standard Test Method for Air Content of Freshly Mixed Concrete by the Pressure Method*, ASTM Standard C143-12, *Standard Test Method for Slump of Hydraulic-Cement Concrete*, and ASTM Standard C138-13, *Standard Test Method for Density (Unit Weight), Yield, and Air Content (Gravimetric) of Concrete*. Concrete cylinder samples were cast in specification to ASTM C31/31M-12, *Standard Practice for Making and Curing Concrete Test Specimens in the Field*, and were 4 in. (102 mm) diameter by 8 in. (203 mm) tall cylinders. Cylinders were cured in the casting area in the same conditions as the push-off test specimens (covered in burlap and plastic and wetted two (2) times a day for 3-days) and were demolded within 2 days of casting. Cylinders were tested following ASTM C39/39M-12a, *Standard Test Method for Compressive Strength of Cylindrical Concrete Specimens*. For each cast, a 3-day, 28-day, and test-day compression cylinder tests were performed. The 3-day tests were 2141 psi (14.8 MPa) and 1634 psi (11.3 MPa) for cast 1 and cast 2, respectively. The 28-day results were 4083 psi (28.2 MPa) and 4536 psi (31.3 MPa) for cast 1 and cast 2, respectively. Note that the lab team only ground down the rough, lid portion of the compression cylinders and not the end that was inside of the test cylinder form. This potentially resulted in higher variance as the three tests completed for the 3-day and 28-day cylinders. These specimens did not meet the ASTM specifications within acceptable variance. When both sides were ground for the other cylinders, the specimens fit within the acceptable variance as stated by ASTM C39/39M.

Table 4.7 shows the concrete compressive strengths at time of testing for each the top and bottom casts.

Table 4.5: Concrete mixture proportions per cubic yard (meter)

Sample	W/(C+P)	*Coarse agg. lbs (kg)	Fine agg. 1 lbs (kg)	Fine agg. 2 lbs (kg)	Cement lbs (kg)	Fly ash lbs (kg)	Water lbs (kN)	Ad. Mix. (WRDA-64) oz (g)
Side 1	0.489	1223 (554.8)	1608 (729.2)	273.8 (124.2)	509 (231)	90 (40.8)	175.7 (79.7)	24 (680.4)
Side 2	0.490	1195 (542.2)	1571 (712.5)	272.3 (123.5)	506 (230)	90.2 (40.9)	184.9 (83.9)	24 (680.4)

*Maximum aggregate size of 3/8 in. (9.5 mm)

Table 4.6: Fresh concrete characteristics

Sample	Slump, in (mm)	Air voids, %	Unit weight, pcf ($kg \cdot m^{-3}$)
Side 1	3.75 (95.2)	4.30	141 (2261)
Side 2	6.00 (152.4)	2.85	143 (2284)

Table 4.7: Concrete compressive strength at time of shear specimen testing, psi (MPa)

x	4G60-x		4G80-x		5G60-x		5G80-x	
	Bottom	**Top**	**Bottom**	**Top**	**Bottom**	**Top**	**Bottom**	**Top**
1	5179 (35.7)	4481 (30.9)	5815 (40.1)	4372 (30.1)	5169 (35.6)	4578 (31.6)	5169 (35.6)	4578 (31.6)
2	5179 (35.7)	4481 (30.9)	5028 (34.7)	4198 (28.9)	5169 (35.6)	4578 (31.6)	5257 (36.2)	4149 (28.6)
3	5028 (34.7)	4198 (28.9)	5028 (34.7)	4198 (28.9)	5257 (36.2)	4149 (28.6)	5257 (36.2)	4149 (28.6)
4	5028 (34.7)	4198 (28.9)	5028 (34.7)	4198 (28.9)	5257 (36.2)	4149 (28.6)	5257 (36.2)	4149 (28.6)
5	5028 (34.7)	4198 (28.9)	5028 (34.7)	4198 (28.9)	5257 (36.2)	4149 (28.6)	5257 (36.2)	4149 (28.6)

*No compression cylinder tests were performed within 72 hours of test. Closest compression test was used.

5.0 EXPERIMENTAL RESULTS

5.1 INTRODUCTION

Test results from the push-off test specimens are presented in this chapter. The test matrix and details and experimental procedures can be found in Chapter 3. Graphically, the shear load versus the shear displacement, horizontal crack width, and strain gauge readings are shown in Sections 5.2 and 5.3.

Figure 5.1 illustrates the main variables reported in the tests. These include: (i) the interface shear displacement at maximum interface shear force, Δ_{ult}; (ii) the maximum interface shear force, V_{ult}; (iii) the minimum sustained interface shear force, $V_{sus,min}$; (iv) the maximum sustained interface shear force, $V_{sus,max}$; (v) the interface shear force observed at first bar fracture, V_b; (vi) and the interface shear displacement at first bar fracture, Δ_b. Tables listing these values are provided in sections 5.2 and 5.3.

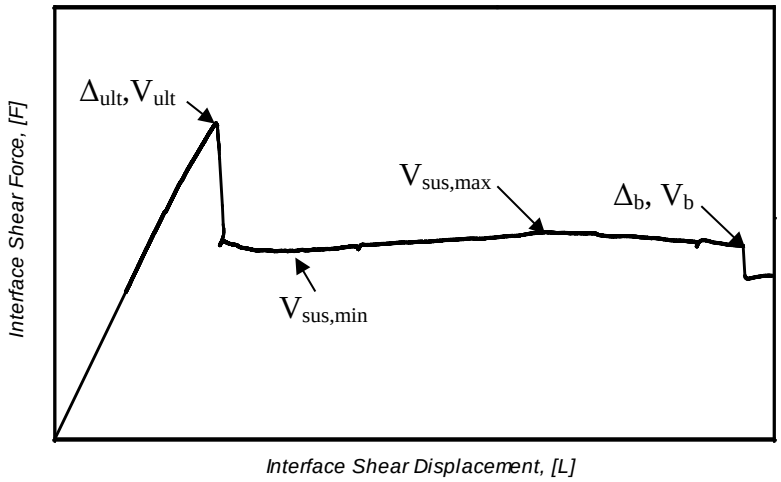

Figure 5.1: Illustration of test result parameters

Figure 5.2a and 5.2b illustrate the interface shear force at initiation of cracking, $V_{cr,}$ versus the reinforcing steel strain across the interface and the crack width, respectively. This is illustrated to show V_{cr} and strain, and crack width at peak load as well as the value at which the interface shear force is at its maximum. Detailed quantitative measured and post-processed data are provided in the tables in sections 5.2 and 5.3.

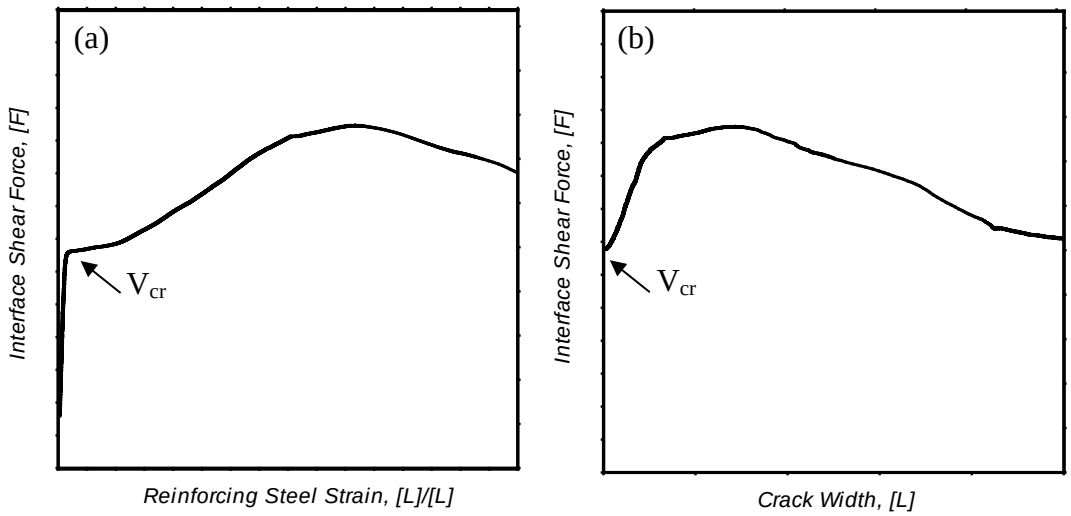

(a) (b)

Figure 5.2: Initiation of cracking definition: (a) Interface shear force versus reinforcing steel strain and (b) interface shear force versus crack width

5.2 PUSH-OFF TESTS: SPECIMEN CONTAINING #4 (#13M) REINFORCING BARS ACROSS THE INTERFACE RESULTS

This section shows the experimental results for the specimens containing #4 (#13M) reinforcing bars across the interface.

5.2.1 Interface Shear Force versus Interface Shear Displacement

The interface slip is important to understanding the interface shear force-interface shear displacement relation of the interface and thus the overall interaction of concrete cohesion, aggregate interlock, and dowel action. The displacement in the plane of the interface along the direction of the application of the load was computed using the four string potentiometers that were parallel to the shear interface. Figure 5.3 and Figure 5.4 show the average of the four string potentiometers taken as the interface shear displacement versus the interface shear force for the specimens containing #4 (#13M) reinforcing bars across the interface.

Figure 5.3 shows the interface shear force versus interface shear displacement relation for the 4G60 specimens. From 0 in. (0 mm) until around 0.05 in. (1.27 mm), the interface shear force versus interface shear displacement shows a mostly linear response until there is a reduction in stiffness before the peak interface shear force. After the peak interface shear force, the specimen interface slips and the interface shear force drops sharply. In some specimen results after the main interface shear force drop, discontinuities are observed at around 0.2 in. (5.1 mm) interface shear displacement. These interface shear load drops are believed to be due to an instantaneous loss of aggregate interlock. These are then followed by an immediate increase in stiffness and strength as the reinforcing steel bar dowel action engages. During the sustained shear capacity stage, which is the segment in which dowel action controls the response, there is a mildly positive slope due to the yielding and strain hardening of the reinforcing steel bars.

Figure 5.4 shows the interface shear force versus interface shear displacement relation for the 4G80 specimens. Overall, the shape of the interface shear force-interface shear displacement curve is similar for specimens 4G60 and 4G80, with the 4G80 specimens achieving larger peak interface shear forces. However, after the peak interface shear force both classes of specimens showed similar behavior regarding the sustained interface shear forces.

Table 5.1 and Table 5.2 show the 4G60 and 4G80 specimen shear test results, respectively. The shear stress at peak interface shear force, σ_{ult}, is the peak interface shear force divided by the area of the interface. Work done on the specimen before the first bar fracture, E_b, is calculated as the area under the interface shear force versus interface shear displacement curve to the first bar fracture. From the table, it can be seen that the coefficient of variation (COV) for all parameters was less than 10%, except for the interface shear displacement at first reinforcing bar fracture, Δ_b, and work done on the specimen before first reinforcing bar fracture, E_b. In addition, it is worth noting that the coefficient of variation for the parameters with a COV less than 10% is similar to the inherent material variability *(Mirza et al. 1979)*. In

Table 5.2, overall, the COV values are mostly at 10% or less, except for the interface shear displacement at the first reinforcing bar fracture, which was at 11%.

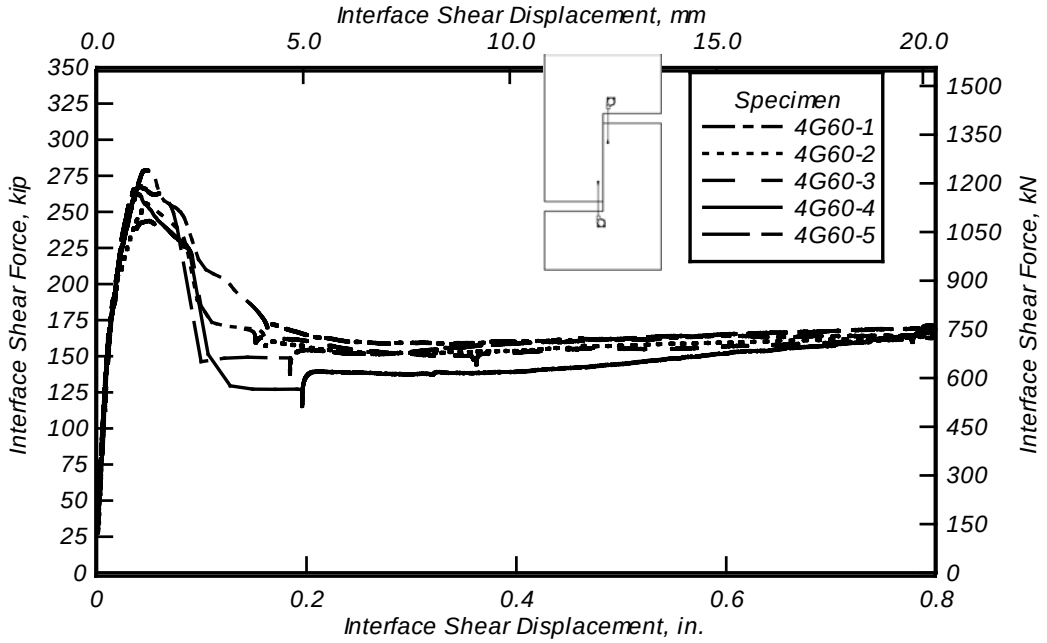

Figure 5.3: Interface shear force versus interface shear displacement for the 4G60 specimens

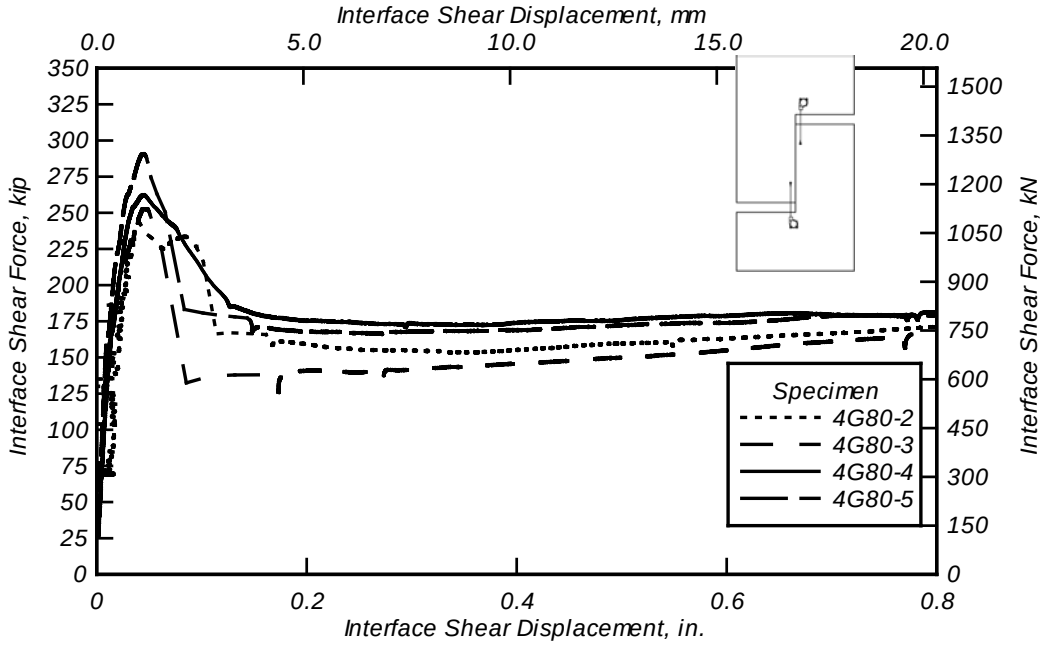

Figure 5.4: Interface shear force versus interface shear displacement for the 4G80 specimen

Table 5.1: 4G60 specimen shear test results

Specimen	**Δ_{ult}, in (mm)**	**V_{ult}, kip (kN)**	**σ_{ult}, ksi (MPa)**	**$V_{sus,min}$, kip (MPa)**	**$V_{sus,max}$, kip (MPa)**	**V_{cr}, kip (MPa)**	**V_b, kip (MPa)**	**Δ_b, in. (mm)**	**E_b, kip-ft (kJ)**
4G60-1	0.047 (1.20)	279.03 (1241.18)	726.64 (5009.98)	159.00 (707.27)	171.20 (761.54)	188.20 (837.16)	163.02 (725.15)	1.174 (29.81)	17.694 (23.990)
4G60-2	0.042 (1.06)	256.55 (1141.18)	668.09 (4606.32)	152.80 (679.69)	167.40 (744.63)	185.10 (823.37)	156.28 (695.17)	1.277 (32.44)	18.646 (25.280)
4G60-3	0.050 (1.26)	244.50 (1087.59)	636.72 (4390.02)	145.30 (646.33)	166.30 (739.74)	179.10 (796.68)	162.82 (724.27)	1.243 (31.57)	18.004 (24.410)
4G60-4	0.039 (0.98)	264.23 (1175.37)	688.11 (4744.34)	138.70 (616.97)	180.60 (803.35)	198.20 (881.64)	179.23 (797.27)	1.178 (29.93)	16.743 (22.700)
4G60-5	0.042 (1.07)	269.77 (1200.00)	702.53 (4843.75)	153.50 (682.80)	173.90 (773.55)	189.70 (843.83)	172.74 (768.37)	0.842 (21.39)	12.686 (17.200)
Mean	0.044 (1.12)	262.82 (1169.06)	684.42 (4718.88)	149.86 (666.61)	171.88 (764.66)	188.06 (836.53)	166.82 (742.05)	1.143 (29.03)	16.754 (22.716)
Median	0.042 (1.07)	264.23 (1175.37)	688.11 (4744.34)	152.80 (679.69)	171.20 (761.54)	188.20 (837.16)	163.02 (725.15)	1.178 (29.93)	17.694 (23.990)
Stdv	0.0045 (0.114)	13.115 (58.337)	34.153 (235.476)	7.918 (35.221)	5.740 (25.533)	6.974 (31.024)	9.092 (40.441)	0.1737 (4.412)	2.3755 (3.2208)
cov	10%	5%	5%	5%	3%	4%	5%	15%	14%

Table 5.2: 4G80 specimen shear test results

Specimen	Δ_{ult}, in (mm)	V_{ult}, kip (kN)	σ_{ult}, ksi (MPa)	$V_{sus,min}$, kip (MPa)	$V_{sus,max}$, kip (MPa)	V_{cr}, kip (MPa)	V_b, kip (MPa)	Δ_b, in. (mm)	E_b, kip-ft (kJ)
*4G80-1	0.032 (0.81)	232.80 (1035.55)	606.25 (4179.95)	N/A	N/A	158.70 (705.93)	N/A	N/A	N/A
4G80-2	**0.029 (0.73)	243.52 (1183.24)	634.17 (4372.45)	153.50 (682.80)	175.42 (780.31)	187.50 (834.04)	174.58 (776.58)	1.231 (31.27)	18.365 (24.900)
4G80-3	0.047 (1.19)	252.49 (1123.13)	657.52 (4533.47)	141.00 (627.20)	179.20 (797.12)	172.10 (765.54)	176.66 (785.81)	1.118 (28.40)	15.762 (21.370)
4G80-4	0.044 (1.13)	262.25 (1166.55)	682.94 (4708.74)	173.31 (770.92)	180.50 (802.90)	166.80 (741.96)	174.19 (774.82)	0.954 (24.24)	15.209 (20.620)
4G80-5	0.044 (1.12)	290.62 (1292.74)	756.82 (5218.10)	172.80 (768.65)	181.00 (805.13)	201.80 (897.65)	155.32 (690.89)	1.171 (29.75)	18.070 (24.500)
Mean	0.045 (1.14)	262.22 (1166.41)	682.87 (4708.19)	160.15 (712.39)	179.03 (796.37)	182.05 (809.80)	170.19 (757.02)	1.119 (28.42)	16.851 (22.848)
Median	0.044 (1.13)	257.37 (1144.84)	670.23 (4621.11)	163.15 (725.73)	179.85 (800.01)	179.80 (799.79)	174.38 (775.70)	1.145 (29.08)	16.916 (22.935)
Stdv	0.0015 (0.037)	20.419 (90.830)	53.176 (366.633)	15.750 (70.058)	2.523 (11.225)	15.825 (70.395)	9.970 (44.350)	0.1189 (3.020)	1.5983 (2.1670)
cov	3%	8%	8%	10%	1%	9%	6%	11%	9%

*Trial test. Post peak values not available.

**Inadvertently tested at higher strain rate. Δ_{ult} value not analyzed statistically.

5.2.2 Interface Shear Force versus Strain

Figure 5.5 and Figure 5.6 show the average of the strain measured with the four strain gauges located 3 in. (76 mm) from the interface for the 4G60 and 4G80 specimens, respectively. The strains were measured because they can be used to estimate the contribution of the reinforcing steel bars to the clamping force, which enhances aggregate interlock.

Figure 5.5 shows the interface shear force versus the average reinforcing steel microstrain relation for the 4G60 specimens. In this figure, it can be seen that the initial branch to approximately 100 to 200 microstrain is linear. At about 180 kips (800.7 kN), there is a clear change in slope, i.e. stiffness. With a shallower slope, the load increases mildly until the peak interface shear force is reached. A third post-peak softening branch is then observed. For the 4G60 specimens, the reinforcing steel microstrain surpasses both nominal yield strain (2070 microstrain for Grade 60 reinforcing steel) and the mean tested yield strain (2345 microstrain), after the peak interface shear force is reached. The irregularity in the 4G60-4 specimen at about 2800 microstrain is potentially a dynamic effect from the cohesion loss as it corresponds to the discontinuities discussed for Figure 5.3. The other specimens show this behavior at higher microstrains, not shown, that correspond to the discontinuities.

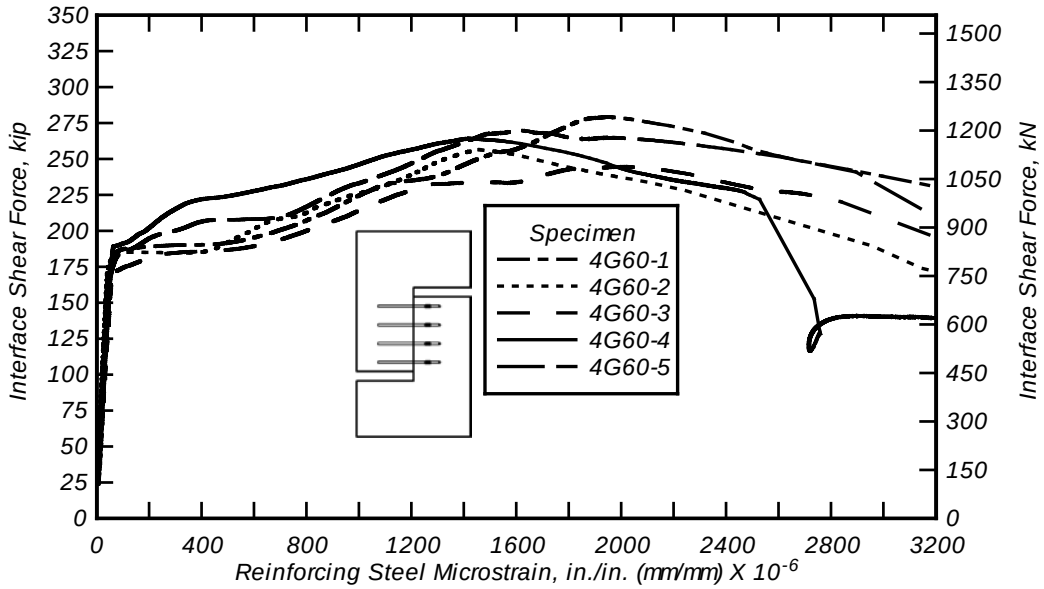

Figure 5.5: Interface shear force versus average reinforcing steel microstrain for the 4G60 specimens

Figure 5.6 shows the interface shear force versus the average reinforcing steel microstrain relation for the 4G80 specimens. For the 4G80 specimens, the reinforcing steel microstrain surpasses both the nominal yield strain (2760 microstrain for Grade 80 reinforcing steel) and the mean tested yield strain (3034 microstain), after the peak interface shear force. Overall, the 4G80 specimens had similar behavior to the 4G60 specimens.

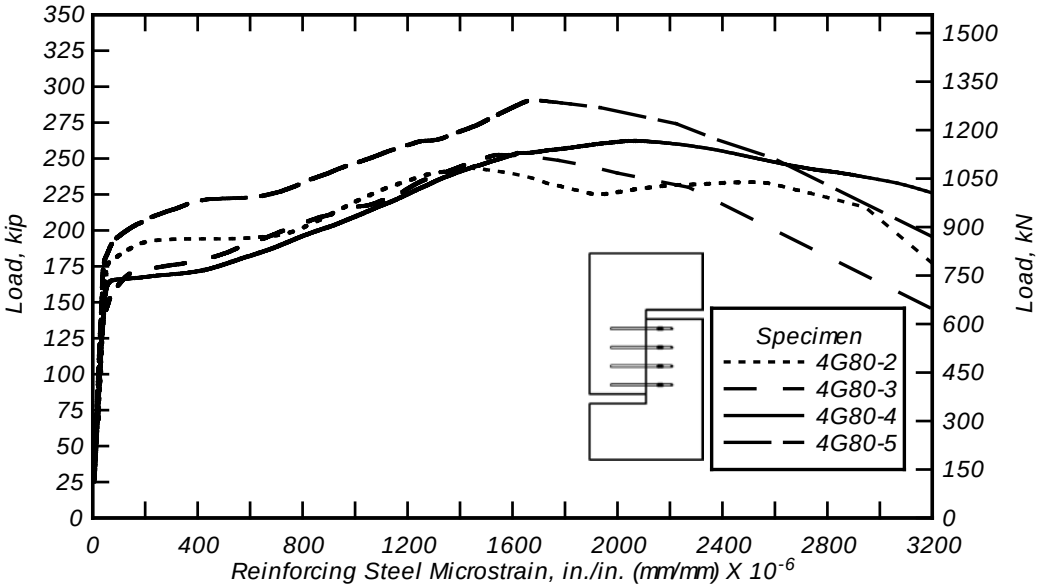

Figure 5.6: Interface shear force versus average reinforcing steel microstrain for the 4G80 specimens

Table 5.3 and Table 5.4 list the strain gauge readings at the peak interface shear force. Strain gauges, s_1-s_5, correspond to the strain gauges from the location on the shear interface closest to the actuator. For example, s_1 is the first strain gauge that is closest to the actuator and s_5 is the

furthest away. For both types of specimens, s_3 is the strain gauge that is located on the opposite U-bar leg 1 in. (25 mm) from the interface. In Table 5.3, all of the coefficients of variation are higher than 10%, except for the strain gauge 1 in. (25 mm) from the interface or s_3. For the 4G80 specimens (Table 5.4), all of the coefficients of variation are higher than 10%, except for the strain gauges s_2 and s_3.

Table 5.3: 4G60 specimen strain gauge readings at peak interface shear force

Specimen	s_1, in./in. (mm/mm)	s_2, in./in. (mm/mm)	s_3, in./in. (mm/mm)	s_4, in./in. (mm/mm)	s_5, in./in. (mm/mm)
4G60-1	0.0022	0.0022	0.0018	0.0019	0.0015
4G60-2	0.0017	0.0015	0.0015	0.0015	0.0012
4G60-3	0.0022	0.0021	0.0017	0.0022	0.0015
4G60-4	0.0019	0.0016	0.0014	0.0012	0.0010
4G60-5	0.0019	0.0019	0.0017	0.0016	0.0010
Mean	0.0020	0.0019	0.0016	0.0017	0.0012
Median	0.0019	0.0019	0.0017	0.0016	0.0012
Stdv	0.00024	0.00028	0.00013	0.00039	0.00027
cov	12%	15%	8%	23%	22%

Table 5.4: 4G80 specimen strain gauge readings at peak interface shear force

Specimen	s_1, in./in. (mm/mm)	s_2, in./in. (mm/mm)	s_3, in./in. (mm/mm)	s_4, in./in. (mm/mm)	s_5, in./in. (mm/mm)
*4G80-1	N/A	N/A	N/A	N/A	N/A
4G80-2	0.0015	0.0018	0.0017	0.0014	0.0009
4G80-3	0.0018	0.0018	0.0016	0.0015	0.0011
4G80-4	0.0032	0.0016	0.0014	0.0022	0.0013
4G80-5	0.0021	0.0019	0.0016	0.0016	0.0011
Mean	0.0022	0.0018	0.0016	0.0017	0.0011
Median	0.0020	0.0018	0.0016	0.0015	0.0011
Stdv	0.00073	0.00014	0.00010	0.00037	0.00015
cov	34%	8%	6%	22%	14%

5.2.3 Interface Shear Force versus Crack Width

Figure 5.7 and Figure 5.8 show the interface shear force versus crack width measured in the direction perpendicular to the interface for the 4G60 and 4G80 specimens, respectively. The positive average of the readings for the string potentiometers was assumed to be the approximate crack width. Crack width was monitored because of its relation to the strain of the reinforcing bars and the contribution of aggregate interlock.

Figure 5.7 shows the interface shear force versus crack width for the 4G60 specimens. In general, the curves exhibit a trilinear form. The first section until the peak interface shear load,

then the curve exhibits a softening branch followed by a decreasing section in the third section which exhibits a sustained interface shear load.

Figure 5.8 shows the interface shear force versus crack width for the 4G80 specimens. The specimens exhibit similar behavior as the 4G60 specimens.

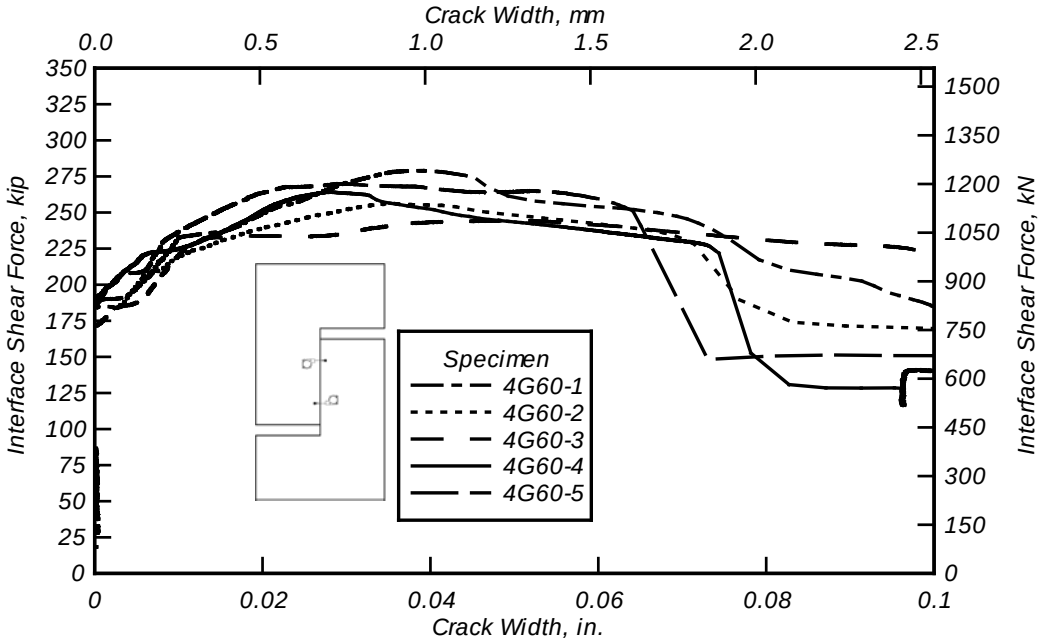

Figure 5.7: Interface shear force versus crack width for the 4G60 specimens

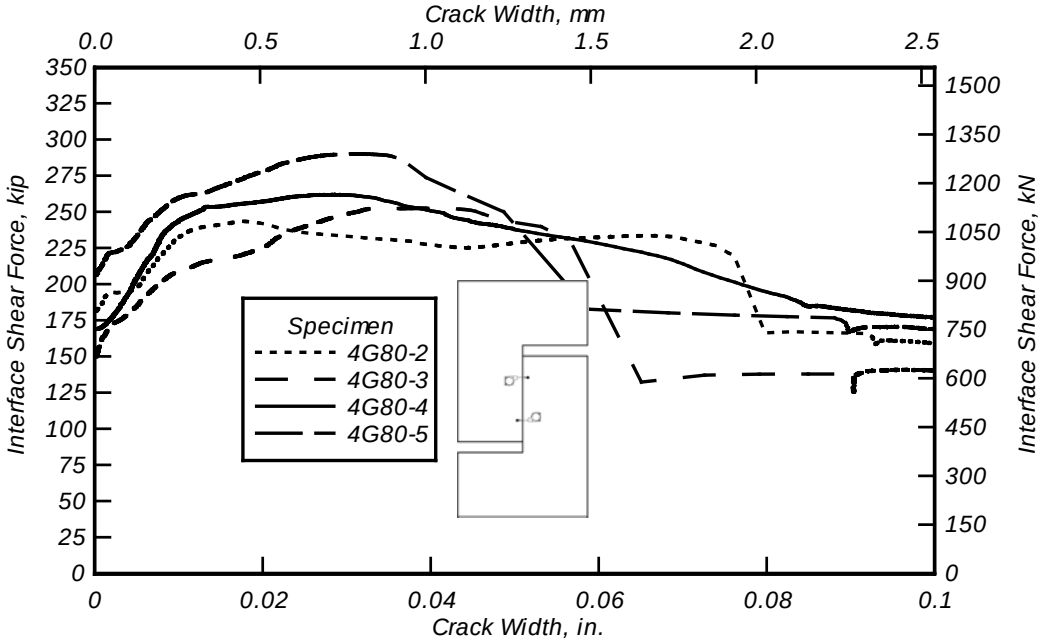

Figure 5.8: Interface shear force versus crack width for the 4G80 specimens

5.3 PUSH-OFF TESTS: SPECIMEN CONTAINING #5(#16M) REINFORCING BARS ACROSS THE INTERFACE RESULTS

This section shows the experimental results for the specimens containing #5 (#16M) reinforcing bars across the interface.

5.3.1 Interface Shear Force versus Interface Shear Displacement

Figure 5.9 and Figure 5.10 show the interface shear force versus the interface shear displacement for the 5G60 and 5G80 specimens, respectively. The specimens containing #5 (#16M) reinforcing bars across the interface were instrumented and measured using the same method as the specimens containing #4 (#13M) reinforcing bars across the interface.

Figure 5.9 shows the interface shear force versus the interface shear displacement for the 5G60 specimens. The general behavior is similar to what was observed for the specimens containing #4 (#13M) reinforcing bars across the interface. The peak interface shear force and sustained interface shear force is consistent, within a range of about 12 kip (53 kN). However, the 5G60-5 specimen showed sustained interface shear force values about 25 kip (111 kN) higher than the other specimens. Table 5.5 shows the 5G60 specimen shear test results. The COV for all parameters was below 10%, except for the interface shear displacement at the first reinforcing bar fracture, Δ_b, and work done on the specimen before first reinforcing bar fracture, E_b.

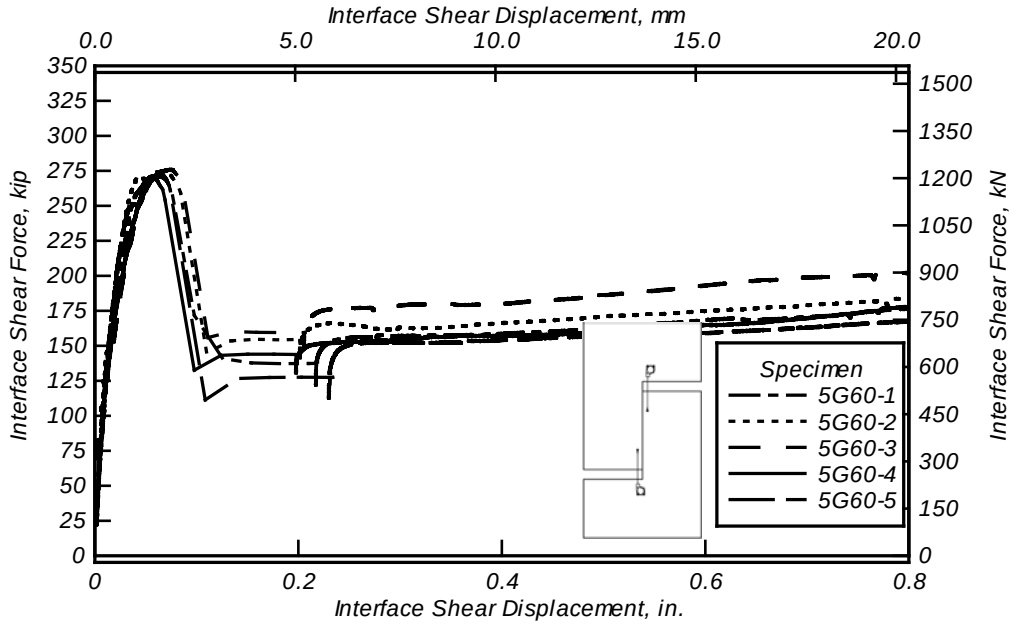

Figure 5.9: Interface shear force versus interface shear displacement for the 5G60 specimens

Table 5.5: 5G60 specimen shear test results

Specimen	$\Delta_{ult,}$ in (mm)	V_{ult}, kip (kN)	σ_{ult}, ksi (MPa)	$V_{sus,min}$, kip (MPa)	$V_{sus,max}$, kip (MPa)	V_{cr}, kip (MPa)	V_b, kip (MPa)	Δ_b, in. (mm)	E_b, kip-ft (kJ)
5G60-1	0.063 (1.60)	273.26 (1215.53)	948.83 (6541.95)	156.49 (696.10)	182.22 (810.55)	143.00 (636.31)	180.52 (802.97)	1.003 (25.46)	15.179 (20.580)
5G60-2	0.067 (1.71)	275.84 (1227.00)	957.78 (6603.66)	162.80 (724.17)	184.80 (822.03)	146.50 (651.66)	182.45 (811.59)	0.837 (21.25)	13.224 (17.930)
5G60-3	0.074 (1.88)	277.37 (1233.78)	963.08 (6640.17)	178.30 (793.12)	204.70 (910.55)	141.50 (629.42)	201.41 (895.92)	0.820 (20.83)	14.412 (19.540)
5G60-4	0.058 (1.49)	272.15 (1210.58)	944.96 (6515.29)	154.70 (688.14)	195.90 (871.41)	135.20 (601.40)	194.62 (865.73)	1.153 (29.28)	17.709 (24.010)
5G60-5	0.063 (1.60)	275.15 (1223.95)	955.40 (6587.23)	156.60 (696.59)	187.50 (834.04)	144.70 (643.66)	184.94 (822.65)	1.457 (37.02)	22.201 (30.100)
Mean	0.065 (1.66)	274.75 (1222.17)	955.30 (6586.59)	161.78 (719.62)	191.02 (849.72)	142.18 (632.45)	188.79 (839.77)	1.054 (26.77)	16.545 (22.432)
Median	0.063 (1.60)	275.15 (1223.95)	955.30 (6587.23)	156.60 (696.59)	187.50 (834.04)	143.00 (636.10)	184.94 (822.65)	1.003 (25.46)	15.179 (20.580)
Stdv	0.0059 (0.149)	2.072 (9.216)	7.604 (52.427)	9.733 (43.293)	9.212 (40.979)	4.326 (19.244)	8.899 (39.586)	0.2631 (6.684)	3.5631 (4.8309)
cov	9%	1%	1%	6%	5%	1%	5%	25%	22%

Figure 5.10 shows the interface shear force versus the interface shear displacement for the 5G80 specimens. The overall behavior is similar to the 5G60 specimens. However, the interface shear force is greater for all portions of the test for the 5G80 specimens than the 5G60 specimens at and beyond the interface shear displacement corresponding to the peak interface shear force. The 5G80 specimens show strong correlation during the sustained interface shear force, meeting a range of about 25 kip (111 kN). Table 5.6 shows the 5G80 specimen shear test results. Overall, all COV values are less than 10%.

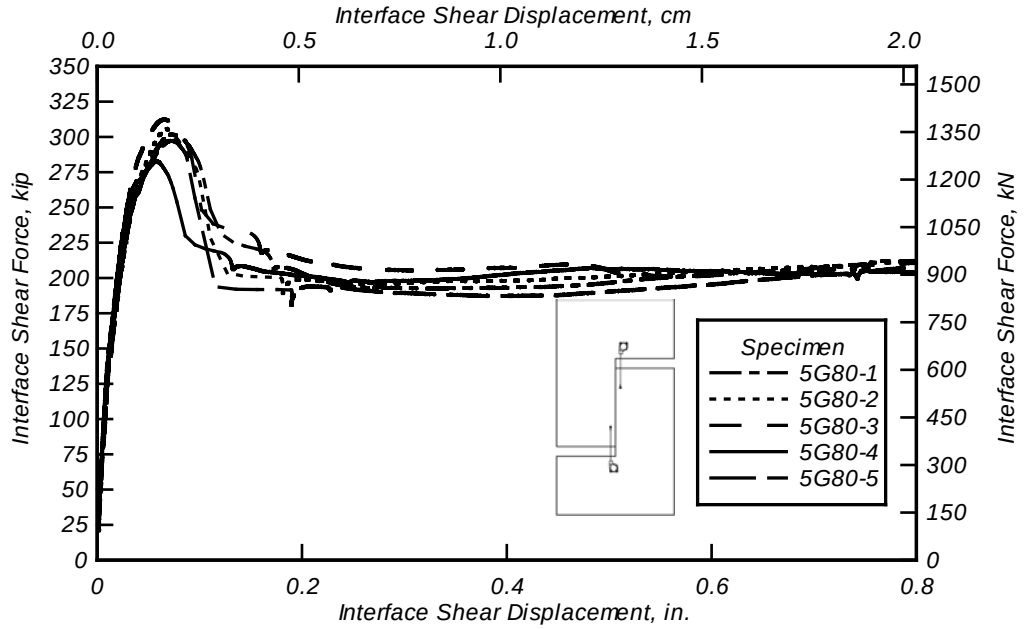

Figure 5.10: Interface shear force versus interface shear displacement for the 5G80 specimens

Table 5.6: 5G80 specimen shear test results

Specimen	Δ_{ult}, in (mm)	V_{ult}, kip (kN)	σ_{ult}, ksi (MPa)	$V_{sus,min}$, kip (MPa)	$V_{sus,max}$, kip (MPa)	V_{cr}, kip (MPa)	V_b, kip (MPa)	Δ_b, in. (mm)	E_b, kip-ft (kJ)
5G80-1	0.072 (1.84)	301.71 (1342.06)	1047.60 (7222.93)	192.80 (857.62)	218.80 (973.27)	145.10 (645.44)	214.77 (955.34)	1.178 (29.93)	21.552 (29.220)
5G80-2	0.068 (1.73)	305.67 (1359.70)	1061.37 (7317.86)	195.90 (871.41)	211.30 (939.91)	150.70 (670.35)	202.11 (899.03)	0.997 (25.32)	18.446 (25.010)
5G80-3	0.065 (1.66)	312.41 (1389.69)	1084.77 (7479.25)	201.00 (894.09)	215.60 (959.04)	148.20 (659.23)	215.59 (959.01)	1.004 (25.51)	19.213 (26.050)
5G80-4	0.058 (1.46)	282.66 (1257.33)	981.45 (6766.87)	197.60 (878.97)	207.00 (920.78)	138.70 (616.97)	198.13 (881.33)	1.008 (25.61)	18.469 (25.040)
5G80-5	0.073 (1.86)	297.24 (1322.19)	1032.08 (7115.94)	187.30 (833.15)	215.00 (956.37)	135.90 (604.51)	203.26 (904.13)	1.104 (28.04)	19.811 (26.860)
Mean	0.067 (1.71)	299.94 (1334.19)	1039.92 (7169.98)	194.92 (867.05)	213.54 (949.87)	143.72 (639.30)	206.77 (919.77)	1.058 (26.88)	19.498 (26.436)
Median	0.068 (1.73)	301.71 (1342.06)	1047.60 (7222.93)	195.90 (871.41)	215.00 (956.37)	145.10 (645.44)	203.26 (904.13)	1.008 (25.61)	19.213 (26.050)
Stdv	0.0063 (0.159)	11.153 (49.612)	44.541 (307.102)	5.188 (23.078)	4.523 (20.120)	6.266 (27.872)	7.915 (35.208)	0.0801 (2.034)	1.2808 (1.7365)
cov	9%	4%	4%	3%	2%	2%	4%	8%	7%

5.3.2 Interface Shear Force versus Strain

Figure 5.11 and Figure 5.12 show the average of the strain measured by three strain gauges located 3 in. (76 mm) from the interface for the 5G60 and 5G80 specimens, respectively. The strains were measured because they can be used to estimate the contribution of the reinforcing steel bars to the clamping force, which enhances aggregate interlock.

Figure 5.11 shows the interface shear force versus the average reinforcing steel microstrain relation for the 5G60 specimens. In this figure, it can be seen that the initial branch of the curve is linear up to 100-200 microstrain. At about 140 kip [623 kN], there is a clear change in stiffness. With a shallower slope, the load increases until the peak interface shear force is reached. A third branch post-peak softening branch can be seen. It is also seen that the peak interface shear force happens after the 2241 microstrain (tested yield strain value) limit for the Grade 60 ksi [550 MPa] reinforcing steel nominal yield stress.

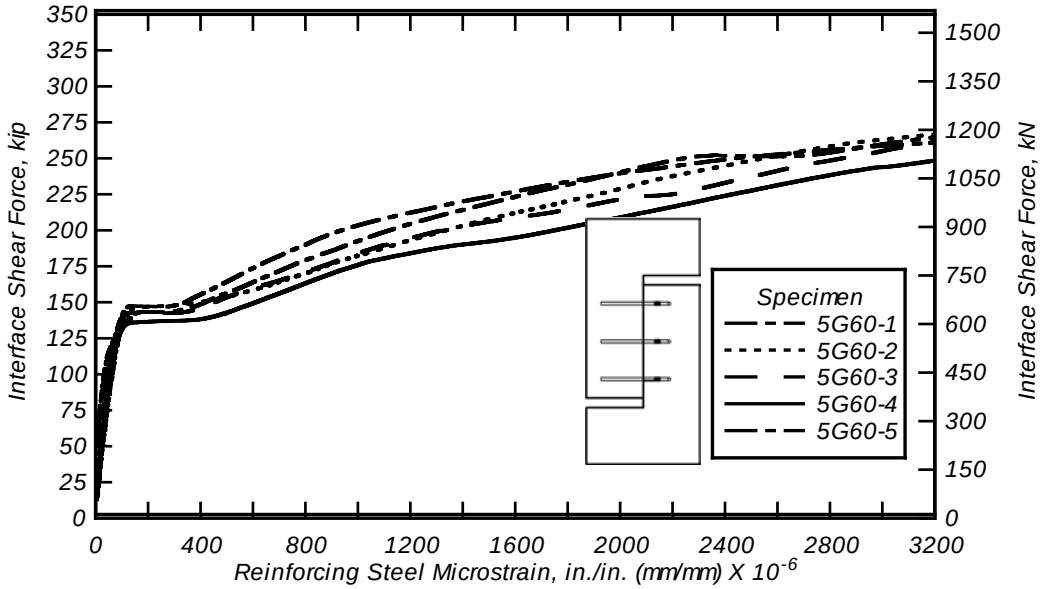

Figure 5.11: Interface shear force versus average reinforcing steel microstrain for the 5G60 specimens

Figure 5.12 shows the interface shear force versus average reinforcing steel microstrain relation for the 5G80 specimens. For the 5G80 specimens, the reinforcing steel microstrain surpasses the nominal yield strain, which is 2966 microstrain for Grade 80 (550) reinforcing steel, before the peak interface shear force. Overall, the 5G80 specimens had similar behavior to the 5G60 specimens.

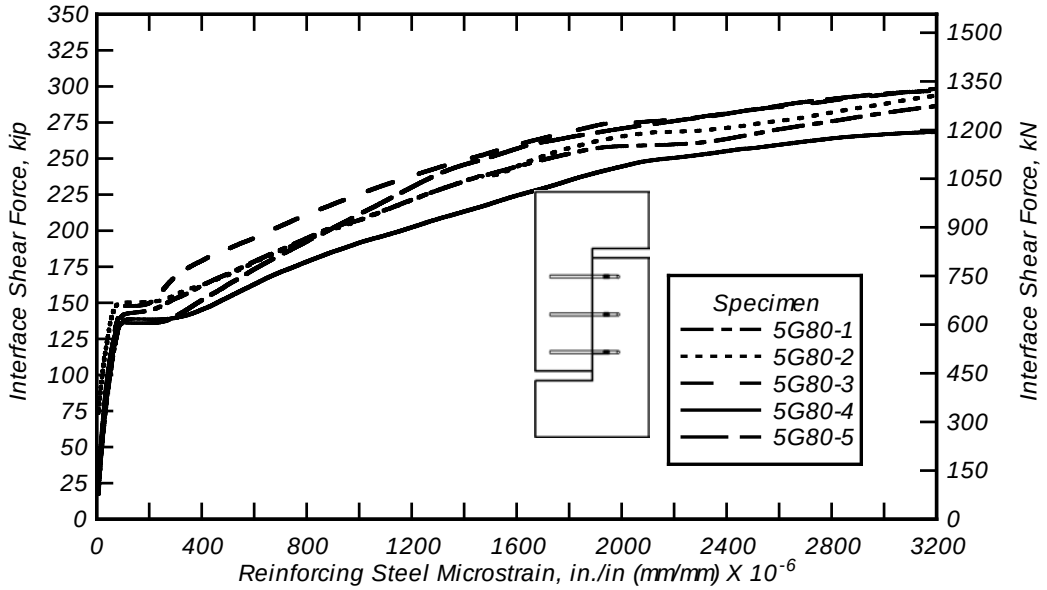

Figure 5.12: Interface shear force versus average reinforcing steel microstrain for the 5G80 specimens

Table 5.7 and Table 5.8 list the strain gauge readings at peak interface shear force for the 5G60 and 5G80 specimens, respectively. Table 5.7 shows the 5G60 specimen strain gauge readings at the peak interface shear force. It can be seen that the bars near the center of the interface (s_2) have larger strain, which can be associated with the fact that these have a larger tributary area than the end bars. In addition, it can also be seen from this table that all of the COV values are higher than 10%, except for the strain gauge 1 in. [25 mm] from the interface or s_3 and s_1 for the 5G60 specimens.

Table 5.8 shows the 5G80 specimen strain gauge readings at the peak interface shear force. All of the coefficients of variation are higher than 10%, except for the strain gauge 1 in. (25 mm) from the interface or s_3.

Table 5.7: 5G60 specimen strain gauge readings at peak interface shear force

Specimen	s_1, in./in. (mm/mm)	s_2, in./in. (mm/mm)	s_3, in./in. (mm/mm)	s_4, in./in. (mm/mm)
5G60-1	0.00549	0.00725	0.00233	0.00393
5G60-2	0.00595	0.00685	0.00255	0.00470
5G60-3	0.00536	0.00522	0.00290	0.00498
5G60-4	0.00577	0.00585	0.00274	0.00360
5G60-5	0.00561	0.00710	0.00233	0.00501
Mean	0.00564	0.00620	0.00257	0.00444
Median	0.00561	0.00585	0.00255	0.00470
Stdv	0.00023	0.00083	0.00025	0.00064
cov	4%	13%	10%	14%

Table 5.8: 5G80 specimen strain gauge readings at peak interface shear force

Specimen	s_1, in./in. (mm/mm)	s_2, in./in. (mm/mm)	s_3, in./in. (mm/mm)	s_4, in./in. (mm/mm)
5G80-1	0.00452	0.00461	0.00272	0.00357
5G80-2	0.00332	0.00569	0.00252	0.00330
5G80-3	0.00504	0.00526	0.00279	0.00314
5G80-4	0.00485	0.00593	0.00287	0.00340
5G80-5	0.00379	0.00350	0.00282	0.00264
Mean	0.00430	0.00500	0.00274	0.00321
Median	0.00561	0.00585	0.00274	0.00470
Stdv	0.00073	0.00098	0.00014	0.00035
cov	17%	20%	5%	11%

5.3.3 Interface Shear Force versus Crack Width

Figure 5.13 and Figure 5.14 show the interface shear force versus crack width measured in the direction perpendicular to the interface for the 5G60 and 5G80 specimens, respectively.

Figure 5.13 shows the interface shear force versus crack width for the 5G60 specimens. In general, the curves exhibit a general trilinear form after cracking. The first section occurs up until the peak interface shear load, then the curve exhibits a softening branch followed by a decreasing section in the third section which exhibits a sustained interface shear load.

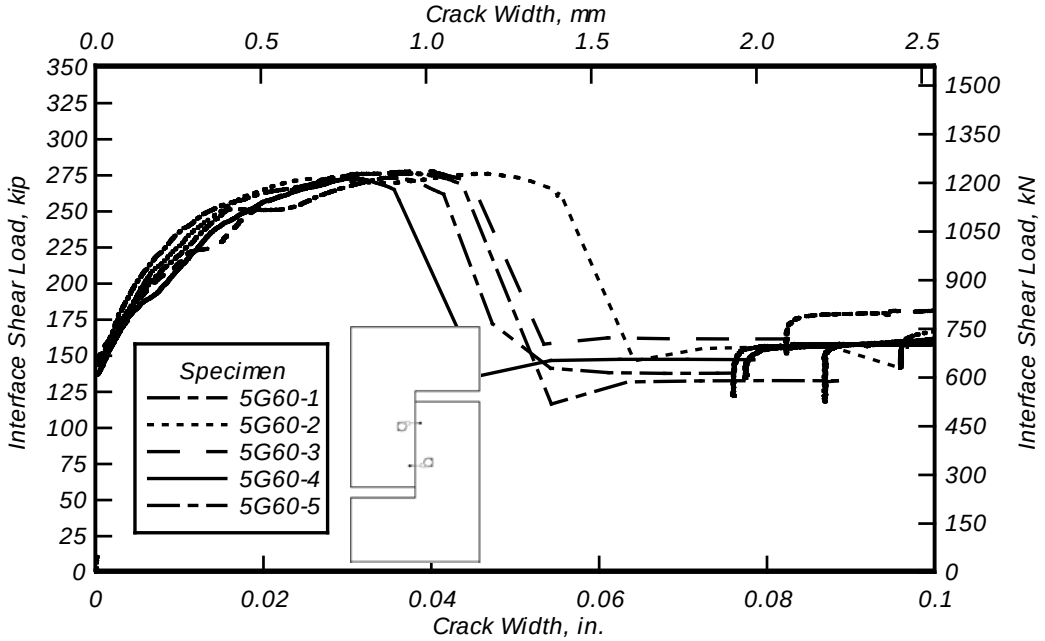

Figure 5.13: Interface shear force versus crack width for the 5G60 specimens

Figure 5.14 shows the interface shear force versus crack width for the 5G80 specimens. The specimens have similar behavior to the 5G60 specimens.

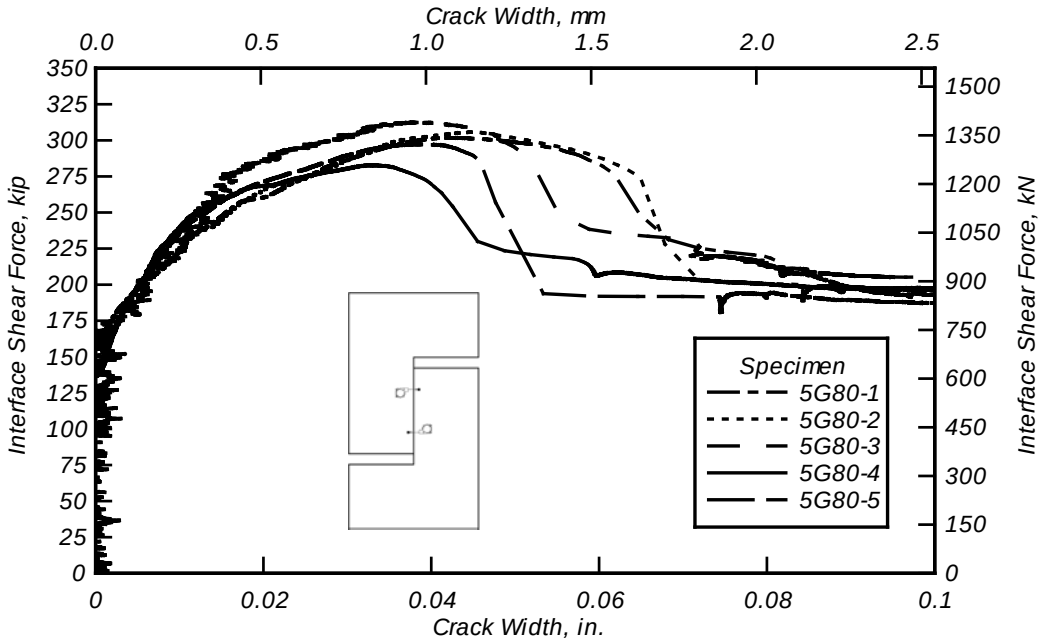

Figure 5.14: Interface shear force versus crack width for the 5G80 specimens

5.4 DISCUSSION RESULTS

5.4.1 Comparison of Specimens Containing #4 (#13M) Reinforcing Bars across the Interface

This section compares the results from the 4G60 and 4G80 specimens.

Figure 5.3 and Figure 5.4 show the interface shear force versus interface shear displacement charts for the 4G60 and 4G80 specimens. The 4G60 and 4G80 specimens show similar response under loading, although the 4G80 specimens show higher sustained interface shear force.

The following is a discussion from the Table 5.1 and Table 5.2 results for the 4G60 and 4G80 specimens, respectively. The interface shear displacement at the peak interface shear stress, Δ_{ult}, was very similar for both types of specimens. The peak interface shear stresses, σ_{ult}, of the specimens were similar, though the results for the 4G60 specimens had 7% lower COV values in the repetitions than the results for the 4G80 specimen repetitions. The higher variability in the repetitions of the 4G80 specimen results may be attributed to the interaction of the HSS with the concrete.

The minimum sustained interface shear force and the maximum sustained interface shear force are higher for the 4G80 specimens, which are expected due to the greater yield stress of the reinforcing bars. The greater yield stress would increase the dowel action resistance of the interface reinforcing bars for any dowel action mode. The initiation of cracking, V_{cr}, median was about 6 kip (27 kN) higher for the 4G60 specimens than the 4G80 specimens, though both types had similar peak interface shear forces. The interface shear force at first bar fracture was higher for the 4G80 specimens, which is consistent with the increased maximum shear interface shear force from the Grade 80 (550) reinforcing steel. Work done on the specimen for both the 4G60

and 4G80 specimens and their respective COV were both around 12%. In addition, the average of the interface shear displacement at the first reinforcing bar fracture was within 0.025 in. (0.635 mm), indicating a similar behavior. This finding was unexpected as the Grade 80 ksi (550 MPa) reinforcing steel has a lower material ultimate strain than the Grade 60 ksi (410 MPa) reinforcing steel. Local fracturing of the concrete for the higher yield steel may be enabling a longer length, thus allowing more stretch for the strain limit.

Figure 5.5 and Figure 5.6 showed the relation between the interface shear force versus the reinforcing steel microstrain for the 4G60 and 4G80 specimens, respectively. The figures use data from the strain gauges 3 in. (76 mm) from the interface. It is shown in these figures that the initiation of cracking is also the initiation of a sudden increase in the strain of the interface reinforcing bars. It is also seen graphically that the peak interface shear force happens before the 2345 microstrain tested yield limit for the Grade 60 ksi (420 MPa) steel nominal yield stress and the 3034 microstrain tested yield limit for the Grade 80 ksi (550 MPa) steel nominal yield stress. Neither grade of steel reached the strain corresponding to the specified nominal yield stress. The strain that the reinforcing bars did obtain at peak interface shear force corresponded to a stress of about 45 ksi [310 MPa] of stress for both grades.

Table 5.3 and Table 5.4 showed the strain at the peak interface shear force for the 4G60 and 4G80 specimens, respectively. It is noted that there are many strain gauges with COV values greater than 10% in the strain at peak interface shear force for the 4G60 and 4G80 specimens. The average strain levels in the strain gauges 1 in. (25 mm) from the interface for the 4G60 and 4G80 specimens did not reach strain corresponding to Grade 60 (420) steel yield stress before the peak interface shear force.

Figure 5.7 and Figure 5.8 show the relation between the interface shear force versus crack width for the 4G60 and 54G80 specimens, respectively. It can be seen that the 4G60 specimens are more consistent than the 4G80 specimens and that the peak interface shear force is sustained for a greater interface shear displacement. This may be from the increased ductility of the Grade 60 (420 MPa) reinforcing bars or from the HSS reinforcing bars fracturing the concrete locally.

5.4.2 Comparison of Specimens Containing #5 (#16M) Reinforcing Bars across the Interface

This section compares the results from the 5G60 and 5G80 specimens.

Figure 5.9 and Figure 5.10 show the interface shear force versus interface shear displacement charts for the 5G60 and 5G80 specimens, respectively. The 5G60 and 5G80 specimens show similar response under loading, although the 5G80 specimens show higher sustained interface shear force and peak interface shear force.

The following is a discussion of Table 5.5 and Table 5.6 for the 5G60 and 5G80 specimens, respectively. The interface shear displacement at the peak interface shear stress, Δ_{ult}, was very similar for both types of specimens. The mean peak interface shear stresses, σ_{ult}, of the specimens were around 85 psi (0.6 MPa) higher for the 5G80 specimens than the 5G60 specimens. The 5G80 specimens showed a higher COV than the 5G60 specimens for the peak interface shear force, V_u. This higher variability in the repetitions of the 5G80 specimen results

may be attributed to the interaction of the HSS reinforcement with the concrete. However, a difference in COV of 3% is within the inherent material variability *(Mirza et al. 1979)*.

The minimum sustained interface shear force and the maximum sustained interface shear force are higher for the 5G80 specimens, which are expected due to the greater yield stress of the reinforcing bars. The greater yield stress would increase the dowel action resistance of the interface reinforcing bars for any dowel action mode. The median of the initiation of cracking, V_{cr}, was about 2 kip (9 kN) higher for the 5G60 specimens than the 5G80 specimens, even though the 5G80 specimens had significantly higher peak interface shear forces. This indicates that the reinforcement grade had minimal effect on the initiation of concrete-concrete cohesion loss. The interface shear force at first bar fracture was higher for the 5G80 specimens, which is consistent with the increased maximum sustained interface shear force from the Grade 80 (550) reinforcing steel. Work done on the specimen before first reinforcing bar fracture, E_b, for the 5G60 specimens was about 3 kip-ft (4 kJ) lower than the 5G80 specimens. This is a reasonable finding as the 5G80 specimens had higher peak and sustained interface shear forces. The 5G60 specimens had much more variation in the work done before the first reinforcing bar fracture as the COV was about 15% higher than the 5G80 specimens. It is unknown why this occurred, although it may be related to the greater material ultimate strain values of the reinforcing steel across the interface in the 5G80 specimens. In addition, the average of the interface shear displacement at the first reinforcing bar fracture was within 0.004 in. (0.01 mm), indicating a similar behavior. This is unexpected as the Grade 80 ksi (550 MPa) reinforcing steel has a lower material ultimate strain than the Grade 60 ksi (410 MPa) reinforcing steel. Local fracturing of the concrete for the higher yield steel may be enabling a longer unrestrained length, thus allowing more displacement before the strain at fracture for the reinforcing steel is reached.

Figure 5.11 and Figure 5.12 show the relation between the interface shear force versus the reinforcing steel microstrain for the 5G60 and 5G80 specimens, respectively. The figures use data from the strain gauges 3 in. (76 mm) from the interface. It is shown in these figures that the initiation of cracking is also the initiation of a sudden increase in the strain of the interface reinforcing bars. It is also illustrated in these figures that the peak interface shear force occurs after strain corresponding to Grade 60 ksi (420 MPa) steel nominal yield stress (2241 microstrain tested yield strain) and Grade 80 ksi (550 MPa) steel nominal yield stress (2966 microstrain tested yield strain). Both grades of steel are strained to levels corresponding to stress that is higher than their nominal grade for the strain gauges 3 in. (76 mm) from the interface.

Table 5.7 and Table 5.8 showed the strain at the peak interface shear force for the 5G60 and 5G80 specimens, respectively. It is noted that there are many strain gauges with coefficients of variation higher than 10% in the strain at peak interface shear force for the 5G60 and 5G80 specimens. The average strain levels in the strain gauges 1 in. (25 mm) from the interface, s_3, for the 5G60 and 5G80 specimens reached strain corresponding to Grade 60 (420) steel yield stress before the peak interface shear force. However, the average values did not reach strain corresponding to Grade 80 (550) steel yield stress.

Figure 5.13 and Figure 5.14 show the relation between the interface shear force versus crack width for the 5G60 and 5G80 specimens, respectively. It can be seen that the 5G80 specimen peak interface shear forces are sustained for a greater interface shear displacement. This is likely due to the Grade 80 (550) reinforcing bars having a higher yield stress than the Grade 60 (420)

reinforcing bars; the interface system stiffness is sustained for more of the crack width as there is more resistance before strain hardening of the material.

5.4.3 Comparison of Specimens Containing #4 (#13M) Reinforcing Bars across the Interface and Specimens Containing #5 (#16M) Reinforcing Bars across the Interface

This section compares the specimens containing #4 (#13M) reinforcing bars across the interface to the specimens containing #5 (#16M) reinforcing bars across the interface. Overall, both the Grade 60 ksi (420 MPa) and the Grade 80 ksi (550 MPa) reinforcing bars achieved comparable behavior, though the higher yield stress specimens did have more scatter in the results.

The peak interface shear load and stress, V_{ult} and σ_{ult}, of the 5G80 specimens were about 15 kips (67 kN) higher than the 5G60 specimens, indicating that the higher yield stress reinforcing bars were effective at increasing the shear friction resistance of the interface. However, this was not the case for the specimens containing #4 (#13M) reinforcing bars across the interface, which exhibited similar peak shear stresses and loads for both grades of reinforcing steel. The peak shear load and stress, V_{ult} and σ_{ult}, for the 5G60 and 5G80 specimens were consistently higher than the 4G60 and 4G80 specimens, even though they all were designed to have similar capacities. Because all 20 specimens were cast at the same time to reduce the variability in concrete strength, results seem to indicate that the rebar size may contribute to this increased strength. However, because the specimens containing #5 (#16M) reinforcing bars across the interface also had the debonded area, the debonding may not have been fully effective and may have contributed to some of this difference.

The minimum and maximum sustained shear loads, $V_{sus,min}$, and $V_{sus,max}$ respectively, are higher for the Grade 80 (550) specimens than for the Grade 60 (420) specimens. This is consistent with the greater dowel action resistance that would be present for the higher yield stress reinforcing steel.

The initiation of cracking, V_{cr}, is comparable for each set, indicating that, at least for varying grades at a constant reinforcement ratio, V_{cr} is most likely controlled by concrete cohesion rather than the reinforcement parameter.

The shear load at fracture of the first reinforcing bar, V_b, was higher for the Grade 80 (550) specimens, which is again expected because of the higher yield stress reinforcing steel. The displacement at first bar fracture, Δ_b, was relatively consistent for each set, which is unexpected as each type of reinforcing steel had varying ultimate strain properties.

The work done on the specimen, E_b, was consistent for all sets except for the 5G80 specimen, which exhibited higher values. The consistency of E_b may be from the similarity of the design parameters of each set. Because the 5G80 specimens achieved a higher peak interface shear stress and sustained interface shear load than the other three groups, the work done before first bar fracture is increased.

Figure 5.15 shows the average strain gauge readings for all specimens with +/- 1 standard deviation shown. Points labeled in this figure with a "+" correspond to half of peak interface

shear force values and points labeled with an “x” correspond to peak interface shear force values. Note, shear interface at 12 in. (~300 mm) corresponds to the center of the horizontal interface and the locations of the “+” and “x” points represent the location of the U-bars within that interface. This figure shows the results for the strain gauges 3 in. (76 mm) from the interface. The specimens containing #4 (#13M) reinforcing bars across the interface do not reach strain corresponding to the 60 ksi (420 MPa) nominal yield stress before the peak interface shear force. However, the specimens containing #5 (#16M) reinforcing bars across the interface reach strain corresponding to 80 ksi (550 MPa) nominal yield stress. The measured strain of the strain gauges 3 in. (76 mm) from the interface were greater in magnitude and this may be from their location on the inside of the U-bar bend. This location may have had bending effects on the strain gauges. This effect was assumed minimal on the strain gauges 1 in. (25 mm) from the interface as discussed in Section 5.4.2.

Figure 5.16 shows the strain at peak shear load for the s_3 gauges. The ε_{60} corresponds to the strain at approximately 60 ksi (420 MPa) and ε_{80} corresponds to the strain at approximately 80 ksi (550 MPa). It can be seen that the 4G60 and 4G80 specimens achieved a strain corresponding to about 45 ksi (310 MPa). In addition, the 5G60 specimens reached a strain corresponding to roughly 70 ksi (480 MPa) and the 5G80 specimens reached a strain corresponding to about 80 ksi (550 MPa).

The curves in Figure 5.17 through Figure 5.19 are averages for each specimen set. The figures were created by taking data points from adjusted corresponding interface shear displacement string potentiometer values for each specimen in a series.

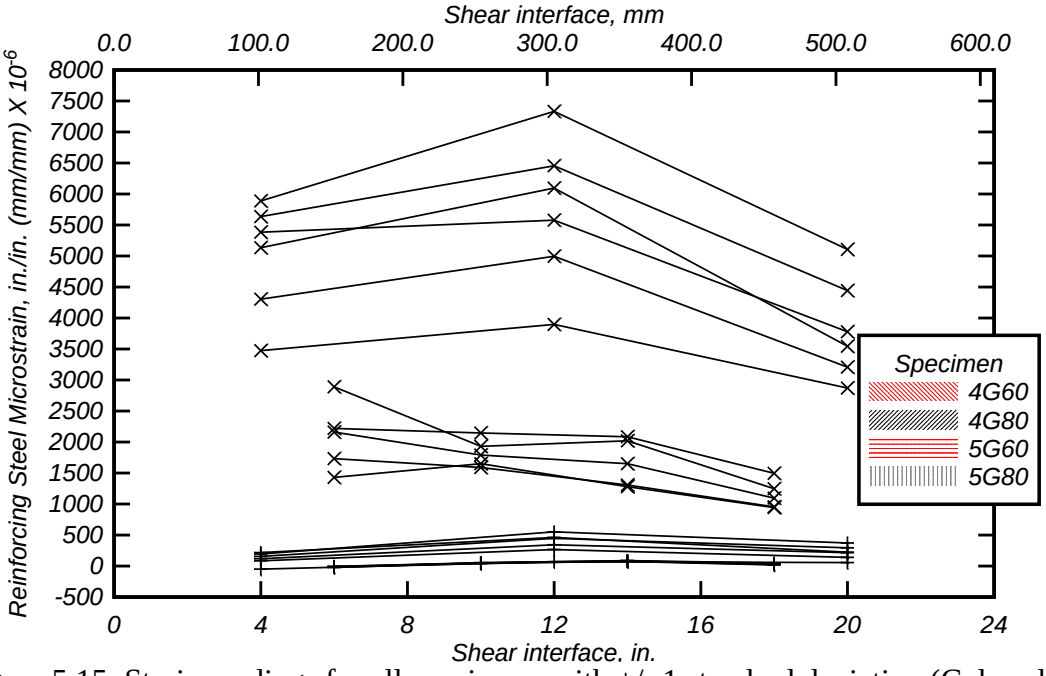

Figure 5.15: Strain readings for all specimens with +/- 1 standard deviation (Color plot)

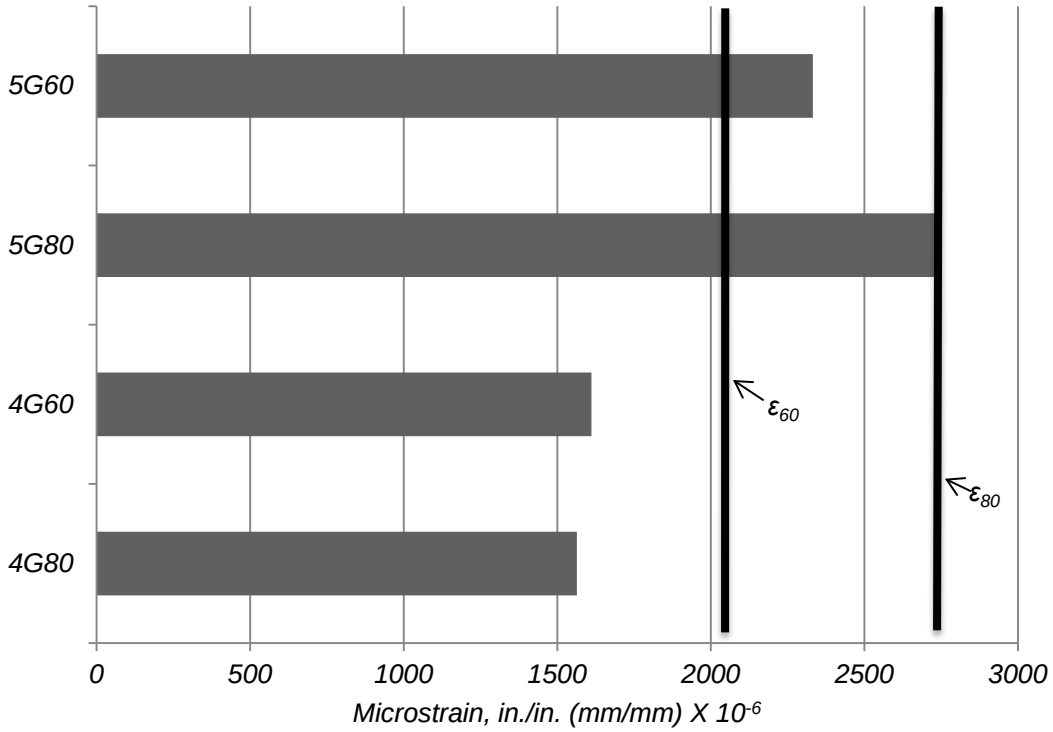

Figure 5.16: Microstrain at peak shear load for average of strain gauges 1 in. (25 mm) from the interface for each specimen set

Figure 5.17 shows the curves for the interface shear force versus interface shear displacement. It is noted through this curve that the 5G80 specimens have significantly higher peak interface shear force and sustained interface shear force than the other three (3) sets of specimens. For the other specimen sets, the results are reasonably consistent. Note that the 5G60 specimens were designed to have similar capacity to the 4G60 specimens. Also, the 4G60, 4G80, and 5G60 specimens are within 25 kips (111 kN) of sustained interface shear force for this analysis method.

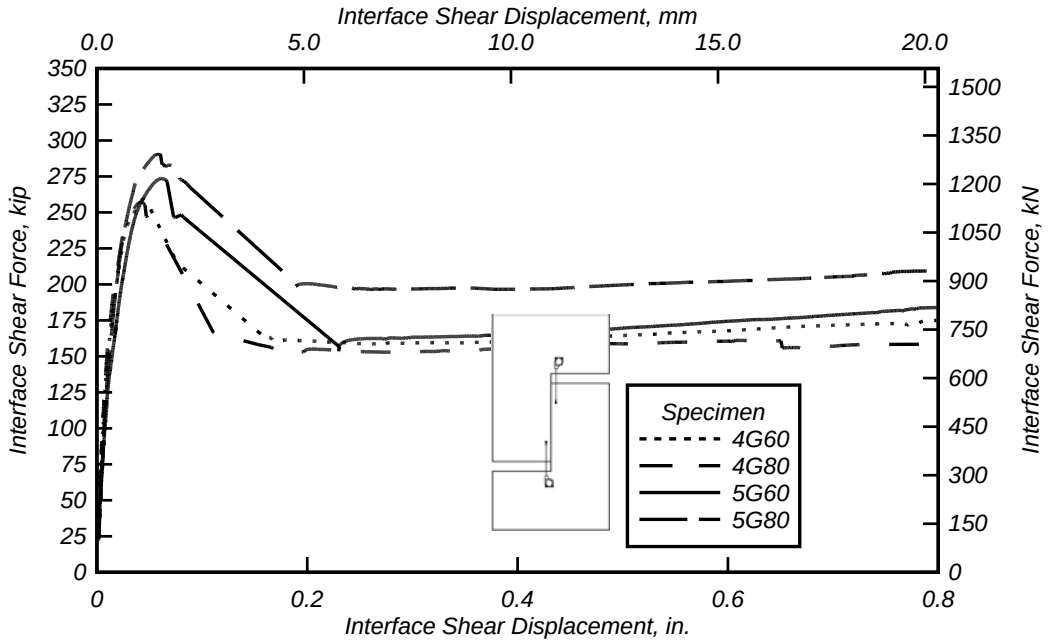

Figure 5.17: Average interface shear force versus displacement for all specimens

Figure 5.18 shows the interface shear force versus reinforcing steel microstrain for all specimens from strain gauges 3 in. (76 mm) from the interface. It is noted that the specimens containing #5 (#16M) reinforcing bars across the interface undergo initial cracking before the specimens containing #4 (#13M) reinforcing bars across the interface. This difference is mainly due to the fact that the specimens containing #5 (#16M) reinforcing bars across the interface had a smaller concrete interface area, thus exhibiting a smaller force due to concrete-concrete cohesion. From the point of cohesion loss until the peak load, the curves show a hardening branch. For the specimens containing #4 (#13M) reinforcing bars across the interface, the reinforcing steel microstrain only surpasses the nominal yield strain, which is 2070 microstrain for Grade 60 ksi (420 MPa) reinforcing steel, after the peak interface shear load is reached. However, for the specimens containing #5 (#16M) reinforcing bars across the interface, the bars reach the nominal yield strain before the peak interface shear load was observed. The slopes of each of the sets are similar, indicating that the global specimen stiffness of all sets of specimens are similar.

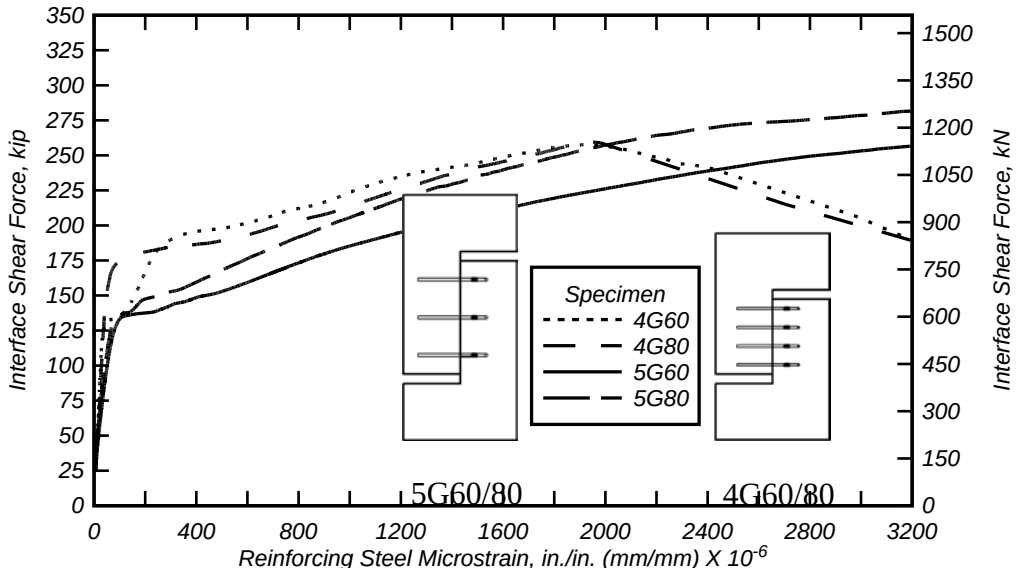

Figure 5.18: Average interface shear force versus reinforcing steel strain for all specimens

Figure 5.19 shows the interface shear force versus crack width relation for all specimens. The 5G80 specimen results were cropped because the data was erratic and interfered with the figure display during the sustained interface shear force. This was due to a malfunctioning string pot. The relation corresponds well for all specimens, with the 5G80 specimens again showing a higher peak interface shear force. Figure 5.19 illustrates that the specimens behaved similarly with regard to crack width. This indicates that the difference in the development of the reinforcing bars may be why the 5G60 and 5G80 specimens had higher reinforcing steel strains at peak interface shear force than the 4G60 and 4G80 specimens.

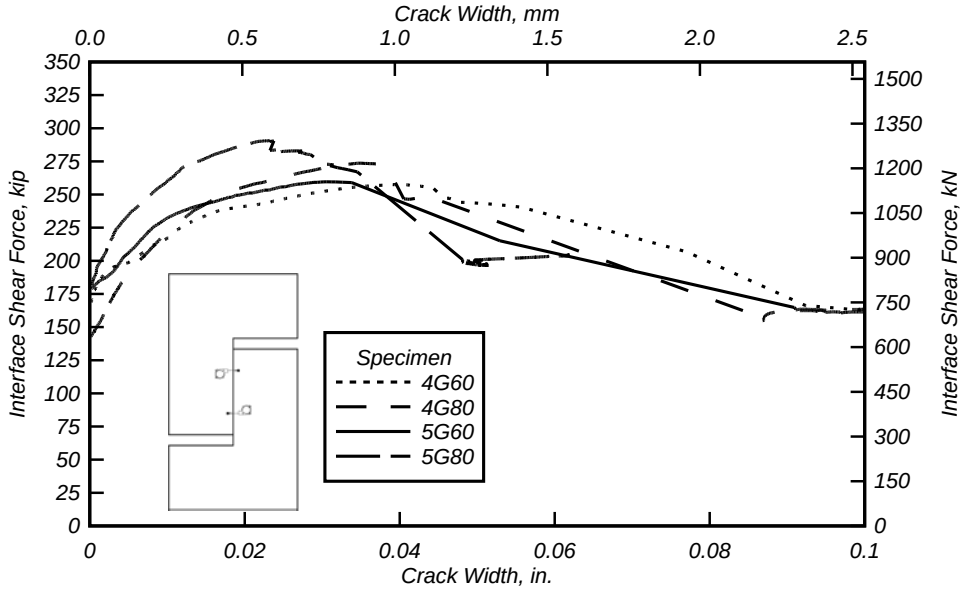

Figure 5.19: Average interface shear force versus crack width for all specimens

5.5 DESIGN EQUATION

Harries et al. *(Harries et al. 2012)* recently proposed an equation for the interface shear capacity based on the three stages of shear friction mechanism:

$$\mathbf{V_{ni} = \alpha A_{cv} f_c^{'} + 0.002 A_{vf} E_s \leq 0.2 A_{cv} f_c^{'}} \qquad \mathbf{(5.1)}$$

where ($\alpha A_{cv} f_c^{'}$) represents the concrete component during the linear, precracked stage of the shear friction mechanism. The α variable is 0.075, 0.040, and 0 for monolithically cast, cold-jointed, and precracked specimens, respectively; Acv is the area of the concrete interface; and f′c is the design concrete compressive strength. For the second or postcracked stage, the term ($0.002 A_{vf} E_s$) represents the friction force generated by the reinforcing steel component. A coefficient 0.002 is the strain corresponding to approximately 60 ksi [420 MPa]. Avf is the area of reinforcing steel, and Es is the modulus of elasticity of the reinforcing steel. For the third and final stage, before cohesion is lost, or the stage in which the interface has cracked and experienced sufficient slip to reach the peak interface shear force is limited to ($0.2 A_{cv} f_c^{'}$). This is where 0.2 is a coefficient determined by Kahn and Mitchell *(Kahn and Mitchell 2002)* and Acv and f′c have been defined. Equation 5.1 is similar to the equations used by current US codes and the reinforcing steel strain parameter could be potentially modified for HSS. However, the 0.002 coefficient in Equation 5.2 limits the strain because the reinforcing steel is assumed that it will not yield *(*Harries et al. 2012). Results in this paper, for the 4G60 and 4G80 specimens, show that this assumption is valid for specimens containing #4 (#13M) reinforcing bars across the interface. The reinforcing bar strains in the 5G60 and 5G80 specimens were higher than the 0.002 strain value for the strain gauges located 1 in. (25 mm) from the interface. Thus, from these test results, the equation proposed should account for bar size. As such, the following equation is proposed:

$$\mathbf{V_{ni}} = \begin{cases} \mathbf{\alpha A_{cv} f_c^{'} + 0.002 A_{vf} E_s, \text{ for No. 4 bar size}} \\ \mathbf{\alpha A_{cv} f_c^{'} + A_{vf} f_y, \text{ for No. 5 bar size}} \end{cases} \leq \mathbf{0.2 A_{cv} f_c^{'}} \qquad \mathbf{(5.2)}$$

where f_y would be limited to 80 ksi (550 MPa). However, as limited testing has been done, it is recommended that further specimens with larger bar sizes be tested and that full-sized girders and shear key specimens be tested to further validate the proposed equation.

5.6 COMPARISON TO AASHTO AND ACI EQUATIONS

Figure 5.20 shows the clamping force computed from the measurements from the strain gauge that was 1 in. [25 mm] from the interface. Even though this only corresponds to one strain gauge this value was used for two reasons. First, the value underestimates the clamping force since it was observed that this measured strain value was consistently lower and thus this will provide for a conservative estimate of the clamping force, and second this value is closest to the interface and thus corresponds to the force transferred near the interface. The clamping force, *P*, is given by:

$$\mathbf{P = A_s E_s \varepsilon_s + P_c} \qquad \mathbf{(5.3)}$$

where A_s is the total area of the reinforcing bar steel across the interface, E_s is the Young's modulus of the reinforcing steel, and ε_s is the strain of the reinforcing steel, and P_c is the net compressive force normal to the shear plane measured by the load cell. The stress-strain curves for the reinforcing steel obtained from the material testing *(see Barbosa et al. 2015)* were used in this computation. The intercept value (value at zero clamping stress) of the peak shear stress versus clamping stress line is 0.47 ksi (3.24 MPa). It is worth noting that the intercept corresponds to the cohesion factor specified in codes. This value is comparable to the 0.28 ksi (1.93 MPa) specified by AASHTO *(AASHTO 2012)* for 1/4 in. (6.35 mm) amplitude roughened surface, with a 1.68 factor of safety. Note that the specimens in the testing program reported here had a 1/8 in. (3.2 mm) amplitude roughened surface, so the factor of safety would actually be larger than 1.68.

For comparison purposes, Figure 5.20 also shows the design curves from Harries et al. (2012), the equation from AASHTO *(AASHTO 2012)* for 1/4 in. (3.2 mm) roughened surface, the equation from AASHTO *(AASHTO 2012)*for not intentionally roughened surface (0 in.), and the expression proposed in Equation 5.2.

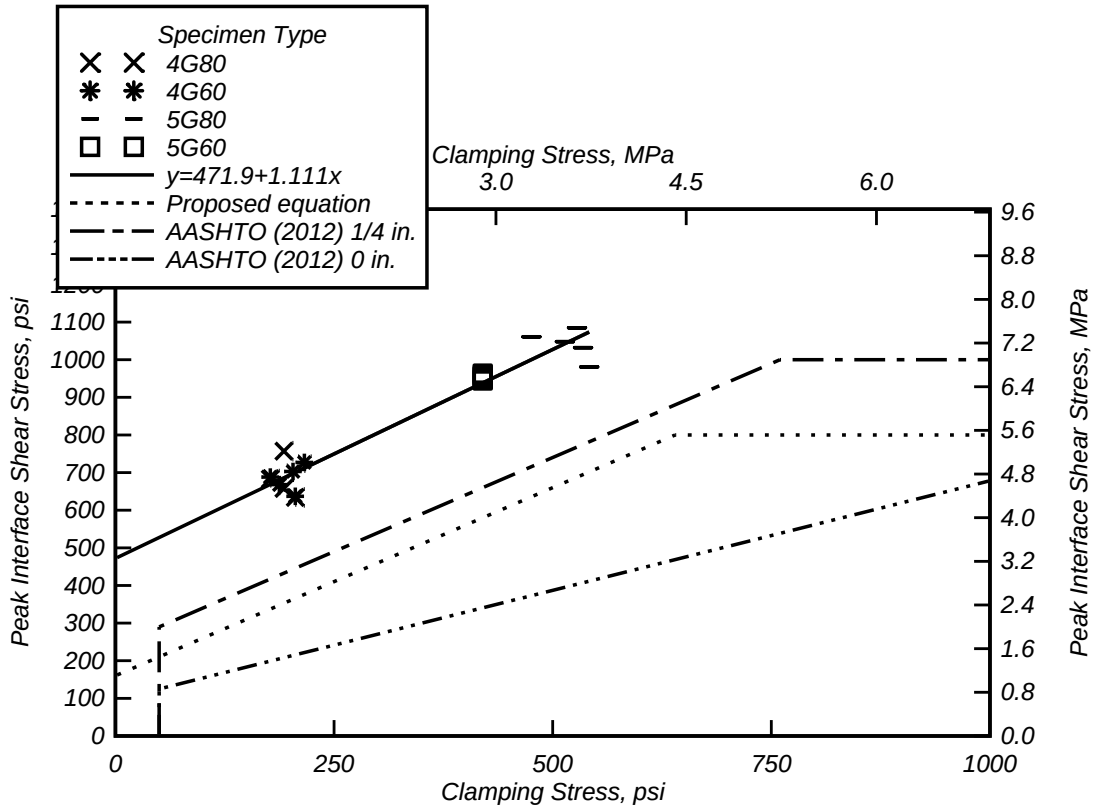

Figure 5.20: Experimental peak shear stress and clamping stress relation

Table 5.9 and Figure 5.21 show the ratios of the mean of the peak interface shear load measured in the test results with the values determined based on AASHTO *(AASHTO 2012)*, ACI 318 *(ACI 2011)*, and the Harries et al. *(Harries et al. 2012)* equation, but using measured values, which has here been defined as the probable strength. Note that the experimentally determined values for concrete compressive strength and reinforcing steel yield stress were used with the respective

equations. The calculations were performed without limiting the values as specified by the corresponding code and researchers. In addition, the nominal values of the concrete compressive strength and reinforcing steel yield stress was taken with respective equation limitations for comparison. For the ratios computed using the AASHTO *(AASHTO 2012)* equations, values for an 1/8 in. (3.2 mm) roughness was interpolated between the AASHTO *(AASHTO 2012)*values for 1/4 in. (6.4 mm) roughness and for surfaces that are not intentionally roughened. For the Harries et al. equation a value of 0.04 for was used for "alpha". For the ACI, Section 17 equation a value of "d" equal to the interface length was used. Other parameters used in the calculations include c = 0.1575, μ = 0.8, K_1 = 0.225, and K_2 = 1.15. For all four sets of equations, the V_m/V_p ratio ranged from 1.28 to 2.38. Note that the Harries et al. *(Harries et al. 2012)* equation best represents the data for this research. This means that the equation produces factor of safety values that are closest to, but always greater than 1.0.

Table 5.9: Ratio of measured strength, V_m, to probable strength, V_p

Specimen	V_m (kip)	Equation	V_p (kip)	V_m/V_p
4G80	262.20	AASHTO	173.57	1.51
4G60	262.80		149.63	1.76
5G80	299.90		174.59	1.72
5G60	274.80		142.44	1.93
4G80	262.20	ACI 17	183.94	1.43
4G60	262.80		165.98	1.58
5G80	299.90		171.08	1.75
5G60	274.80		146.97	1.87
4G80	262.20	ACI 11	140.16	1.87
4G60	262.80		110.24	2.38
5G80	299.90		160.33	1.87
5G60	274.80		120.16	2.29
4G80	262.20	Harries	204.64	1.28
4G60	262.80		176.46	1.49
5G80	299.90		209.12	1.43
5G60	274.80		170.04	1.62

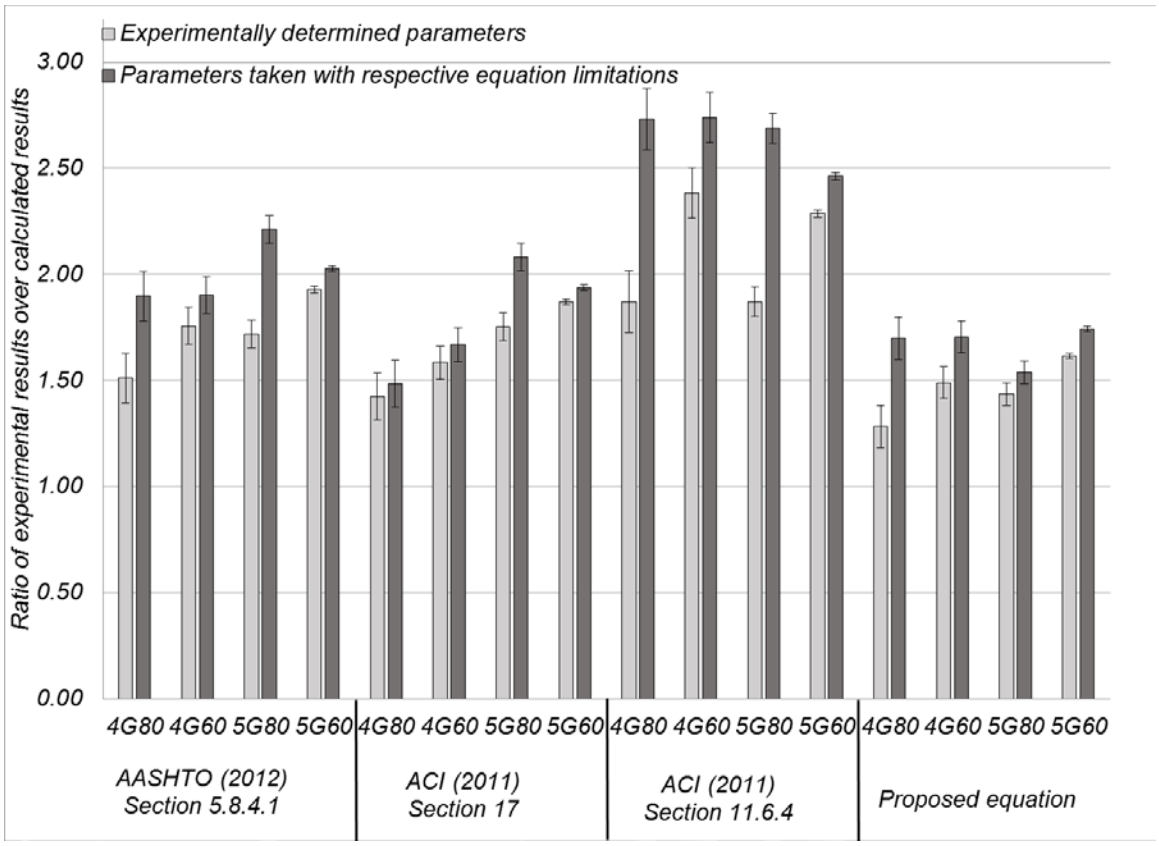

Figure 5.21: Comparison of push-off test results with values from US codes. Ratio of measured strength, Vm, to probable strength, Vp

6.0 CONCLUSION

HSS is commercially available today though its use is still limited. The use of HSS has the potential to reduce the amount of reinforcing steel to be transported, reduce construction costs, and increase constructability. Insufficient research has been completed on shear friction applications of HSS. The research presented assessed the behavior of Grade 80 (550) in a girder-slab shear friction connection. One set of push-off test specimens was constructed with Grade 60 (420) reinforcing steel and the other set was constructed with Grade 80 (550) steel. Both sets had identical reinforcing bar layouts and the grade of steel was the only variable.

The main conclusions that can be drawn from these test results are:

1. Significantly higher peak interface shear forces were observed for the specimens containing #5 (#16M) reinforcing bars across the interface constructed with Grade 80 ksi (550 MPa) reinforcing bars when compared with results from the specimens of the same bar size with Grade 60 (420) reinforcing bars. However, the results were not consistent across bar sizes. For the specimens containing #4 (#13M) reinforcing bars across the interface, the type with Grade 80 ksi (550 MPa) reinforcing bars across the shear friction interface showed no significant change in peak interface shear resistance. This indicates that for the specimens tested the reinforcing bar size is likely as significant and influencing variable for design and performance.

2. All specimens with Grade 80 (550) reinforcing bars across the shear friction interface achieved higher sustained interface shear force than the specimens with the Grade 60 ksi (420 MPa) reinforcing bars across the shear friction interface, which provides evidence that greater loads were developed due to dowel action when the higher strength steel is used.

3. For the specimens containing #4 (#13M) reinforcing bars across the interface, the strain gauges at 1 in. (25 mm) from the interface did not reach the strain level corresponding to the 60 ksi (420 MPa) nominal stress. The strain level reached corresponded to about 45 ksi (310 MPa)

4. For the specimens with #5 (#16M) reinforcing bars across the interface, taking the Grade 80 ksi (550 MPa) reinforcing steel at its nominal design value was conservative for all cases considered. In other words, the strain level reached the nominal strain level corresponding to the Grade 80 (550) reinforcing steel, but not the actual material yield strain.

5. The reinforcement parameter proved to be an important factor, which is not currently explicitly considered in the design equations, since the nominal stress values used for design are currently limited to 60 ksi (420 MPa).

6. Taking the Grade 80 ksi (550 MPa) reinforcing steel at its nominal design value was conservative for all cases considered. However, more research would need to be completed to determine if this trend holds for all applicable cases.

7. The current design equations in AASHTO (2012) and ACI (2011) showed larger safety factors for the HSS reinforcement than for the conventional reinforcement. For the HSS, the factors in AASHTO (2012) range from 1.50 to 2.25ACI equations provide safety factors that are all in excess of 1.43. Specifically, ACI 318 section 11.6.4 provides safety factors in excess of 1.87.

The results in this study add depth to the knowledge of HSS in shear friction applications within the bounds of the test program. Shear transfer across concrete-concrete interfaces is a complex phenomenon. Older models assumed that the clamping force could be estimated using the full yield stress of the bars. However, as shown in this testing program, bar size seems to play a role and development length and bond are also important parameters. In summary, a reinforcement parameter should be explicitly considered in design. Such a proposal is in order, but further analyses of the results in from this thesis are on-going. Other parameters outside of the ones studied in this paper should be evaluated to determine if they affect the ability for HSS to engage before the peak interface shear force. Those parameters may include reinforcing bar spacing, reinforcement ratio, reinforcing bar size, and reinforcing bar development length. Studying these parameters may enable design specifications that allow the use of high strength reinforcing bars in concrete shear friction connections.

If subsequent testing is to be performed, the following test set-up suggestions should be considered:

(1) Number of stirrup-legs: it is suggested that at least four (4) legs are used for each specimen group, which may yield a different length of the shear interface per group;

(2) Width of the shear interface: The same width of the specimens should be used to facilitate comparisons, even though longer lengths can be considered.

(3) Clear cover: clear cover between the first and last stirrups and the concrete surface should be kept consistent across the specimens. This will also influence the overall specimen lengths.

Until the parameters for bar spacing, reinforcement ratio, reinforcing bar size, and reinforcing bar development length are studied, using the AASHTO *(AASHTO 2012)* equation is recommended. The equation could be used with a limit on the reinforcing bar yield strength of 80 ksi (550 MPa) instead of 60 ksi (420 MPa), as the factors of safety from testing using the nominal values were at least 1.5 for each case. Note that the factors of safety were calculated using the interpolated values for 1/8 in. (3.2 mm) from AASHTO *(AASHTO 2012)* between the values for 1/4 in. (6.4 mm) roughness and for surfaces that are not intentionally roughened.

7.0 REFERENCES

AASHTO. *AASHTO Load Resistance Factor Design Bridge Design Specifications, Customary U.S. Units*. American Association of State Highway and Transportation Officials, Washington, D.C., 2014.

AASHTO. *AASHTO Load Resistance Factor Design Bridge Design Specifications, Customary U.S. Units*. American Association of State Highway and Transportation Officials, Washington, D.C., 2012.

AASHTO. *AASHTO Load Resistance Factor Design Bridge Design Specifications, Customary U.S. Units.* American Association of State Highway and Transportation Officials, Washington, D.C., 2007.

AASHTO. *AASHTO Load Resistance Factor Design Bridge Design Specifications, Customary U.S. Units.* American Association of State Highway and Transportation Officials, Washington, D.C., 2004.

AASHTO. *AASHTO Load Resistance Factor Design Bridge Design Specifications, Customary U.S. Units*. American Association of State Highway and Transportation Officials, Washington, D.C., 1998.

ACI. *Building Code Requirements for Structural Concrete (ACI 318-11) and Commentary*. American Concrete Institute, Farmington Hills, MI, 2011.

ACI. *Building Code Requirements for Structural Concrete (ACI 318-02) and Commentary*. American Concrete Institute, Farmington Hills, MI, 2002.

ASTM Standard A615/A615M, 2014. *Standard Specification for Deformed and Plain Carbon-Steel Bars for Concrete Reinforcement.* ASTM International, West Conshocken, PA, 2014. DOI: 10.1520/A0615_A0615M. www.astm.org

ASTM Standard A706/A706M, 2014. *Standard Specification for Low-Alloy Steel Deformed and Plain Bars for Concrete Reinforcement*. ASTM International, West Conshocken, PA, 2014. DOI: 10.1520/A0706_A0706M. www.astm.org

ASTM Standard C31/31M, 2012. *Standard Practice for Making and Curing Concrete Test Specimens in the Field*. ASTM International, West Conshocken, PA, 2012. DOI: 10.1520/C0031_C0031M-12. www.astm.org

ASTM Standard C39, 2012a. *Standard Test Method for Compressive Strength of Cylindrical Concrete Specimens*. ASTM International, West Conshocken, PA, 2012. DOI: 10.1520/C0039_C0039M-12A. www.astm.org

ASTM Standard C138, 2013. *Standard Test Method for Density (Unit Weight), Yield, and Air Content (Gravimetric) of Concrete*. ASTM International, West Conshocken, PA, 2013. DOI: 10.1520/C0138_C0138M. www.astm.org

ASTM Standard C143, 2012. *Standard Test Method for slump of Hydraulic-Cement Concrete*. ASTM International, West Conshocken, PA, 2012. DOI: 10.1520/C0143_C0143M-12. www.astm.org

ASTM Standard C231, 2014. *Standard Test Method for Air Content of Freshly Mixed Concrete by the Pressure Method*. ASTM International, West Conshocken, PA, 2014, DOI: 10.1520/C0231_C0231M-14. www.astm.org

ASTM Standard E8/E8M, 2013a. *Standard Test Methods for Tension Testing of Metallic Materials*. ASTM International, West Conshocken, PA, 2013, DOI: 10.1520/E0008_E0008M. www.astm.org

ASTM Standard E83, 2010a. *Standard Practice for Verification and Classification of Extensometer Systems*. ASTM International, West Conshocken, PA, 2010. DOI: 10.1520/E0083-10A. www.astm.org

Birkeland, P.W., and H.W. Birkeland. Connections in Precast Concrete Construction. *ACI Journal Proceedings*, Vol. 63, No. 3, 1966, pp. 345-368.

Caltrans. *California Amendments to AASHTO LRFD Bridge Design Specifications*. 6th Edition. California Department of Transportation, Sacramento, CA. 2014.

Caltrans. *Standard Specifications*. California Department of Transportation, Sacramento, CA. 2010.

DOT and PF. *Alaska Highway Preconstruction Manual*. Alaska Department of Transportation and Public Facilities, Juneau, AK. 2013.

Harries, K.A., G.A. Zeno, and B. Shahrooz. Toward an Improved Understanding of Shear-Friction Behavior. *ACI Structural Journal*, Vol. 109, No.6, 2012, pp. 835-844.

Hofbeck, J.A., I.O. Ibrahim, and A.H. Mattock. Shear Transfer in Reinforced Concrete. *ACI Journal Proceedings*, Vol. 66, No. 2, 1969, pp. 119-128.

Hwang, S.-J., H.-W. Yu, and H.-J. Lee. Theory of Interface Shear Capacity of Reinforced Concrete. *Journal of Structural Engineering*, Vol. 126, No. 6, 2000, pp. 700-707.

ITD. *LRFD Bridge Design Manual*. Idaho Transportation Department, Boise, ID. 2008.

Julio, E.N.B.S., F.A.B. Branco, and V.D. Silva. Concrete-to-Concrete Bond Strength. Influence of the Roughness of the Substrate Surface. *Construction and Building Materials*, Vol. 18, No. 9, 2004, pp. 675-681.

Kahn, L.F., and A.D. Mitchell. Shear Friction Tests with High-Strength Concrete. *ACI Structural Journal*, Vol.99, No. 1, 2002, pp. 98-103.

Kahn, L.F., and A. Slapkus. Interface Shear in High Strength Composite T-Beams. *PCI Journal*, Vol. 49, No. 4, 2004, pp. 102-110.

Kim, Y.H., M.B.D. Huste, D. Trejo, and D.B.H. Cline. Shear Characteristics and Design for High-Strength Self-Consolidating Concrete. *Journal of Structural Engineering*, Vol. 136, No. 8, 2010, pp. 989-1000.

Kovach, J.D. *Horizontal Shear Capacity of Composite Concrete Beams without Interface Ties*. (Master's thesis). Lehigh University. 2008.

Loov, R.E., and A.K. Patnaik. Horizontal Shear Strength of Composite Concrete Beams with a Rough Interface. *PCI Journal*, Vol. 39, No. 1, 1994, pp. 48-69.

Mattock, A.H., W.K. Li, and T.C. Wang. Shear Transfer in Lightweight Reinforced Concrete. *PCI Journal*, Vol. 21, No. 1, 1976, pp. 20-39.

Mansur, M.A., T. Vinayagam, and K.-H. Tan. Shear Transfer across a Crack in Reinforced High-Strength Concrete. *Journal of Materials in Civil Engineering*, Vol. 20, No. 4, 2008, pp. 294-302.

Menzel, C.A. Some Factors Influencing Results of Pull-Out Bond Tests. *ACI Journal Proceedings*, Vol. 35, No. 6, 1939, pp. 517-542.

Mirza, S.A., J.G. MacGregor, and M. Hatzinikolas. Statistical Descriptions of Strength of Concrete. *Journal of the Structural Division*, Vol. 105, No. 6, 1979, pp. 1021-1037.

Mirza, S.A., and J.G. MacGregor. Variability of Mechanical Properties of Reinforcing Bars. *Journal of the Structural Division*, Vol. 105, No. 5, 1979, pp. 921-937.

ODOT. *Bridge Design and Drafting Manual*. Oregon Department of Transportation, Salem, OR. 2014.

ODOT. Standard Specifications. Oregon Department of Transportation, Salem, OR. 2015.

Park, P., and T. Paulay. *Reinforced Concrete Structures*, John Wiley and Sons, New York. 1975.

Patnaik, A.K. Behavior of Composite Concrete Beams with Smooth Interface. *Journal of Structural Engineering*, Vol. 127, No. 4, 2001, pp. 359-366.

Rehm, G. *Über die Grundlagen des Verbundes zwischen Stahl und Beton*. Ernst. 1961.

Santos, P.M.D., and E.N.B.S. Júlio. A State-of-the-Art Review on Shear-Friction." *Engineering Structures*, Vol. 45, 2012, pp.435-448.

Saemann, J.C., and G.W. Washa. Horizontal Shear Connections Between Precast Beams and Cast-in-Place. *ACI Journal Proceedings*, Vol. 61, No. 11, 1964, pp. 1383-1408.

Scholz, D.P., J.A. Wallenfelsz, C. Lijeron, and C.L. Roberts-Wollmann. *Recommendations for the Connection between Full-Depth Precast Bridge Deck Panel Systems and Precast I-Beams*." Virginia Tech, VTechWorks. 2007.

Scott, J. *Interface Shear Strength in Lightweight Concrete Bridge Girders*. (Master's thesis). Virginia Polytechnic Institute and State University. 2010.

Trejo, D., A.R. Barbosa, and T. Link. *Seismic Performance of Circular Reinforced Concrete Bridge Columns Constructed with Grade 80 Reinforcement*. Publication No. FHWA-OR-RD-15-02. 2014.

Trejo, D., and Y.H. Kim. *Development of Precast Bridge Deck Overhang System: Technical Report*. Texas Transportation Institute, Texas A&M University System. 2011.

WSDOT. *Bridge Design Manual LRFD*. M 23-50. Washington Department of Transportation. 2014.

Wallenfelsz, J.A. *Horizontal Shear Transfer for Full-Depth Precast Concrete Bridge Deck Panels*. (Master's thesis). Virginia Polytechnic Institute and State University. 2006.

Walraven, J.C., and H.W. Reinhardt. Theory and Experiments on the Mechanical Behaviour of Cracks in Plain and Reinforced Concrete Subjected to Shear Loading. *HERON*, Vol. 26, No. 1A, 1981, pp. 1-68.

Waweru, R., G. Palacios, and S.-H. Chao. Horizontal Shear Strength of Full-Scale Composite Box and Slab Bridge Beams Having Horizontal Shear Reinforcement with Limited Development Length. 2014 PCI Convention and National Bridge Conference, September 6-9, 2014, Washington, D.C., 2014.

Zeno, G.A. *Use of High-Strength Steel Reinforcement in Shear Friction Applications*. (Master's thesis). University of Pittsburgh. 2009.

APPENDICES

4G60 specimens

Calculated Input Manual check

From AASHTO (2012) section 5.8.4-Interface Shear Transfer-Shear Friction

AASHTO (2012) Section 5.8.4.3: Values interpolated between a cast-in-place concrete slab on clean concrete girder surfaces, free of laitance with surface roughened to an amplitude of 0.25 in. and concrete placed against a clean concrete surface, free of laitance, but not intentionally roughened.

Fraction of concrete strength available to resist the interface shear

$K_1 := 0.250$

Limiting interface shear resistance

$K_2 := 1.3ksi$ (1.8 ksi for normalweight)

Cohesion factor

$c_c := 0.1775ksi$

Coefficient of friction

$\mu := 0.8$

Specimen properties

Yield strength of the shear reinforcement

$f_y := 60 \frac{kip}{in^2}$

Strength of concrete

$f_c := 4ksi$

Length of contact area

$L_s := 16in$

Width of contact area

$b := 24in$

Interface area of the concrete engaged in shear transfer

$A_{cv} := L_s \cdot b$ $A_{cv} = 384 \cdot in^2$

Size No. of rebar

$R_{no} := 4$

Number of U-bars

$N_r := 4$

Number of bar crossings through shear interface

$N_c := N_r \cdot 2$

Cross section of the shear reinforcement

$A_{vf} := \left(\frac{R_{no}\, in}{8 \cdot 2} \right)^2 \cdot \pi \cdot N_c$ $A_{vf} = 1.571 \cdot in^2$

Specimen shear strength determination

AASHTO (2012) 5.8.4.4
Minimum area of interface shear reinforcement

$Asmin := 0.05 \cdot \frac{A_{cv}}{\frac{f_y}{ksi}}$ $Asmin = 0.32 \cdot in^2$

Minimum area check

$A_{vf} > Asmin = 1$ If 1, then O.K.

AASHTO (2012) 5.5.4.2.1
LRFD shear factor

$\phi := 0.90$

Pressure normal to interface

$p_i := 3 \frac{lbf}{in^2}$

Required force normal to interface

$P_c := p_i \cdot A_{cv}$ $P_c = 1.152 \cdot kip$

AASHTO (2012) 5.8.4.1-3
Nominal shear strength

$V_n := c_c \cdot A_{cv} + \mu \cdot (A_{vf} \cdot f_y + P_c)$

$V_n = 144.48 \cdot kip$

Factored nominal shear strength

$\phi \cdot V_n = 130.032 \cdot kip$

V_n shall not be greater than the lesser of:

AASHTO (2012) 5.8.4.1-4

$V_{ni1} := K_1 \cdot f_c \cdot A_{cv}$ $V_{ni1} = 384 \cdot kip$

$V_n < V_{ni1} = 1$ If 1, then O.K.

AASHTO (2012) 5.8.4.1-5

$V_{ni2} := K_2 \cdot A_{cv}$ $V_{ni2} = 499.2 \cdot kip$

$V_n < V_{ni2} = 1$ If 1, then O.K.

4G80 specimens

Calculated Input Manual check

From AASHTO (2012) section 5.8.4-Interface Shear Transfer-Shear Friction

AASHTO (2012) Section 5.8.4.3: Values interpolated between a cast-in-place concrete slab on clean concrete girder surfaces, free of laitance with surface roughened to an amplitude of 0.25 in. and concrete placed against a clean concrete surface, free of laitance, but not intentionally roughened.

Fraction of concrete strength available to resist the interface shear

$K_1 := 0.250$

Limiting interface shear resistance

$K_2 := 1.3ksi$ (1.8 ksi for normalweight)

Cohesion factor

$c_c := 0.1775ksi$

Coefficient of friction

$\mu := 0.8$

Specimen properties

Yield strength of the shear reinforcement

$f_y := 80 \frac{kip}{in^2}$

Strength of concrete

$f_c := 4ksi$

Length of contact area

$L_s := 16in$

Width of contact area

$b := 24in$

Interface area of the concrete engaged in shear transfer

$A_{cv} := L_s \cdot b$ $A_{cv} = 384 \cdot in^2$

Size No. of rebar

$R_{no} := 4$

Number of U-bars

$N_r := 4$

Number of bar crossings through shear interface

$N_c := N_r \cdot 2$

Cross section of the shear reinforcement

$A_{vf} := \left(\frac{R_{no}\, in}{8 \cdot 2} \right)^2 \cdot \pi \cdot N_c$ $A_{vf} = 1.571 \cdot in^2$

Specimen shear strength determination

AASHTO (2012) 5.8.4.4
Minimum area of interface shear reinforcement

$Asmin := 0.05 \cdot \frac{A_{cv}}{\frac{f_y}{ksi}}$ $Asmin = 0.24 \cdot in^2$

Minimum area check

$A_{vf} > Asmin = 1$ If 1, then O.K.

AASHTO (2012) 5.5.4.2.1
LRFD shear factor

$\phi := 0.90$

Pressure normal to interface

$p_i := 3 \frac{lbf}{in^2}$

Required force normal to interface

$P_c := p_i \cdot A_{cv}$ $P_c = 1.152 \cdot kip$

AASHTO (2012) 5.8.4.1-3
Nominal shear strength

$V_n := c_c \cdot A_{cv} + \mu \cdot (A_{vf} \cdot f_y + P_c)$

$V_n = 169.613 \cdot kip$

Factored nominal shear strength

$\phi \cdot V_n = 152.651 \cdot kip$

V_n shall not be greater than the lesser of:

AASHTO (2012) 5.8.4.1-4

$V_{ni1} := K_1 \cdot f_c \cdot A_{cv}$ $V_{ni1} = 384 \cdot kip$

$V_n < V_{ni1} = 1$ If 1, then O.K.

AASHTO (2012) 5.8.4.1-5

$V_{ni2} := K_2 \cdot A_{cv}$ $V_{ni2} = 499.2 \cdot kip$

$V_n < V_{ni2} = 1$ If 1, then O.K.

5G60 specimens

Calculated Input Manual check

From AASHTO (2012) section 5.8.4-Interface Shear Transfer-Shear Friction

AASHTO (2012) Section 5.8.4.3: Values interpolated between a cast-in-place concrete slab on clean concrete girder surfaces, free of laitance with surface roughened to an amplitude of 0.25 in. and concrete placed against a clean concrete surface, free of laitance, but not intentionally roughened.

Fraction of concrete strength available to resist the interface shear

$K_1 := 0.250$

Limiting interface shear resistance

$K_2 := 1.3ksi$ (1.8 ksi for normalweight)

Cohesion factor

$c_c := 0.1775ksi$

Coefficient of friction

$\mu := 0.8$

Specimen properties

Yield strength of the shear reinforcement

$f_y := 60 \frac{kip}{in^2}$

Strength of concrete

$f_c := 4ksi$

Length of contact area

$L_s := 24in$

Width of contact area

$b := 12in$

Interface area of the concrete engaged in shear transfer

$A_{cv} := L_s \cdot b$ $A_{cv} = 288 \cdot in^2$

Size No. of rebar

$R_{no} := 5$

Number of U-bars

$N_r := 3$

Number of bar crossings through shear interface

$N_c := N_r \cdot 2$

Cross section of the shear reinforcement

$A_{vf} := \left(\frac{R_{no}\, in}{8 \cdot 2} \right)^2 \cdot \pi \cdot N_c$ $A_{vf} = 1.841 \cdot in^2$

Specimen shear strength determination

AASHTO (2012) 5.8.4.4
Minimum area of interface shear reinforcement

$Asmin := 0.05 \cdot \frac{A_{cv}}{\frac{f_y}{ksi}}$ $Asmin = 0.24 \cdot in^2$

Minimum area check

$A_{vf} > Asmin = 1$ If 1, then O.K.

AASHTO (2012) 5.5.4.2.1
LRFD shear factor

$\phi := 0.90$

Pressure normal to interface

$p_i := 3 \frac{lbf}{in^2}$

Required force normal to interface

$P_c := p_i \cdot A_{cv}$ $P_c = 0.864 \cdot kip$

AASHTO (2012) 5.8.4.1-3
Nominal shear strength

$V_n := c_c \cdot A_{cv} + \mu \cdot (A_{vf} \cdot f_y + P_c)$

$V_n = 140.168 \cdot kip$

Factored nominal shear strength

$\phi \cdot V_n = 126.152 \cdot kip$

V_n shall not be greater than the lesser of:

AASHTO (2012) 5.8.4.1-4

$V_{ni1} := K_1 \cdot f_c \cdot A_{cv}$ $V_{ni1} = 288 \cdot kip$

$V_n < V_{ni1} = 1$ If 1, then O.K.

AASHTO (2012) 5.8.4.1-5

$V_{ni2} := K_2 \cdot A_{cv}$ $V_{ni2} = 374.4 \cdot kip$

$V_n < V_{ni2} = 1$ If 1, then O.K.

5G80 specimens

Calculated Input Manual check

From AASHTO (2012) section 5.8.4-Interface Shear Transfer-Shear Friction

AASHTO (2012) Section 5.8.4.3: Values interpolated between a cast-in-place concrete slab on clean concrete girder surfaces, free of laitance with surface roughened to an amplitude of 0.25 in. and concrete placed against a clean concrete surface, free of laitance, but not intentionally roughened.

Fraction of concrete strength available to resist the interface shear

$K_1 := 0.250$

Limiting interface shear resistance

$K_2 := 1.3ksi$ (1.8 ksi for normalweight)

Cohesion factor

$c_c := 0.1775ksi$

Coefficient of friction

$\mu := 0.8$

Specimen properties

Yield strength of the shear reinforcement

$f_y := 80 \frac{kip}{in^2}$

Strength of concrete

$f_c := 4ksi$

Length of contact area

$L_s := 24in$

Width of contact area

$b := 12in$

Interface area of the concrete engaged in shear transfer

$A_{cv} := L_s \cdot b$ $A_{cv} = 288 \cdot in^2$

Size No. of rebar

$R_{no} := 5$

Number of U-bars

$N_r := 3$

Number of bar crossings through shear interface

$N_c := N_r \cdot 2$

Cross section of the shear reinforcement

$A_{vf} := \left(\frac{R_{no}\, in}{8 \cdot 2} \right)^2 \cdot \pi \cdot N_c$ $A_{vf} = 1.841 \cdot in^2$

Specimen shear strength determination

AASHTO (2012) 5.8.4.4
Minimum area of interface shear reinforcement

$Asmin := 0.05 \cdot \frac{A_{cv}}{\frac{f_y}{ksi}}$ $Asmin = 0.18 \cdot in^2$

Minimum area check

$A_{vf} > Asmin = 1$ If 1, then O.K.

AASHTO (2012) 5.5.4.2.1
LRFD shear factor

$\phi := 0.90$

Pressure normal to interface

$p_i := 3 \frac{lbf}{in^2}$

Required force normal to interface

$P_c := p_i \cdot A_{cv}$ $P_c = 0.864 \cdot kip$

AASHTO (2012) 5.8.4.1-3
Nominal shear strength

$V_n := c_c \cdot A_{cv} + \mu \cdot (A_{vf} \cdot f_y + P_c)$

$V_n = 169.621 \cdot kip$

Factored nominal shear strength

$\phi \cdot V_n = 152.659 \cdot kip$

V_n shall not be greater than the lesser of:

AASHTO (2012) 5.8.4.1-4

$V_{ni1} := K_1 \cdot f_c \cdot A_{cv}$ $V_{ni1} = 288 \cdot kip$ $V_n < V_{ni1} = 1$ If 1, then O.K.

AASHTO (2012) 5.8.4.1-5

$V_{ni2} := K_2 \cdot A_{cv}$ $V_{ni2} = 374.4 \cdot kip$ $V_n < V_{ni2} = 1$ If 1, then O.K.

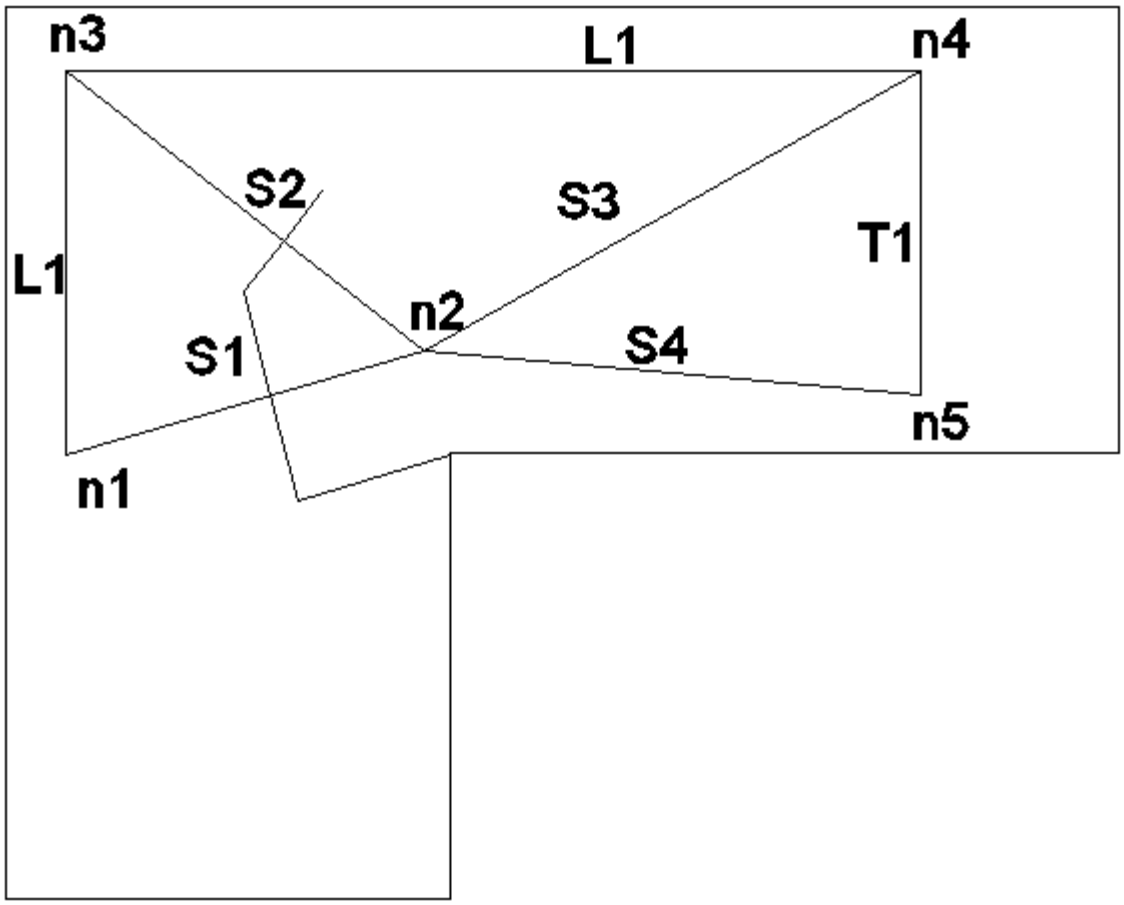

Strut and tie method for the 4G60 and 4G80 specimens

Step 1.) Adjust input values according to specimen properties

Need to check value according to instructions highlighted

Input Values

Design load $P := 300kip$

Reinforced concrete specific weight. $\gamma_c := 150 \frac{lbf}{ft^3}$

Nominal compressive strength of concrete used in the footing. $f'_c := 4500psi$

Nominal yield stress of reinforcing steel. $f_y := 60ksi$

L shape width $b := 24in$

Phi factor for tension in steel in anchorage zones $\phi_{stm} := 0.7$

Phi factor for compression in strut and tie model, Sec. 5.5.4.2. $\phi_n := 0.9$

Forces from SAP2000 analysis

Step 2.) Compute and check strut s1 according to AASHTO (2012) Sec. 5.6.3.3

Vertical Distance Between Node 1 and 2 $L_{p12} := 2.875in$

Horizontal Distance between Node 1 and 2 $L_{w12} := 9.625in$

$\varepsilon_{s1} := 0.002$ Tensile strain in the concrete in the direction of the tension tie (in./in.)

$L_{s1} := \left(L_{w12}^{\ 2} + L_{p12}^{\ 2}\right)^{\frac{1}{2}} = 10.045 \cdot in$ Length of compression strut s1.

$a_1 := \operatorname{atan}\left(\frac{L_{p12}}{L_{w12}}\right) \cdot rad \quad a_1 = 16.631 \cdot deg$ Angle of strut one measured to the horizontal.

AASHTO (2012) Figure 5.6.3.3.2-1

$l_{b1} := 7.118in$ Height of effective bearing plate

$h_{a1} := 6 \cdot \left(\frac{6}{8}\right) in + 0.75 \frac{in}{2}$

$l_{a1s} := l_{b1} \cdot \sin(a_1) + h_{a1} \cdot \cos(a_1) \quad l_{a1s} = 6.708 \cdot in$ Width of strut 1 on n1 side

$l_{a1t} := 2.9in \cdot 2 \quad l_{a1t} = 5.8 \cdot in$ Width of strut 1 on node 2 side

$A_{cs1} := \min(l_{a1s} \cdot b, l_{a1t} \cdot b) \quad A_{cs1} = 139.2 \cdot in^2$ Approximation of the effective area of strut s1.

$\varepsilon_{1s1} := \varepsilon_{s1} + (\varepsilon_{s1} + 0.002) \cdot \cot(90deg - a_1)^2$ Eq. 5.6.3.3.3-2

$f_{cus1} := \left\lceil \frac{f'_c}{(0.8 + 170 \cdot \varepsilon_{1s1})} \right\rceil \quad f_{cus1} = 3.748 \cdot ksi$ Eq. 5.6.3.3.3-1

$0.85f'_c = 3.825 \cdot ksi$ Maximum value for fcu. Eq. 5.6.3.3.3-1

$P_{ns1} := A_{cs1} \cdot \min(0.85f'_c, f_{cus1}) \quad P_{ns1} = 521.708 \cdot kip$ Eq. 5.6.3.3.4-1

Note that longitudinal bar 1 passes through node 1.

$P_{r1} := \phi_{stm} \cdot P_{ns1} \quad P_{r1} = 365.196 \cdot kip$ Eq. 5.6.3.2-1

$F_{s1} := \frac{P}{\cos(a_1)} = 313.097 \cdot kip$ Compressive force in strut s1.

$0.75 \cdot \phi_{stm} \cdot f'_c \cdot A_{cs1} - F_{s1} = 15.763 \cdot kip$ If positive, then node is O.K.

$check\_s1 := P_{r1} - F_{s1}$ $check\_s1 = 52.098 \cdot kip$ $check\_s1 > 0 = 1$

If the above value is less than zero then the compressive force in strut is higher than the capacity of the strut and the design needs to be adjusted

Step 3.) Compute the required amount of reinforcing steel for longitudinal bar 1 at n3 to AASHTO LRFD Bridge Design Specifications 6th Ed. Sec. 5.6.3.4

From node 3 to 1:

$F_{l1.31} := 60.71kip$ Tension force in longitudinal bar 1

$A_{l1.31} := \frac{F_{l1.31}}{\phi_n \cdot f_y}$ $A_{l1.31} = 1.124 \cdot in^2$ Required area of reinforcement for longitudinal bar 1

$n_{l1.31} := \frac{A_{l1.31}}{0.44in^2}$ $n_{l1.31} = 2.555$ Required number of #6 bars for longitudinal bar 1

3 #6 bars are req. for longitudinal bar 1

From node 3 to 4:

$F_{l1.34} := 75.40kip$ Tension force in longitudinal bar 1

$A_{l1.34} := \frac{F_{l1.34}}{\phi_n \cdot f_y}$ $A_{l1.34} = 1.396 \cdot in^2$ Required area of reinforcement for longitudinal bar 1

$n_{l1.34} := \frac{A_{l1.34}}{0.44in^2}$ $n_{l1.34} = 3.173$ Required number of #6 bars for longitudinal bar 1

4 #6 bars are req. for longitudinal bar 1 - CONTROLS

Step 4.) Compute and check strut s2 according to AASHTO (2012) Sec. 5.6.3.3

Vertical Distance Between Node 2 and 3 $L_{p23} := 7.625in$

Horizontal Distance between Node 2 and 3 $L_{w23} := 9.625in$

$\varepsilon_{s2} := 0.002$ Tensile strain in the concrete in the direction of the tension tie (in./in.)

$L_{s2} := \left(L_{w23}^2 + L_{p23}^2\right)^{\frac{1}{2}} = 12.279 \cdot in$ Length of compression strut s2.

$a_2 := atan\left(\frac{L_{p23}}{L_{w23}}\right) \cdot rad$ $a_2 = 38.387 \cdot deg$ Angle of strut one measured to the horizontal.

AASHTO (2012) Figure 5.6.3.3.2-1

$h_{a2} := 2 \cdot 6 \cdot \left(\frac{5}{8}\right) in$

$l_{a2s} := h_{a2} \cdot \sin(a_2)$ $l_{a2s} = 4.657 \cdot in$ Width of strut 2 on node 3 side

$l_{a2t} := 1.7in \cdot 2$ $l_{a2t} = 3.4 \cdot in$ Width of strut 2 on node 2 side

$A_{cs2} := \min(l_{a2s} \cdot b, l_{a2t} \cdot b)$ $A_{cs2} = 81.6 \cdot in^2$ Approximation of the effective area of strut s1.

$\varepsilon_{1s2} := \varepsilon_{s2} + (\varepsilon_{s2} + 0.002) \cdot \cot(a_2)^2$ Eq. 5.6.3.3.3-2

$f_{cus2} := \left\lceil \frac{f'_c}{(0.8 + 170 \cdot \varepsilon_{1s2})} \right\rceil$ $f_{cus2} = 2.024 \cdot ksi$ Eq. 5.6.3.3.3-1

$0.85 f'_c = 3.825 \cdot ksi$ Maximum value for fcu. Eq. 5.6.3.3.3-1

$P_{ns2} := A_{cs2} \cdot \min(0.85 f'_c, f_{cus2})$ $P_{ns2} = 165.145 \cdot kip$ Eq. 5.6.3.3.4-1

Note that longitudinal bar 1 passes through node 1.

$P_{r2} := \phi_{stm} \cdot P_{ns2}$ $P_{r2} = 115.601 \cdot kip$ Eq. 5.6.3.2-1

$F_{s2} := 96.41 kip$ Compressive force in strut s1.

$0.65 \cdot \phi_{stm} \cdot f'_c \cdot A_{cs2} - F_{s2} = 70.666 \cdot kip$ If positive, then node is O.K.

$check\_s2 := P_{r2} - F_{s2}$ $check\_s2 = 19.191 \cdot kip$ $check\_s2 > 0 = 1$

If the above value is less than zero then the compressive force in strut is higher than the capacity of the strut and the design needs to be adjusted

Step 5.) Compute and check strut s3 according to AASHTO LRFD Bridge Design Specifications 6th Ed. Sec. 5.6.3.3

Vertical Distance Between Node 2 and 4 $L_{p24} := 7.5in$

Horizontal Distance between Node 2 and 4 $L_{w24} := 13.375in$

$\varepsilon_{s3} := 0.002$ Tensile strain in the concrete in the direction of the tension tie (in./in.)

$L_{s3} := \left(L_{w24}^2 + L_{p24}^2\right)^{\frac{1}{2}} = 15.334 \cdot in$ Length of compression strut s3

$a_3 := \operatorname{atan}\left(\frac{L_{p24}}{L_{w24}}\right) \cdot rad$ $a_3 = 29.281 \cdot deg$ Angle of strut one measured to the horizontal.

AASHTO (2012) Figure 5.6.3.3.2-1

$l_{a3t} := 12.5in$ Width of strut 3 on Node 2 side (compression node)

$l_{a4t} := (0.625in \cdot 2 \cdot 6 + 2.5in)$ $l_{a4t} = 10 \cdot in$ Width of strut 3 on Node 4 side

$A_{cs3} := \min\left(l_{a3t} \cdot b \cdot \sin\left(a_3\right), l_{a4t} \cdot b \cdot \sin\left(a_3\right)\right)$ Approximation of the effective area of strut s3

$A_{cs3} = 117.384 \cdot in^2$

$\varepsilon_{1s3} := \varepsilon_{s3} + \left(\varepsilon_{s3} + 0.002\right) \cdot \cot\left(a_3\right)^2$ Eq. 5.6.3.3.3-2

$f_{cus3} := \left[\frac{f'_c}{\left(0.8 + 170 \cdot \varepsilon_{1s3}\right)}\right]$ $f_{cus3} = 1.363 \cdot ksi$ Eq. 5.6.3.3.3-1

$0.85f'_c = 3.825 \cdot ksi$ Maximum value for fcu Eq. 5.6.3.3.3-1

$P_{ns3} := A_{cs3} \cdot \min\left(0.85f'_c, f_{cus3}\right)$ $P_{ns3} = 159.944 \cdot kip$ Eq. 5.6.3.3.4-1

Note that longitudinal bar 2 passes through node 3, 5, & subsequent bottom nodes.

$P_{r3} := \phi_{stm} \cdot P_{ns3}$ $P_{r3} = 111.96 \cdot kip$ Eq. 5.6.3.2-1

$F_{s3} := 91.24kip$ Compressive force in strut s3

$0.75 \cdot \phi_{stm} \cdot f'_c \cdot A_{cs3} - F_{s3} = 186.08 \cdot kip$ If positive, then node is O.K.

$check\_s3 := P_{r3} - F_{s3}$ $check\_s3 = 20.72 \cdot kip$ $check\_s3 > 0 = 1$

If the above value is less than zero then the compressive force in strut is higher than the capacity of the strut and the design needs to be adjusted

Step 6.) Compute and check strut s4 and sn according to AASHTO (2012) Sec. 5.6.3.3

Vertical Distance Between Node 2 and 5 $L_{p25} := 1.25in$

Horizontal Distance between Node 2 and 5 $L_{w25} := 13.375in$

$\varepsilon_{s4} := 0.002$ Tensile strain in the concrete in the direction of the tension tie (in./in.)

$L_{s4} := \left(L_{w25}^2 + L_{p25}^2\right)^{\frac{1}{2}} = 13.433 \cdot in$ Length of compression strut s4.

$a_4 := \operatorname{atan}\left(\frac{L_{p25}}{L_{w25}}\right) \cdot rad$ $a_4 = 5.339 \cdot deg$ Angle of strut one measured to the horizontal.

AASHTO (2012) Figure 5.6.3.3.2-1

$l_{a5t} := 2.75in \cdot 2$ $l_{a5t} = 5.5 \cdot in$ Width of strut 4 on Node 2 side (compression node)

$l_{a6t} := 2.75in \cdot 2$ $l_{a6t} = 5.5 \cdot in$ Width of strut 2 on Node 5 side (1.5in cover)

$A_{cs4} := \min(l_{a5t} \cdot b)$ Approximation of the effective area of strut s4 or sn.

$A_{cs4} = 132 \cdot in^2$

$\varepsilon_{1s4} := \varepsilon_{s4} + (\varepsilon_{s4} + 0.002) \cdot \cot(90deg - a_4)^2$ Eq. 5.6.3.3.3-2

$f_{cus4} := \left[\frac{f'_c}{(0.8 + 170 \cdot \varepsilon_{1s4})} \right]$ $f_{cus4} = 3.927 \cdot ksi$ Eq. 5.6.3.3.3-1

$0.85f'_c = 3.825 \cdot ksi$ Maximum value for fcu. Eq. 5.6.3.3.3-1

$P_{ns4} := A_{cs4} \cdot \min(0.85f'_c, f_{cus4})$ $P_{ns4} = 504.9 \cdot kip$ Eq. 5.6.3.3.4-1

Note that longitudinal bar 2 passes through node 3, 5, & subsequent bottom nodes.

$P_{r4} := \phi_{stm} \cdot P_{ns4}$ $P_{r4} = 353.43 \cdot kip$ Eq. 5.6.3.2-1

$F_{s4} := 301.16kip$ Compressive force in strut s4.

$0.75 \cdot \phi_{stm} \cdot f'_c \cdot A_{cs4} - F_{s4} = 10.69 \cdot kip$ If positive, then node is O.K.

$check\_s4 := P_{r4} - F_{s4}$ $check\_s4 = 52.27 \cdot kip$ $check\_s4 > 0 = 1$

If the above value is less than zero then the compressive force in strut is higher than the capacity of the strut and the design needs to be adjusted

Step 7.) Compute and check strut s5 according to AASHTO LRFD (2012) Sec. 5.6.3.3

Vertical Distance Between Node 5 and 5 $L_{p56} := 8.75in$

Horizontal Distance between Node 5 and 6 $L_{w56} := 6in$

$\varepsilon_{s5} := 0.002$ Tensile strain in the concrete in the direction of the tension tie (in./in.)

$L_{s5} := \left(L_{w56}^2 + L_{p56}^2 \right)^{\frac{1}{2}} = 10.61 \cdot in$ Length of compression strut s5.

$a_5 := \operatorname{atan}\left(\frac{L_{p56}}{L_{w56}} \right) \cdot rad$ $a_5 = 55.561 \cdot deg$ Angle of strut one measured to the horizontal.

AASHTO LRFD BDS Figure 5.6.3.3.2-1

$l_{a7t} := (0.625in \cdot 2 \cdot 6)$ $l_{a7t} = 7.5 \cdot in$ Width of strut 5 on Node 5 side

$l_{a8t} := (0.625in \cdot 2 \cdot 6)$ $l_{a8t} = 7.5 \cdot in$ Width of strut 5 on Node 6 side

$A_{cs5} := \min\left(l_{a7t} \cdot b \cdot \sin\left(a_5\right), l_{a8t} \cdot b \cdot \sin\left(a_5\right)\right)$ Approximation of the effective area of strut s5 or sn.

$A_{cs5} = 148.451 \cdot in^2$

$\varepsilon_{1s5} := \varepsilon_{s5} + \left(\varepsilon_{s5} + 0.002\right) \cdot \cot\left(90deg - a_5\right)^2$ Eq. 5.6.3.3.3-2

$f_{cus5} := \left[\frac{f'_c}{\left(0.8 + 170 \cdot \varepsilon_{1s5}\right)}\right]$ $f_{cus5} = 1.74 \cdot ksi$ Eq. 5.6.3.3.3-1

$0.85f'_c = 3.825 \cdot ksi$ Maximum value for fcu. Eq. 5.6.3.3.3-1

$P_{ns5} := A_{cs5} \cdot \min\left(0.85f'_c, f_{cus5}\right)$ $P_{ns5} = 258.308 \cdot kip$ Eq. 5.6.3.3.4-1

Note that longitudinal bar 2 passes through node 3, 5, & subsequent bottom nodes.

$P_{r5} := \phi_{stm} \cdot P_{ns5}$ $P_{r5} = 180.815 \cdot kip$ Eq. 5.6.3.2-1

$F_{s5} := 17.05kip$ Compressive force in strut s5.

$0.75 \cdot \phi_{stm} \cdot f'_c \cdot A_{cs5} - F_{s5} = 333.666 \cdot kip$ If positive, then node is O.K.

$check\_s5 := P_{r5} - F_{s5}$ $check\_s5 = 163.765 \cdot kip$ $check\_s5 > 0 = 1$

If the above value is less than zero then the compressive force in strut is higher than the capacity of the strut and the design needs to be adjusted

Step 8.) Compute the required amount of reinforcing steel for tie 1 to AASHTO LRFD Bridge Design Specifications 6th Ed. Sec. 5.6.3.4

$F_{t1} := 51.37kip$ Tension force in tie 1

$A_{t1} := \frac{F_{t1}}{\phi_n \cdot f_y}$ $A_{t1} = 0.951 \cdot in^2$ Required area of reinforcement for tie 1

$n_{t1} := \frac{A_{t1}}{2 \cdot 0.20in^2}$ $n_{t1} = 2.378$ Required number of #4 stirrups for tie 1.

Three #4 stirrups will be used for tie 1

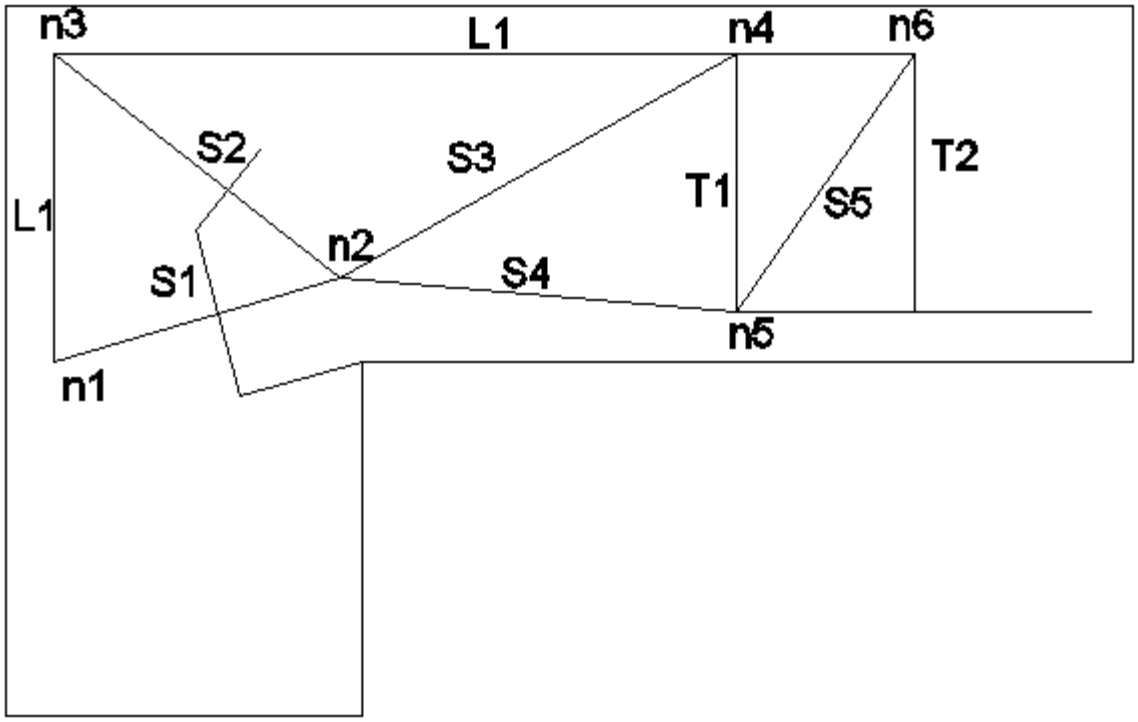

Strut and tie method for the 5G60 and 5G80 specimens

Step 1.) Adjust input values according to specimen properties

Need to check value according to instructions highlighted

Input Values

Design load $P := 300kip$

Reinforced concrete specific weight. $\gamma_c := 150 \frac{lbf}{ft^3}$

Nominal compressive strength of concrete used in the footing. $f'_c := 4500psi$

Nominal yield stress of reinforcing steel. $f_y := 60ksi$

L shape width $b := 24in$

Phi factor for tension in steel in anchorage zones $\phi_{stm} := 0.7$

Phi factor for compression in strut and tie model, Sec. 5.5.4.2. $\phi_n := 0.9$

Forces from SAP2000 analysis

Step 2.) Compute and check strut s1 according to AASHTO (2012) Sec. 5.6.3.3

Vertical Distance Between Node 1 and 2 $L_{p12} := 2.875in$

Horizontal Distance between Node 1 and 2 $L_{w12} := 9.625in$

$\varepsilon_{s1} := 0.002$ Tensile strain in the concrete in the direction of the tension tie (in./in.)

$L_{s1} := \left(L_{w12}^{2} + L_{p12}^{2}\right)^{\frac{1}{2}} = 10.045 \cdot in$ Length of compression strut s1.

$a_1 := \operatorname{atan}\left(\frac{L_{p12}}{L_{w12}}\right) \cdot rad \quad a_1 = 16.631 \cdot deg$ Angle of strut one measured to the horizontal

AASHTO (2012) Figure 5.6.3.3.2-1

$l_{b1} := 7.118in$ Height of effective bearing plate

$h_{a1} := 6 \cdot \left(\frac{6}{8}\right) in + 0.75 \frac{in}{2}$

$l_{a1s} := l_{b1} \cdot \sin\left(a_1\right) + h_{a1} \cdot \cos\left(a_1\right) \quad l_{a1s} = 6.708 \cdot in$ Width of strut 1 on n1 side

$l_{a1t} := 2.9in \cdot 2 \quad l_{a1t} = 5.8 \cdot in$ Width of strut 1 on node 2 side

$A_{cs1} := \min\left(l_{a1s} \cdot b, l_{a1t} \cdot b\right) \quad A_{cs1} = 139.2 \cdot in^{2}$ Approximation of the effective area of strut s1.

$\varepsilon_{1s1} := \varepsilon_{s1} + \left(\varepsilon_{s1} + 0.002\right) \cdot \cot\left(90deg - a_1\right)^{2}$ Eq. 5.6.3.3.3-2

$f_{cus1} := \left\lceil \frac{f'_c}{\left(0.8 + 170 \cdot \varepsilon_{1s1}\right)} \right\rceil \quad f_{cus1} = 3.748 \cdot ksi$ Eq. 5.6.3.3.3-1

$0.85 f'_c = 3.825 \cdot ksi$ Maximum value for fcu. Eq. 5.6.3.3.3-1

$P_{ns1} := A_{cs1} \cdot \min\left(0.85 f'_c, f_{cus1}\right) \quad P_{ns1} = 521.708 \cdot kip$ Eq. 5.6.3.3.4-1

Note that longitudinal bar 1 passes through node 1.

$P_{r1} := \phi_{stm} \cdot P_{ns1} \quad P_{r1} = 365.196 \cdot kip$ Eq. 5.6.3.2-1

$F_{s1} := \frac{P}{\cos\left(a_1\right)} = 313.097 \cdot kip$ Compressive force in strut s1.

$0.75 \cdot \phi_{stm} \cdot f'_c \cdot A_{cs1} - F_{s1} = 15.763 \cdot kip$ If positive, then node is O.K.

$check\_s1 := P_{r1} - F_{s1} \quad check\_s1 = 52.098 \cdot kip \quad check\_s1 > 0 = 1$

If the above value is less than zero then the compressive force in strut is higher than the capacity of the strut and the design needs to be adjusted

Step 3.) Compute the required amount of reinforcing steel for longitudinal bar 1 at n3 to AASHTO (2012) Sec. 5.6.3.4

From node 3 to 1:

$F_{l1.31} := 85.71kip$ Tension force in longitudinal bar 1.

$A_{l1.31} := \frac{F_{l1.31}}{\phi_n \cdot f_y}$ $A_{l1.31} = 1.587 \cdot in^2$ Required area of reinforcement for longitudinal bar 1

$n_{l1.31} := \frac{A_{l1.31}}{0.44in^2}$ $n_{l1.31} = 3.607$ Required number of #6 bars for longitudinal bar 1.

4 #6 bars are req. for longitudinal bar 1

From node 3 to 4:

$F_{l1.34} := 106.45kip$ Tension force in longitudinal bar 1.

$A_{l1.34} := \frac{F_{l1.34}}{\phi_n \cdot f_y}$ $A_{l1.34} = 1.971 \cdot in^2$ Required area of reinforcement for longitudinal bar 1

$n_{l1.34} := \frac{A_{l1.34}}{0.44in^2}$ $n_{l1.34} = 4.48$ Required number of #6 bars for longitudinal bar 1.

5 #6 bars are req. for longitudinal bar 1 - CONTROLS

Step 4.) Compute and check strut s2 according to AASHTO (2012) Sec. 5.6.3.3

Vertical Distance Between Node 2 and 3 $L_{p23} := 7.625in$

Horizontal Distance between Node 2 and 3 $L_{w23} := 9.625in$

$\varepsilon_{s2} := 0.002$ Tensile strain in the concrete in the direction of the tension tie (in./in.)

$L_{s2} := \left(L_{w23}^2 + L_{p23}^2\right)^{\frac{1}{2}} = 12.279 \cdot in$ Length of compression strut s2.

$a_2 := atan\left(\frac{L_{p23}}{L_{w23}}\right) \cdot rad$ $a_2 = 38.387 \cdot deg$ Angle of strut one measured to the horizontal.

AASHTO (2012) Figure 5.6.3.3.2-1

$h_{a2} := 2 \cdot 6 \cdot \left(\frac{5}{8}\right) in$

$l_{a2s} := h_{a2} \cdot \sin\left(a_2\right)$ $l_{a2s} = 4.657 \cdot in$ Width of strut 2 on node 3 side

$l_{a2t} := 2.01in \cdot 2$ $l_{a2t} = 4.02 \cdot in$ Width of strut 2 on node 2 side

$A_{cs2} := \min\left(l_{a2s} \cdot b, l_{a2t} \cdot b\right)$ $A_{cs2} = 96.48 \cdot in^2$ Approximation of the effective area of strut s1.

$\varepsilon_{1s2} := \varepsilon_{s2} + \left(\varepsilon_{s2} + 0.002\right) \cdot \cot\left(a_2\right)^2$ Eq. 5.6.3.3.3-2

$f_{cus2} := \left[\frac{f'_c}{\left(0.8 + 170 \cdot \varepsilon_{1s2}\right)}\right]$ $f_{cus2} = 2.024 \cdot ksi$ Eq. 5.6.3.3.3-1

$0.85f'_c = 3.825 \cdot ksi$ Maximum value for fcu. Eq. 5.6.3.3.3-1

$P_{ns2} := A_{cs2} \cdot \min\left(0.85f'_c, f_{cus2}\right)$ $P_{ns2} = 195.259 \cdot kip$ Eq. 5.6.3.3.4-1

Note that longitudinal bar 1 passes through node 1.

$P_{r2} := \phi_{stm} \cdot P_{ns2}$ $P_{r2} = 136.682 \cdot kip$ Eq. 5.6.3.2-1

$F_{s2} := 136.67kip$ Compressive force in strut s1.

$0.65 \cdot \phi_{stm} \cdot f'_c \cdot A_{cs2} - F_{s2} = 60.873 \cdot kip$ If positive, then node is O.K.

$check\_s2 := P_{r2} - F_{s2}$ $check\_s2 = 0.012 \cdot kip$ $check\_s2 > 0 = 1$

If the above value is less than zero then the compressive force in strut is higher than the capacity of the strut and the design needs to be adjusted

Step 5.) Compute and check strut s3 according to AASHTO (2012) Sec. 5.6.3.3

Vertical Distance Between Node 2 and 4 $L_{p24} := 7.5in$

Horizontal Distance between Node 2 and 4 $L_{w24} := 13.375in$

$\varepsilon_{s3} := 0.002$ Tensile strain in the concrete in the direction of the tension tie (in./in.)

$L_{s3} := \left(L_{w24}^2 + L_{p24}^2\right)^{\frac{1}{2}} = 15.334 \cdot in$ Length of compression strut s3.

$a_3 := \operatorname{atan}\left(\frac{L_{p24}}{L_{w24}}\right) \cdot rad$ $a_3 = 29.281 \cdot deg$ Angle of strut one measured to the horizontal.

AASHTO (2012) Figure 5.6.3.3.2-1

$l_{a3t} := 12.5in$ Width of strut 3 on Node 2 side (compression node)

$l_{a4t} := (0.625in \cdot 2 \cdot 6 + 4.25in$ $l_{a4t} = 11.75 \cdot in$ Width of strut 3 on Node 4 side

$A_{cs3} := \min\left(l_{a3t} \cdot b \cdot \sin\left(a_3\right), l_{a4t} \cdot b \cdot \sin\left(a_3\right)\right)$ Approximation of the effective area of strut s3

$A_{cs3} = 137.926 \cdot in^2$

$\varepsilon_{1s3} := \varepsilon_{s3} + (\varepsilon_{s3} + 0.002) \cdot \cot(a_3)^2$ Eq. 5.6.3.3.3-2

$f_{cus3} := \left[\frac{f'_c}{(0.8 + 170 \cdot \varepsilon_{1s3})} \right]$ $f_{cus3} = 1.363 \cdot ksi$ Eq. 5.6.3.3.3-1

$0.85 f'_c = 3.825 \cdot ksi$ Maximum value for fcu. Eq. 5.6.3.3.3-1

$P_{ns3} := A_{cs3} \cdot \min(0.85 f'_c, f_{cus3})$ $P_{ns3} = 187.934 \cdot kip$ Eq. 5.6.3.3.4-1

Note that longitudinal bar 2 passes through node 3, 5, & subsequent bottom nodes.

$P_{r3} := \phi_{stm} \cdot P_{ns3}$ $P_{r3} = 131.554 \cdot kip$ Eq. 5.6.3.2-1

$F_{s3} := 128.81 kip$ Compressive force in strut s3

$0.75 \cdot \phi_{stm} \cdot f'_c \cdot A_{cs3} - F_{s3} = 197.04 \cdot kip$ If positive, then node is O.K.

check_s3 := $P_{r3} - F_{s3}$ $check\_s3 = 2.744 \cdot kip$ $check\_s3 > 0 = 1$

If the above value is less than zero then the compressive force in strut is higher than the capacity of the strut and the design needs to be adjusted

Step 6.) Compute and check strut s4 and sn according to AASHTO (2012) Sec. 5.6.3.3

Vertical Distance Between Node 2 and 5 & subsequent struts $L_{p25} := 1.25 in$

Horizontal Distance between Node 2 and 5 & subsequent struts $L_{w25} := 13.375 in$

$\varepsilon_{s4} := 0.002$ Tensile strain in the concrete in the direction of the tension tie (in./in.)

$L_{s4} := \left(L_{w25}^2 + L_{p25}^2 \right)^{\frac{1}{2}} = 13.433 \cdot in$ Length of compression strut s4.

$a_4 := \operatorname{atan}\left(\frac{L_{p25}}{L_{w25}} \right) \cdot rad$ $a_4 = 5.339 \cdot deg$ Angle of strut one measured to the horizontal.

AASHTO (2012) Figure 5.6.3.3.2-1

$l_{a5t} := 3 in \cdot 2$ $l_{a5t} = 6 \cdot in$ Width of strut 4 on Node 2 side (compression node)

$l_{a6t} := 2.75 in \cdot 2$ $l_{a6t} = 5.5 \cdot in$ Width of strut 2 on Node 5 side (1.5in cover)

$A_{cs4} := \min\left(l_{a5t} \cdot b, l_{a6t} \cdot b\right)$ Approximation of the effective area of strut s4 or sn.

$A_{cs4} = 132 \cdot in^2$

$\varepsilon_{1s4} := \varepsilon_{s4} + \left(\varepsilon_{s4} + 0.002\right) \cdot \cot\left(90deg - a_4\right)^2$ Eq. 5.6.3.3.3-2

$f_{cus4} := \left[\frac{f'_c}{\left(0.8 + 170 \cdot \varepsilon_{1s4}\right)}\right]$ $f_{cus4} = 3.927 \cdot ksi$ Eq. 5.6.3.3.3-1

$0.85f'_c = 3.825 \cdot ksi$ Maximum value for fcu. Eq. 5.6.3.3.3-1

$P_{ns4} := A_{cs4} \cdot \min\left(0.85f'_c, f_{cus4}\right)$ $P_{ns4} = 504.9 \cdot kip$ Eq. 5.6.3.3.4-1

Note that longitudinal bar 2 passes through node 3, 5, & subsequent bottom nodes.

$P_{r4} := \phi_{stm} \cdot P_{ns4}$ $P_{r4} = 353.43 \cdot kip$ Eq. 5.6.3.2-1

$F_{s4} := 305.20kip$ Compressive force in strut s4.

$0.75 \cdot \phi_{stm} \cdot f'_c \cdot A_{cs4} - F_{s4} = 6.65 \cdot kip$ If positive, then node is O.K.

$check\_s4 := P_{r4} - F_{s4}$ $check\_s4 = 48.23 \cdot kip$ $check\_s4 > 0 = 1$

If the above value is less than zero then the compressive force in strut is higher than the capacity of the strut and the design needs to be adjusted

Step 7.) Compute and check strut s5 according to AASHTO LRFD Bridge Design Specifications 6th Ed. Sec. 5.6.3.3

Vertical Distance Between Node 5 and 5 $L_{p56} := 8.75in$

Horizontal Distance between Node 5 and 6 struts $L_{w56} := 6in$

$\varepsilon_{s5} := 0.002$ Tensile strain in the concrete in the direction of the tension tie (in./in.)

$L_{s5} := \left(L_{w56}^2 + L_{p56}^2\right)^{\frac{1}{2}} = 10.61 \cdot in$ Length of compression strut s5.

$a_5 := \operatorname{atan}\left(\frac{L_{p56}}{L_{w56}}\right) \cdot rad$ $a_5 = 55.561 \cdot deg$ Angle of strut one measured to the horizontal.

AASHTO (2012) Figure 5.6.3.3.2-1

$l_{a7t} := (0.625in \cdot 2 \cdot 6)$ $l_{a7t} = 7.5 \cdot in$ Width of strut 5 on Node 5 side

$l_{a8t} := (0.625in \cdot 2 \cdot 6)$ $l_{a8t} = 7.5 \cdot in$ Width of strut 5 on Node 6 side

$A_{cs5} := \min\left(l_{a7t} \cdot b \cdot \sin\left(a_5\right), l_{a8t} \cdot b \cdot \sin\left(a_5\right)\right)$ Approximation of the effective area of strut s5 or sn.

$A_{cs5} = 148.451 \cdot in^2$

$\varepsilon_{1s5} := \varepsilon_{s5} + \left(\varepsilon_{s5} + 0.002\right) \cdot \cot\left(90deg - a_5\right)^2$ Eq. 5.6.3.3.3-2

$f_{cus5} := \left[\frac{f'_c}{\left(0.8 + 170 \cdot \varepsilon_{1s5}\right)}\right]$ $f_{cus5} = 1.74 \cdot ksi$ Eq. 5.6.3.3.3-1

$0.85f'_c = 3.825 \cdot ksi$ Maximum value for fcu. Eq. 5.6.3.3.3-1

$P_{ns5} := A_{cs5} \cdot \min\left(0.85f'_c, f_{cus5}\right)$ $P_{ns5} = 258.308 \cdot kip$ Eq. 5.6.3.3.4-1

Note that longitudinal bar 2 passes through node 3, 5, & subsequent bottom nodes.

$P_{r5} := \phi_{stm} \cdot P_{ns5}$ $P_{r5} = 180.815 \cdot kip$ Eq. 5.6.3.2-1

$F_{s5} := 100kip$ Compressive force in strut s5.

$0.75 \cdot \phi_{stm} \cdot f'_c \cdot A_{cs5} - F_{s5} = 250.716 \cdot kip$ If positive, then node is O.K.

$check\_s5 := P_{r5} - F_{s5}$ $check\_s5 = 80.815 \cdot kip$ $check\_s5 > 0 = 1$

If the above value is less than zero then the compressive force in strut is higher than the capacity of the strut and the design needs to be adjusted

Step 8.) Compute the required amount of reinforcing steel for tie 1 to AASHTO (2012) Sec. 5.6.3.4

$F_{t1} := 72.53kip$ Tension force in tie 1

$A_{t1} := \frac{F_{t1}}{\phi_n \cdot f_y}$ $A_{t1} = 1.343 \cdot in^2$ Required area of reinforcement for tie 1

$n_{t1} := \frac{A_{t1}}{2 \cdot 0.20in^2}$ $n_{t1} = 3.358$ Required number of #4 stirrups for tie 1.

2 #4 stirrups will be used for tie 1

Step 9.) Compute the required amount of reinforcing steel for tie 2 to AASHTO (2012) Sec. 5.6.3.4

$F_{t2} := 14.06kip$ Tension force in tie 2

$A_{t2} := \frac{F_{t2}}{\phi_n \cdot f_y} = 0.26 \cdot in^2$ Required area of reinforcement for tie 2

$$n_{t2} := \frac{A_{t2}}{2 \cdot 0.20 in^2} \qquad n_{t2} = 0.651$$

Use 1 #4 stirrup at tie 2

$$s_{t2} := \frac{8.75}{3 \cdot n_{t2}} in = 4.481 \cdot in$$